FINAL TECHNICAL REPORT

Hawaii Energy and Environmental Technologies Initiative

Office of Naval Research

Grant Number N00014-01-1-0928

For the period May 17, 2001 to March 31, 2005

Hawaii Natural Energy Institute

HNEI
HAWAII NATURAL ENERGY INSTITUTE

School of Ocean and Earth Science and Technology
University of Hawaii at Manoa

June 2005

Table of Contents

REPORT DOCUMENTATION PAGE

The public reporting burden for this collection of information is estimated to average 1 hour per response, including the time for reviewing instructions, searching existing data sources, gathering and maintaining the data needed, and completing and reviewing the collection of information. Send comments regarding this burden estimate or any other aspect of this collection of information, including suggestions for reducing the burden, to Department of Defense, Washington Headquarters Services, Directorate for Information Operations and Reports (0704-0188), 1215 Jefferson Davis Highway, Suite 1204, Arlington, VA 22202-4302. Respondents should be aware that notwithstanding any other provision of law, no person shall be subject to any penalty for failing to comply with a collection of information if it does not display a currently valid OMB control number. **PLEASE DO NOT RETURN YOUR FORM TO THE ABOVE ADDRESS.**

1. REPORT DATE (DD-MM-YYYY)	2. REPORT TYPE	3. DATES COVERED (From - To)
06-30-2005	Final Technical Report	05/17/01 to 03/31/05

4. TITLE AND SUBTITLE

Hawaii Energy and Environmental Technologies (HEET) Initiative

5a. CONTRACT NUMBER

5b. GRANT NUMBER

N00014-01-1-0928

5c. PROGRAM ELEMENT NUMBER

6. AUTHOR(S)

Rocheleau, Richard E.

5d. PROJECT NUMBER

04PR15136-00

5e. TASK NUMBER

5f. WORK UNIT NUMBER

7. PERFORMING ORGANIZATION NAME(S) AND ADDRESS(ES)

University of Hawaii
2530 Dole Street, Sakamaki D200
Honolulu, HI 96822

8. PERFORMING ORGANIZATION REPORT NUMBER

9. SPONSORING/MONITORING AGENCY NAME(S) AND ADDRESS(ES)

Office of Naval Research
Regional Office Seattle
1107 NE 45th Street, Suite 350
Seattle, WA 98105-4631

10. SPONSOR/MONITOR'S ACRONYM(S)

ONR

11. SPONSOR/MONITOR'S REPORT NUMBER(S)

12. DISTRIBUTION/AVAILABILITY STATEMENT

Approved for public release; distribution is unlimited

13. SUPPLEMENTARY NOTES

14. ABSTRACT

This report summarizes work conducted by the Hawaii Natural Energy Institute of the University of Hawaii under the Hawaii Energy and Environmental Technologies (HEET) Initiative funded through the Office of Naval Research. This initiative focused on critical technology needs associated with the exploration and utilization of seabed methane hydrates and the development and testing of advanced fuel cells and fuel cell systems. The efforts in methane hydrates encompassed six primary components: hydrate thermochemistry and kinetics, hydrate microbiology, subsea power generation, modeling, field studies, and international collaboration. In the fuel cell area, the major accomplishment was the development of the Hawaii Fuel Cell Test Facility to characterize advanced fuel cells and fuel cells systems for Navy applications, specifically for unmanned undersea vehicles.

15. SUBJECT TERMS

Fuel Cells, Fuel Cell Testing, Methane Hydrates

16. SECURITY CLASSIFICATION OF:

a. REPORT	b. ABSTRACT	c. THIS PAGE
U	U	U

17. LIMITATION OF ABSTRACT

UU

18. NUMBER OF PAGES

96

19a. NAME OF RESPONSIBLE PERSON

Kevin Hanaoka, Interim Dir. of Research Services

19b. TELEPHONE NUMBER (Include area code)

(808) 956-7800

Final Technical Report for the
Hawaii Energy and Environmental Technologies (HEET) Initiative
Grant Number N00014-01-1-0928 (May 17, 2001 to March 31, 2005)

1. Executive Summary

This report summarizes work conducted under the first three years of the Hawaii Energy and Environmental Technologies (HEET) Initiative, funded through the Office of Naval Research to the Hawaii Natural Energy Institute (HNEI) of the University of Hawaii. This initiative focuses on critical technology needs associated with the exploration and utilization of seabed methane hydrates and the development and testing of advanced fuel cells and fuel cell systems.

HNEI's efforts in methane hydrates have encompassed six primary components: hydrate thermochemistry and kinetics, hydrate microbiology, subsea power generation, modeling, field studies, and international collaboration. Significant laboratory facilities developed during this period include a hydrate synthesis system, benthic pressure chambers to simulate deep seafloor sediment, and specialized instrumentation for high pressure calorimetry and measurement of hydrate destabilization and evolved gas. Using bioreactors designed and fabricated for this work, HNEI has demonstrated the high probability that a sulfide/oxygen microbial fuel cell can generate electricity in deep ocean sediments, and that prolonged power generation may be possible with methane availability. HNEI researchers and students participated in three research cruises to offshore methane hydrate fields, where electronic data and sediment and microbial samples were collected. Three international workshops were organized by HNEI, with a total attendance of over 200, including representatives from eight countries. In addition, two foreign graduate students were hosted by HNEI as visiting scholars.

The major accomplishment in the area of PEM fuel cell testing was the planning, design and construction of the Hawaii Fuel Cell Test Facility (HFCTF), a 4,000 sq ft facility housing three full-size fuel cell test stands. This facility opened for business in April 2003 and has demonstrated continuous 24/7 operation, with capabilities including performance and life testing of full-size fuel cells over a wide range of operating conditions, including hydrogen or reformate fuel, air or oxygen, and temperatures up to 100°C. The test stands include in-line humidification and active thermal and water management systems allowing precise control and characterization of these functions. The facility also boasts a host of supporting equipment including on-site hydrogen generation (using an electrolyser) and storage, and on-line high-resolution gas analysis.

In addition to installation and commissioning of the test stands, HNEI's fuel cell test program has included development of a fuel cell assembly laboratory, development of fuel cell test protocols, and testing of full-scale and subscale test cells. Efforts with full-scale fuel cells have included long-term durability tests (~2,000 hours) using simulated reformate fuel, and accelerated degradation testing in an oxygen environment. General Motors and Ballard Power Systems each delivered two subscale fuel cell test hardware assemblies to HNEI for use in characterizing the effects of contaminants on fuel cell performance. Preliminary fuels purity tests were run on the cells assembled by HNEI staff. HNEI has completed specifications for specialized subscale fuel cell test stands and two such stands will be delivered to the HFCTF later in 2005.

In support of finding alternative fuel supplies, HNEI has expended efforts in the area of fuel processing and gas conditioning for hydrogen production. This work was based on the potential use of liquefied petroleum gas (LPG). An automated fuel processing testbed was designed and fabricated, and is currently in use. This system has been used to convert LPG to hydrogen, evaluate catalyst performance, study catalyst deactivation, and perform parametric testing of optimized reforming conditions.

In addition to work with traditional PEM fuel cells, HNEI has also conducted research on novel fuel cell components. One area involves the use of biocarbons (carbonized charcoal produced from biomass) in fuel cell bipolar plates. Specialized biocarbons were prepared, electrical and physical properties were measured, and samples were sent for evaluation to organizations fabricating bipolar plates. Another area is enzymatic bio-fuel cells. Such fuel cells can complement traditional cells using expensive catalysts. Work has focused on charge transfer limitations for biological catalysts. A mini-gas diffusion cell was built and tested, whereby enzyme was immobilized and characteristics measured (e.g., charge and mass transfer). A micro enzyme fuel cell was designed to allow electrochemical deposition of conductive polymers to metal supports. This could facilitate charge transfer to the metal supports from immobilized enzyme and allow continuous fuel flow into and out of the cell.

2. Introduction

The Hawaii Energy and Environmental Technologies (HEET) Initiative, funded to the Hawaii Natural Energy Institute (HNEI) of the University of Hawaii through the Office of Naval Research (ONR), was initiated in the summer of 2001 to address critical technology needs associated with the exploration and utilization of seabed methane hydrates and the development and testing of advanced fuel cells and fuel cell systems. During the first three years of operation, the focal point of our activity has been development of the Hawaii Fuel Cell Test Facility (HFCTF) which houses dual facilities for fuel cell testing and for the synthesis and characterization of methane hydrates.

The HEET project at HNEI was funded as a multi-year agreement, with an official end date of March 31, 2005. This HEET Final Technical Report covers the work accomplished during the period May 17, 2001 through March 2005.

Development of the overall HFCTF required an investment of over $3 million, achieved in partnership with ONR, UTC Fuel Cells, and Hawaiian Electric Company. Installations within the facility include a low temperature laboratory to support the methane hydrates work, and three state-of-the-are fuel cell test stands for characterization of full-size PEM fuel cells, together with substantial hydrogen infrastructure and safety systems to support fuel cell testing activities.

In addition to primary efforts in the arenas of methane hydrates and PEM fuel cell testing, HNEI has also conducted two areas of work in support of fuel cell development. One area includes research involving fuel processing and gas conditioning for hydrogen production, with emphasis on hydrogen suitable for use in fuel cells. The other area addresses novel fuel cell components.

The remaining four sections of this report focus on each of the areas covered within the HEET initiative. Section 3 in on methane hydrates, Section 4 covers the Hawaii Fuel Cell Test Facility and PEM fuel cell testing, Section 5 presents fuel processing and gas conditioning for hydrogen production, and Section 6 deals with novel fuel cell component activities.

3. Methane Hydrates

3.1. Objectives

Methane hydrates in ocean sediments constitute an enormous energy reservoir that is estimated to exceed the energy content of all known coal, oil, and conventional natural gas resources. Located on continental margins throughout the world, methane hydrates offer unique opportunities as an onsite source of fuel for various marine applications and are believed to play a major role in seafloor stability and global climate.

National R&D programs on methane hydrates were initiated in Japan and India in the mid-1990's with the goal of commercial gas production within a 20 year time horizon. The U.S. established its own program in May 2000. The Methane Hydrate Research and Development Act of 2000 (Public Law 106-193) included seven technical areas of focus: (1) identification, exploration, assessment, and development of methane hydrate as a source of energy; (2) technology development for efficient and environmentally sound recovery of methane from hydrates; (3) transport and storage of methane produced from methane hydrates; (4) education and training related to methane hydrate resource R&D; (5) assessment and mitigation of environmental impacts of natural and purposeful hydrate degassing; (6) development of technologies to reduce the risks of drilling through methane hydrates; and (7) support of exploratory drilling projects. The objectives of the present Methane Hydrates Task, which was initiated in 2001, reflect most of the priorities of P.L. 106-193, but emphasize those areas of particular relevance to the Office of Naval Research (ONR) and which are consistent to the overall goals of the HEET initiative. Specifically, the development of hydrates and related sources of seafloor methane as logistical fuels for Naval applications or for specialized subsea power applications, and related marine environmental issues, were principal areas of interest; exploratory drilling projects and seafloor stability/safety received limited attention. Task objectives were devised to leverage fully hydrate R&D expertise and infrastructure that had been developed at HNEI during previous research programs on CO_2 ocean sequestration and deep oil spills.

During the present reporting period (2001-2005), the goals of the HEET Methane Hydrates Task were:

- Pursue development of means to recover methane gas from hydrates in the seafloor sediment.
- Utilize seafloor methane to provide power for specialized subsea applications.
- In cooperation with the Naval Research Laboratory, develop biogeochemical methods to supplement seismic techniques to refine the detection and characterization of deep hydrate reservoirs.
- Investigate the microbial processes in the sediment that generate and modulate methane levels.
- Investigate the fate of methane leaking into the water column from the seafloor.
- Investigate other engineering applications for methane hydrates of relevance to U.S. Naval operations.
- In cooperation with NRL and ONR Global (previously ONR-IFO), promote international collaborative research on methane hydrates.

As indicated above, a key component of the Methane Hydrates Task was the coordination and integration of the HNEI effort with related activities at the NRL and ONR Global.

Specific technical objectives that were pursued to attain the above goals included:

- Development of laboratory facilities to conduct fundamental studies of hydrate thermochemistry and decomposition kinetics.
- Development of laboratory facilities and protocols to investigate microbial methane generation and consumption in seafloor sediments.
- Development of models of hydrate stability.
- Development of models of methane in the oceanic water column.
- Conduct of laboratory experiments on marine microbial fuel cells.
- Conduct of laboratory experiments on hydrate destabilization by thermal, pressure, and chemical methods.
- Collaborative field studies of offshore hydrate biogeochemistry with NRL.
- Organization of workshops to promote international collaboration on methane hydrate R&D.

3.2. Scope of Work and Approach

Pursuant to the goals and technical objectives identified above, the scope of work of the Methane Hydrates Task comprises the six primary components described below.

Hydrate Thermochemistry and Kinetics

Review of the literature indicated that a substantial, albeit not comprehensive, database existed for a limited number of thermodynamic properties (e.g., phase boundaries; densities) of pure and mixed gas hydrates, in contact with water and the hydrate-forming gases, at pressures and temperatures representative of conditions in the deep seafloor. The influence of the seafloor sediment matrix on hydrate stability (while not strictly a thermodynamic effect), however, had not been extensively investigated. Less information was available on other properties relevant to analyses of hydrate dissociation for methane production, such as heat capacity, enthalpy, and thermal conductivity. Hydrate formation and dissociation kinetics, which in most practical scenarios may be dominated by heat and mass transfer effects rather than chemistry, were not as well documented as thermodynamic properties, and the available data exhibited significant variation between different experiments.

It was determined that substantial contributions could still be made in the area of fundamental measurements of hydrate thermochemistry and, to an even greater extent, kinetics. Since the practical goal of the HEET Methane Hydrates Task was the extraction of methane from hydrates for energy, efforts focused on the measurement of properties and investigation of phenomena which would be useful in the development of models and methods to destabilize hydrates *in situ* and to collect the released gas.

During Years 1 through 3 of the HEET initiative, the scope of work for this subtask comprised the design, fabrication, and shakedown testing of four facilities that provided unique capabilities to conduct experimental research on hydrate thermochemistry and kinetics in areas directly relevant to methane extraction. These facilities were: (1) a hydrate synthesis system; (2) high pressure calorimeter; (3) benthic pressure chambers to simulate the deep seafloor sediment; and (4) hydrate destabilization and evolved gas measurement apparatus.

The hydrate synthesis system was needed to produce uniform and consistent samples of single- and mixed gas hydrates and hydrate sediment composites for calorimeter studies and destabilization kinetics experiments. The high pressure calorimeter can perform accurate measurements of heat capacity, enthalpies of formation and decomposition of hydrates, and can be used to deduce phase stability regimes. HNEI has substantial expertise in utilizing laboratory benthic chambers to simulate conditions in the deep ocean. The chambers designed for this subtask would be employed to form and decompose hydrates in sediment columns under pressurized seawater. In addition, they would also be used to investigate transport phenomena in the sediment and water phase, incubate seafloor sediment and deep ocean microbes, and test prototype subsea power generation components and systems. Finally, in order to investigate the kinetics of destabilization, a unique facility was developed that allows outgassing rates to be monitored when methane hydrate samples prepared in the synthesis facility are warmed, depressurized, or exposed to various chemical reagents.

Hydrate Microbiology

Methane and other hydrocarbon fuel gases (typically alkanes) found in seafloor hydrates can be derived from thermogenic sources (such as conventional natural gas and oil) or be produced biologically by microbes in the sediment. Most of the methane in hydrates is believed to be the product of methanogenic bacteria.

A large fraction of methane produced in the sediment is intercepted before it enters the water column. This significantly reduces the impact of the enormous seafloor methane source on the ocean environment and on global climate, since methane that escapes from the ocean into the atmosphere is a major greenhouse gas. The mechanism for methane consumption has not been definitively identified, although it is postulated that microbial sinks (methanotrophs) are responsible.

Methane can provide both carbon and energy to the bacteria that constitute the base of the ocean food web. Vigorous chemosynthetic communities have been observed on methane hydrate outcroppings and near methane seeps, suggesting that the local benthic ecosystem will opportunistically exploit methane if it is available.

Understanding microbial methanogenesis and methane consumption has fundamental scientific value with respect to ocean carbon cycling, sediment geochemistry, benthic biology, and global climate change. From a practical perspective, the microbial community in the sediment plays a critical role in producing the methane that will be recovered or utilized for energy as well as in modulating the leakage of methane into the ocean and atmosphere. Methane recovery for energy will likely alter the local flux of methane through the sediment. The response of the microbial community to these changes and the impact on the local benthic ecology will need to be evaluated to respond to questions that will inevitably be raised by environmental groups, and for the preparation of any required Environmental Impact Statements. Furthermore, as discussed in the following section on subsea power generation, the sediment microbial community may be applied to generate low level electricity via a biological fuel cell.

During Years 1 through 3 of the HEET initiative, the scope of work for this subtask on hydrate microbiology comprised developing protocols to characterize the microbial diversity of methane hydrate sediments and to investigate the metabolic pathways and rates of methane generation and consumption; and the application of these protocols to identify key organisms in hydrate sediments.

Molecular biological techniques were utilized to detect methanotrophic/genic bacteria and sulfate reducers. Bacterial cells from collected hydrate sediment pore water samples were harvested by centrifugation and DNA extracted using standard phenol and chloroform. Various primer sets were tested to determine if they were appropriate for the target organisms. PCR and cloning were employed for species identification.

Subsea Power Generation

The development of technologies and systems that can exploit methane hydrates, or the associated free gas (i.e., seafloor seeps) and methane dissolved in sediment pore water, for *in situ* power generation would have a profound impact on fuel logistics and mission constraints for a host of navy operations. In particular, underwater surveillance and monitoring would stand to benefit significantly. The mission duration of thousands of instruments deployed on the seafloor that currently are powered by batteries could be greatly extended. Seafloor methane could also be applied as a source of energy for certain deep submersibles, such as AUVs, allowing them to remain submerged for much longer periods without surfacing to refuel or recharge.

Low-power (on the order of 1 W) microbial fuel cells have been proposed that are based on a consortium of sulfate reducing bacteria and methanotrophs metabolizing sulfate and methane in the upper layer of the sediment. This system may be appropriate for application in locations with limited methane content, to provide long-term power to certain instruments. In regions with methane hydrates or methane seeps, higher power output (10^2 W or larger) may be feasible using PEM, solid oxide, or other types of conventional fuel cells. The performance of these systems is anticipated to depend primarily on the rate, quality, and sustainability of the fuel and oxidizer supply.

At the time the HEET initiative began, a limited number of conceptual studies of microbial fuel cells had recently been performed which suggested that the concept might be feasible. Higher-power seafloor fuel cell systems and submersible refueling/recharging stations based on methane hydrates or seeps had not been explored beyond a few very rudimentary analyses. As a consequence, it was decided that pursuing development of microbial fuel cells for instrument power would be the most effective application of resources in the near term. The scope of work of this subtask during Years 1 through 3 of the HEET initiative therefore focused on experimental studies to determine the potential and limitations of microbial fuel cells in methane hydrate sediments. Higher power systems would be investigated indirectly via efforts of the hydrate thermochemistry and kinetics subtask related to methane extraction.

The specific objectives of the microbial fuel cell experiments were to identify the most probable oxidation reactions that will occur on an anode exposed to the microbial metabolites and identify the bacteria that produce these reactants; quantify important system parameters including exchange current density and charge transfer coefficient; and establish baseline fuel cell power output, potential, and current density.

A host of laboratory bioreactors were constructed utilizing natural sediment collected from a number of different offshore hydrate beds, and naturally-occurring bacteria from these samples were extracted, cultured, and identified using molecular biological techniques. The availability of nutrients was controlled along with the levels of methane and sulfate to establish the effects of these parameters on fuel cell performance. Liquid media was substituted for sediment in tests to determine mass transfer limitations of the system. Cyclic voltammetry and sampled-current voltammetry techniques were employed.

Modeling

Although resources were concentrated on experimental activities, a limited range of complementary modeling activities were undertaken as part of the scope of work of the HEET Methane Hydrates Task. Two topics were investigated: (1) hydrate dissolution in undersaturated water; and (2) production, oxidation, and transport of methane in the oceanic water column. Hydrate dissolution in undersaturated water is directly relevant to certain hydrate destabilization/gas recovery strategies and the behavior of methane in the water column is an important environmental issue. The modeling efforts during Years 1 through 3 were largely analytical; the objective was to develop submodels that could be incorporated into larger numerical codes to evaluate decomposition strategies and assess environmental impacts of methane leakage from the sediment.

Field Studies

The HEET Methane Hydrates Task was conceived as a collaborative effort between HNEI and NRL. NRL has conducted extensive field studies of methane hydrates and a component of the HNEI scope of work was to participate in the NRL research cruises and collect sediment and other samples that could be utilized in our investigations of hydrate thermochemistry and kinetics, microbiology, and subsea power generation. This interaction would also provide opportunities to better integrate the HNEI and NRL programs on methane hydrates and to develop new joint projects.

International Collaboration

With the exception of the Japanese national program, resources for methane hydrate R&D have been relatively modest. International collaboration would better leverage these limited resources and enhance the exchange of information to the mutual benefit of all participants. Toward this end, promoting cooperative research activities was included in the present scope of work and was pursued through the organization of international workshops and by hosting foreign graduate students to participate in the experiments conducted at the University of Hawaii.

3.3. Technical Accomplishments

The principal technical accomplishments of the HEET Methane Hydrates Task for each of the six components identified in the previous section on Scope of Work and Approach are summarized below. Additional details are available in the related papers, presentations, and thesis resulting from this effort (see Section 3.4).

Hydrate Thermochemistry and Kinetics

During Years 1 through 3 of the HEET initiative, accomplishments of this subtask included the design, fabrication, and shakedown testing of four facilities: (1) a hydrate synthesis system; (2) high pressure calorimeter; (3) benthic pressure chambers to simulate the deep seafloor sediment; and (4) hydrate destabilization and evolved gas measurement apparatus. Each of these is described in the following paragraphs.

Hydrate Synthesis System

A facility to synthesize uniform cores of gas hydrates and hydrate-sand or hydrate-sediment composites was developed. Synthesis is based on the technique of Stern *et al.* (2000) which was modified to accommodate the selected equipment. Hydrate cores are produced by filling Teflon

lined cylindrical pressure vessels (High Pressure Products Tubular Series Reactors) with fine ice crystals in the 150 to 500 μm size range. The ice crystals are generated inside a scientific freezer equipped with a glove box by spraying distilled and deionized water onto liquid nitrogen. If composites are desired, then sand or sediment is added to the ice crystals. The pressure vessels are enclosed in a separate scientific freezer that has been modified to allow computer control of the refrigeration compressor to cycle the temperature inside. An automated gas supply system infuses the pressure vessels with high pressure hydrate-forming gas. The mixture of gas and ice (and sand or sediment) is subject to a predetermined pressure-temperature cycle to convert it to hydrate. For methane hydrate, pressures are cycled between about 20 and 30 MPa as temperature slowly varies (approximately 4 K/hour) between about 250 K and 290 K. Temperature control is based on readings from thermistors or thermocouple probes inserted into the pressure vessels through penetration in the removable bottom closures. The facility can produce 2.86 cm o.d. hydrate cores up to 50 cm long. A typical core of these dimensions will contain between 30 and 40 standard liters of methane. A photograph of the pressure vessels inside the freezer is provided in Figure 3-1 below.
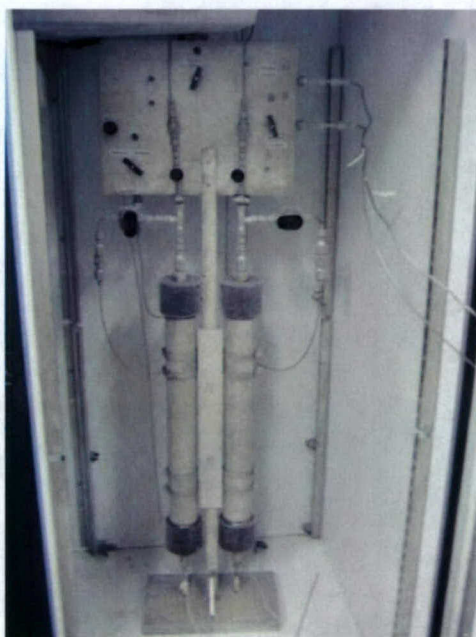

Figure 3-1. Photograph of the hydrate synthesis pressure vessels inside the computer controlled freezer.

N_2, CH_4, and mixed hydrocarbon (CH_4 and C_2H_6) hydrates, and hydrate-sand composites, have been synthesized with the facility. The cores have been tested using Raman spectroscopy (performed by Dr. Shiv Sharma of the Hawaii Institute for Geophysics and Planetology of UH) to confirm that they are hydrates and not ice, and gas content has been measured. These tests have verified the ability of the system to produce uniform hydrate samples. Figure 3-2 provides a representative Raman trace of one of our early synthesized cores. The spectrum indicates the presence of Structure I methane hydrate with methane occupancy in both the large, $5^{12}6^2$, and small, 5^{12}, cages (2899 and 2912 cm^{-1}) as well as ice (3080 cm^{-1}). The Structure I methane hydrate peaks are relatively large compared with the ice peak, indicating a high proportion of

hydrate mixed with some ice. Figure 3-3 is a photograph that was taken when one of the methane hydrate cores was burned.
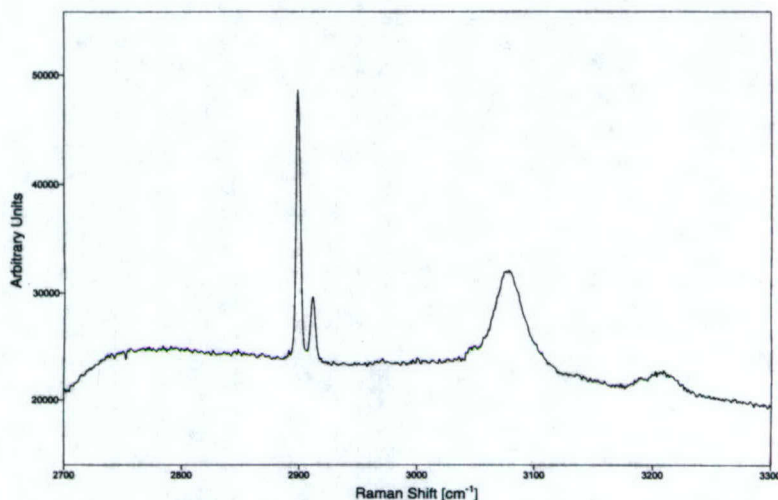

Figure 3-2. Raman spectrum of synthesized methane hydrate core.

Figure 3-3. Photograph of burning methane hydrate core synthesized by the UH facility.

Calorimetery

Differential Scanning Calorimetry (DSC) is commonly used for thermal characterization of physico-chemical transformations. The technique monitors the heat exchange between a sample and its surrounding versus time or temperature. It can be applied in the study of thermodynamics, kinetics or simply as an analytical tool. It has been used to study the composition, dissociation enthalpies and heat capacities of various gas hydrates (Dalmazzone, 2000).

In the case of methane hydrates, measurements need to be performed at relative high pressures and low temperatures. After conducting an extensive screening of commercially available instruments, it was determined that a Calvet-Tien calorimeter produced by Setaram had the appropriate capabilities for our study. The Setaram Model BT2.15 can resolve heat flows as low as 0.10 µW and has rms noise of 0.20 µW. Samples can be maintained at pressures up to 100 bar and temperatures between –196°C and +200°C. A variety of sample cells are available from Setaram to conduct measurements of a wide range of properties including heats of mixing, heat capacity, etc. The sample volume of the BT2.15, ranging up to 12.5 ml for atmospheric pressure cells, is an order of magnitude larger than most micro-DSCs.

The BT2.15 calorimeter was procured in 2003. After some initial problems with high pressure cells, we have begun measuring the dissociation enthalpy of various hydrates including THF, methane, and ethane. Figure 3-4 below is a representative thermogram of the decomposition of THF hydrate. Figure 3-5 on the next page is a thermogram of the formation and decomposition of methane hydrate.
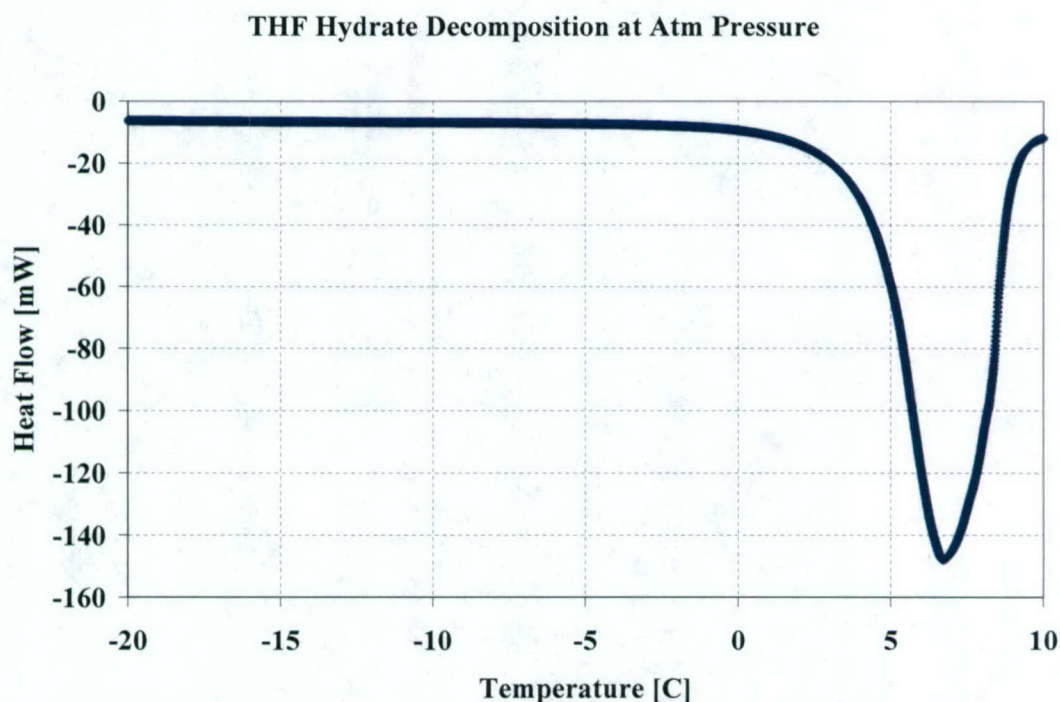
THF Hydrate Decomposition at Atm Pressure

Figure 3-4. Calorimeter thermogram of decomposition of THF hydrate at atmospheric pressure.

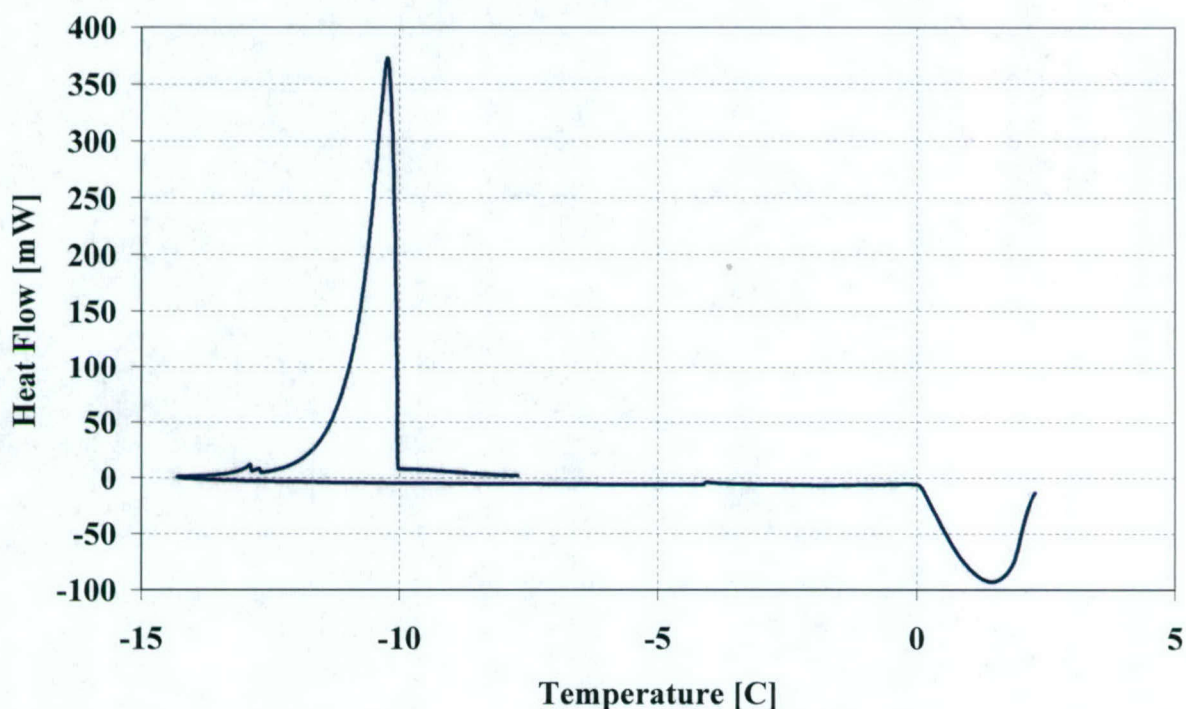## Methane Hydrate Formation and Decomposition

Figure3-5. Calorimeter thermogram of methane hydrate formation and decomposition.

The DSC has also been tested to determine if it is sufficiently sensitive to monitor microbial activity in sediments collected from methane hydrate zones on the Cascadia Margin and the Gulf of Mexico. Figure 3-6 on the next page presents a thermogram of sulfate-reducing bacteria isolated from these sediments and used to inoculate nutrient-rich media contained in a sample cell. The trace is typical of initially dormant bacteria which then give off heat as they utilize the carbon substrate in the medium. As the carbon substrate source is depleted, the bacteria return to their dormant state, and the heat trace returns to the baseline.

The BT2.15 calorimeter will be employed in upcoming hydrate dissociation experiments as well as studies of the metabolism of microbes collected from the seafloor sediment and water column. Investigation of microbial methane oxidation and assimilation will be assigned priority.

In addition to conventional calorimetry, we have recently started work to modify a cell to perform simultaneous spectroscopic measurements. A fiber-optic link to the interior of the cell will allow us to couple an external light source (e.g., laser or lamp) to the sample and also to monitor radiative scattering. This will provide additional information about the state of the sample that can be correlated with the measured energy transfers. The fiber-optic link can also be used to investigate photochemistry. Fabrication and testing is anticipated to be completed by the end of 2005. As a first experiment, we plan to perform Raman measurements as methane and mixed gas hydrates form and decompose.
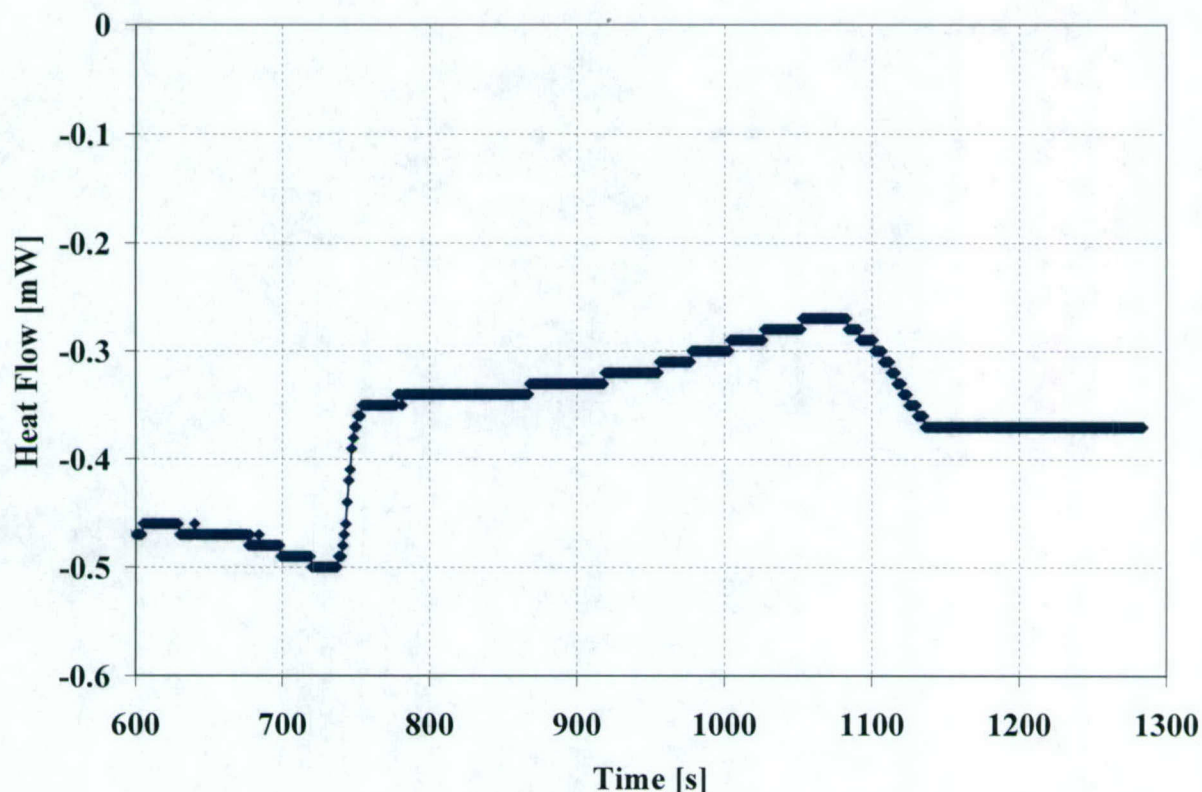
Figure 3-6. Thermogram of microbial metabolism of SRB isolated from methane hydrate sediment.

Benthic Simulators

HNEI previously has employed laboratory benthic simulators to reproduce conditions in the deep ocean to study CO_2 sequestration and deep oil spills, and has developed considerable expertise in the design and operation of these types of facilities. This expertise was leveraged in the present Methane Hydrate Task to produce several new benthic simulators to investigate transport phenomena in the sediment and water phase, incubate seafloor sediment and deep ocean microbes, and test prototype subsea power generation components and systems.

The benthic simulators comprise a pressure chamber, pressurization system, temperature control system, and instrumentation. Figure 3-7 provides a photograph of two new pressure chambers that were designed and fabricated during Years 1 through 3 of HEET. To minimize costs, the chambers are constructed from standard pipe components wherever possible. Most chambers we currently employ consist of a section of schedule 80, nominal 6 inch, 316 stainless steel pipe with bolted end flanges. The larger chamber shown in the photograph was fabricated from nominal 12 inch pipe to provide a larger volume to test subsea power system components. Most chambers are approximately 1 m in height and can be stacked to extend the length of the sediment or water columns. ¾ inch NPT threadolets are welded at multiple points along the axis of the pipe to provide internal access for instruments, windows, or liquid or gas injections and sample extraction. The pressure chambers are surface treated and passivated after welding and the interiors are Teflon coated to provide an inert environment for biological investigations. All

chambers are ASME certified for continuous operation at 1500 psig, equivalent to conditions at about 1,000 m depth in the ocean. HNEI has designed similar chambers for methane hydrate studies at NRL and the National Energy Technology Laboratory of the Department of Energy.
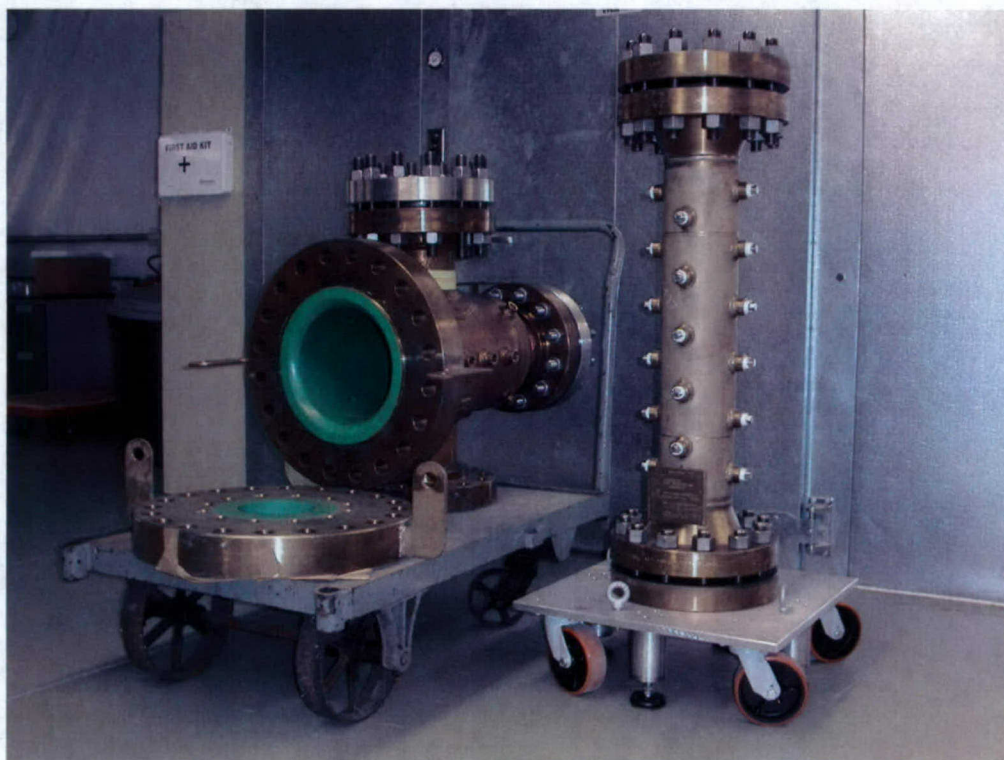

Figure 3-7. Photograph of benthic simulator pressure chambers.

The benthic simulators can be pressurized with water and/or gas, depending on the application. A large inventory of pressurization systems are available from previous HNEI research programs. A walk-in refrigerator has been installed in the Hawaii Fuel Cell Test Facility to provide temperature control. The pressure chambers can be placed inside the refrigerator to attain the low temperatures characteristic of the deep ocean. If finer control is required, then the chambers can be fully immersed into large temperature-regulated liquid baths.

One of the new simulators was put into service during Year 3 as a component of the new hydrate destabilization facility described below. A second simulator will be employed for microbial incubations in Year 4.

Hydrate Destabilization

Several methods to extract gas from hydrates for energy have been proposed: depressurization, thermal stimulation, and inhibitor injection. These schemes are all based on the *in-situ* dissociation of hydrates into gas and water. In order to develop such methods safely and economically, it is necessary to understand the underlying physical phenomena as well as possible. Of particular importance are the kinetics of methane hydrate decomposition, since any practical exploitation of hydrate resources would depend on the basic time scales of the process.

For given thermodynamic conditions, there exists a fundamental intrinsic rate of hydrate decomposition, a speed limit of sorts imposed by molecular constraints (e.g., activation energy). Clarke and Bishnoi (2001) recently provided updated measurements of intrinsic rates for methane hydrates. In most cases, however, whether in the laboratory or *in situ*, heat and mass transfer tend to limit the extent of hydrate decomposition. Such a complex problem requires both careful experimental investigation and thorough analytical modeling (for a basic description of modeling approaches see, for example, Gao, 2004). Jamaluddin *et al.* (1989) provided an early analysis of complete dissociation kinetics in a simple one-dimensional context.

The rapid depressurization of hydrate samples, to ambient pressures of one to a few atmospheres, has been well studied in the laboratory (e.g., Circone *et al.*, 2000a; Komai *et al.*, 2004). It not only represents a possible means of exploiting hydrate resources (which could be accomplished by drawing off gas from beneath the hydrate stability zone in sediments), but the avoidance of high pressures does facilitate experimental procedures. On the other hand, very low pressures (e.g., 200 Pa) have been used to examine the effect of heat, provided as radiation, on hydrate dissociation kinetics (Ullerich *et al.*, 1987). Recently, Sakamoto *et al.* (2004) investigated methane hydrate decomposition by the heat stimulation method in a high-pressure cell. Liberated methane was monitored with a flow meter as it was discharged from the cell through a back-pressure regulator. High pressures of a few tens of atmospheres are more representative of *in situ* conditions that would prevail for hydrates embedded in marine sediments.

It is well known that inhibitors such as methanol and glycol may cause the decomposition of gas hydrates by shifting their thermodynamic-equilibrium curve (Englezos *et al.*, 2001; Svartas and Fadnes, 1992). Only a few studies to date have reported the effects of inhibitor concentration and injection rate on hydrate dissociation kinetics (e.g., Sira *et al.*, 1990). In order to develop viable engineering systems to extract methane from hydrates, particularly for unconventional subsea applications, additional data on inhibitor-induced decomposition are desirable since this would allow quantitative comparison of the merits and risks of the three destabilization approaches (i.e., heating, depressurization, and inhibitors). Toward this end, a unique experimental facility was developed in which the liberated methane gas exhausts freely into a reservoir at the same pressure as the hydrate sample to minimize artifacts of any pressure let-down devices (e.g., throttling valves or regulators) in the gas flow train. To account for mass and heat transport effects that arise as the destabilization front moves away from the inhibitor injection point (and liquid inhibitor accumulates and is diluted by the released water from the hydrate), a model of the process also was developed for comparison with the data.

In addition to studies of inhibitor-induced decomposition, the new facility can also be used to investigate a wide range of thermal and pressure destabilization phenomena at hydrate temperatures and pressures characteristic of the deep ocean sediment.

Figure 3-8 presents a schematic diagram of the experimental apparatus used to destabilize hydrate samples. Hydrate or hydrate-sand composites are prepared in the synthesis facility described previously. The cylindrical synthesis cell was modified to include a coaxial injector inserted through a compression fitting in the top closure (end cap). The injector delivers liquid reagent through a central tube and gas is infused (during synthesis) or flows out of the cell (during destabilization) through the annulus between the outer and inner tubes. A single point thermistor probe or a multipoint thermocouple probe (Sandelius, Inc.) with nine junctions evenly spaced at 5 cm intervals along the probe axis is inserted through a penetration in the bottom closure to monitor temperatures inside the cell. The multipoint probe allows measurement of the

temperature gradient along the decomposing hydrate core due to local release of the heat of fusion at the destabilization front that moves progressively away from the liquid injection point. The entire cell is enclosed within a computer-controlled freezer which allows selection of operating temperature; the cell can also be immersed in an open tank in the freezer containing liquid circulated through a constant temperature bath unit if additional control is required. Pure methane gas from the synthesis supply cylinders is infused in the cell to set the pressure at the start of the experiment. Pressure in the cell is monitored continuously with a pressure transducer ($\leq \pm 1.3$ psi/9000 Pa accuracy).
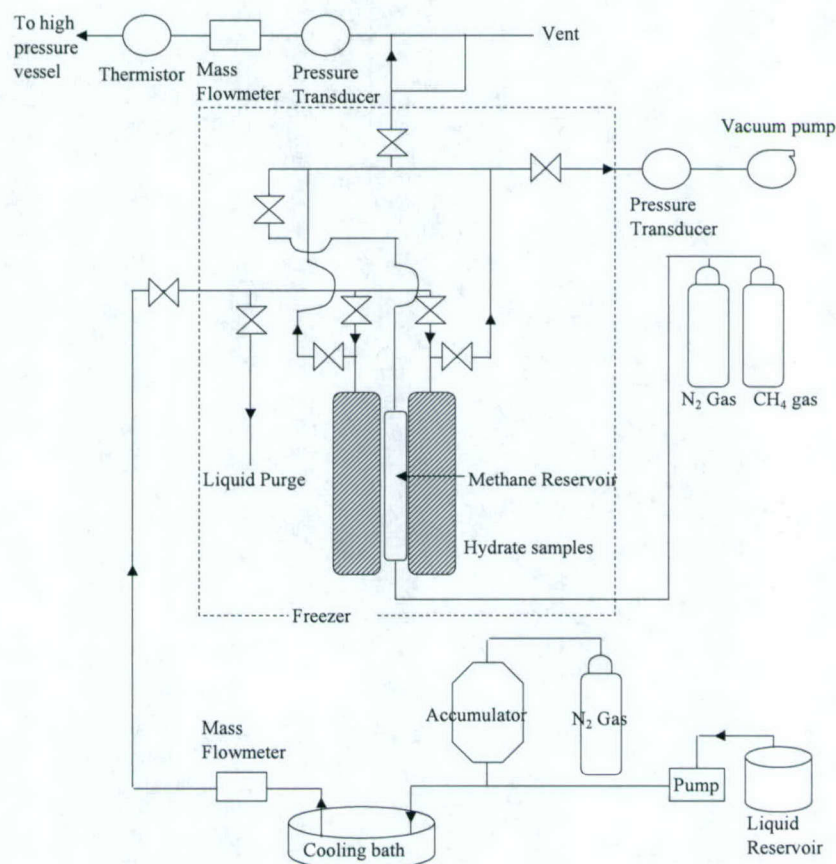

Figure 3-8. Schematic drawing of the hydrate destabilization apparatus.

Liquid reagents are stored in a bladder accumulator reservoir that maintains an essentially constant supply pressure. Flow rate is controlled with a metering valve and is monitored with a coriolis flow meter (AW Company) with better than $\pm 0.5\%$ (of measurement) accuracy. The temperature of the liquid is adjusted in a heat exchanger comprising a long coil of tubing immersed in a constant temperature bath.

Figure 3-9 presents a schematic diagram of the system used to monitor gas evolution rates from the destabilizing hydrate cores. This represents the main point of departure from previous investigations. Gas liberated from the hydrate flows freely into a large pressure vessel containing a custom-built flow meter based on the principle of the Torricelli tube. Circone *et al.* (2000b) employed a similar instrument to conduct studies of pressure destabilization. In that

investigation, hydrates were exposed to room pressure and allowed to decompose. Evolved gas was monitored by directing it into the ambient pressure Torricelli tube flow meter. In order to study hydrate destabilization occurring at elevated pressures characteristic of deep marine sediments, our flow meter is housed in a pressure vessel that is maintained at essentially the same pressure as the decomposing hydrate sample. The internal diameter of this vessel is 146 cm, and its length is 105 cm. The vessel is rated for continuous operation at 10.3 MPa (about the pressure equivalent of 1,000 m depth in the ocean), which is lower than the rating of the synthesis cell (about 40 MPa) and, hence, establishes the upper pressure limit of the experiments. It is equipped with multiple penetrations along its axis and end flanges which are fitted with windows and instruments and used for material addition and extraction. A photograph of the assembly is provided in Figure 3-10.
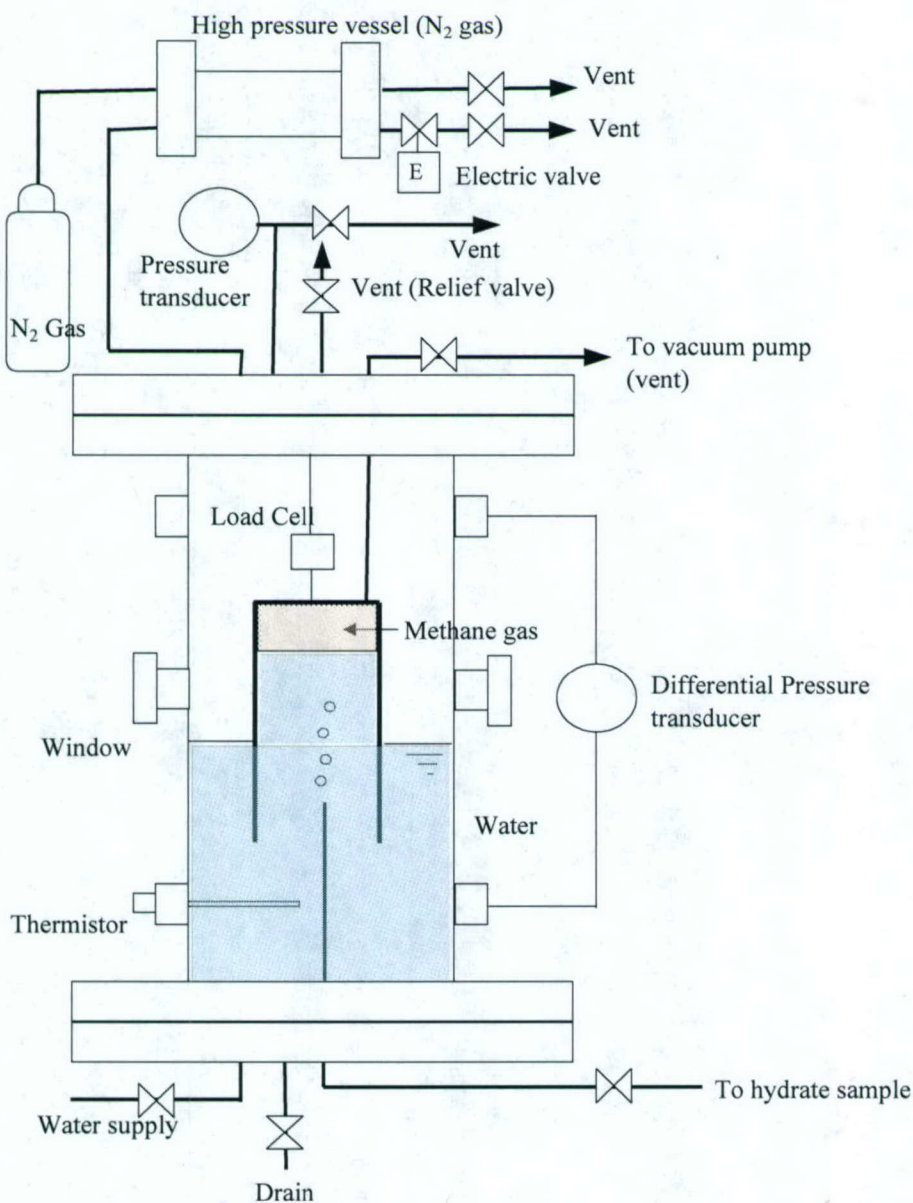
Figure 3-9. Schematic diagram of the system to measure gas evolution rates.
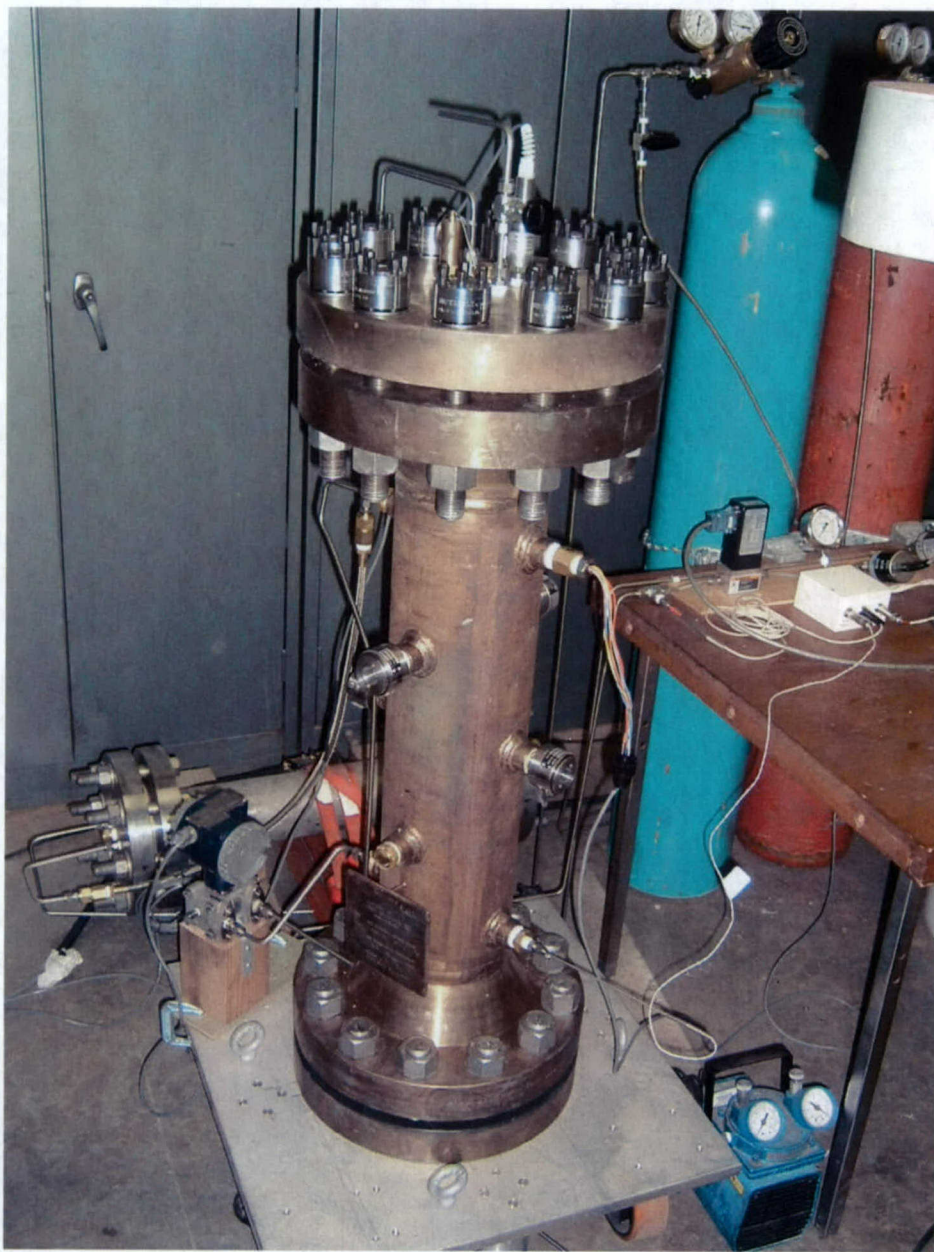
Figure 3-10. Photograph of the assembled system.

Pressure in the vessel is set by charging the space above the water used for the Torricelli tube with N_2 or Ar gas. Once the pressure in the entire system (hydrate cell and pressure vessel) is balanced, the plug valve in the evolved gas line is opened, allowing gas to flow from the hydrate cell into the pressure vessel as it is released by destabilization. As this gas displaces water in the inverted cup (which is initially drawn up above the surrounding water level with a vacuum pump) the suspended load cell (Transducer Techniques model MDB-10) connected to the cup measures the change in the weight of the water column, so that the volume of evolved gas may be calculated. The displaced water causes the water level in the vessel to rise and this is exploited to provide a check on the load cell data by means of the differential pressure transducer shown in Figures 3-9 and 3-10. Note that a process controller is employed to vent the inert gas

from the vessel through an electronic valve to maintain constant pressure as the rising water level compresses the gas. A third redundant measurement of the methane evolution rate is provided by an in-line thermal mass flow meter (shown in Figure 3-8). Although the flow meter introduces a small back-pressuring of the hydrate cell (estimated to be less than 0.007 MPa for the flow rates in these experiments), it is insensitive to dissolution of methane gas into the water in the pressure vessel, which can affect the Torricelli tube and water level measurements. The amount of dissolved methane is estimated by collecting a pressurized water sample at the end of an experiment through one of the side ports and analyzing the amount of methane contained in this sample.

The digital time histories of liquid temperature and injection rate; temperature gradient along the decomposing hydrate core; methane evolution rate; and system pressure are analyzed to obtain destabilization kinetics information.

Initial shakedown experiments that were recently completed indicate that the facility and instrumentation are operating well. Pressures across the system could be held well within ± 1% of the selected operating point over extended periods. The three independent measurements of evolved gas flow rate agreed well. Injection of both warm water and methanol solutions were performed. Minor problems were detected with the liquid flow (injection) control system and the coriolis meter, which are currently being resolved.

A full suite of destabilization experiments are planned during the second half of 2005.

Hydrate Microbiology

Extensive trial-and-error testing was performed to determine protocols to identify, isolate, and culture the key microbes that produce and consume methane in the seafloor sediment. Protocols were found that could successfully identify methanogens, methanotrophs, and sulfate-reducing bacteria (SRB). SRB isolates and cultures were relatively easy to produce. Isolating and culturing methanogen and methanotrophs has been a major challenge due, in part, to the apparently slow growth rates of these microbes and other factors that remain unclear. Work continues on developing appropriate procedures to culture methanogens and methanotrophs.

Initial molecular biological studies have indicated the presence of methanogenic *archaea* and the existence of methanotrophic bacteria in samples collected from the Blake Ridge and Cascadia Margin (Figure 3-11).

DNA was extracted at various points along the length of a geochemically active piston core recovered from the Gulf of Mexico. These samples currently are in the process of being utilized for molecular analysis with the primers described in Table 3-1. Sediment from the same core was used to inoculate vials of various types of sterilized growth media and incubated to attempt to isolate methanogenic *archaea*, methanotrophic bacteria and sulfate-reducing organisms.

Molecular work also is being performed on an active push core that has been characterized by fatty acid analysis.
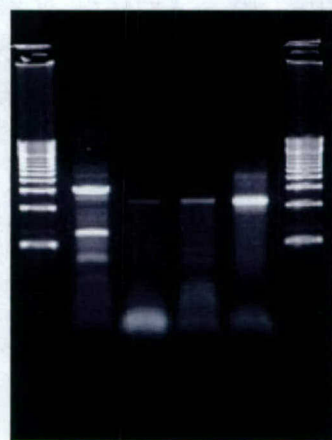
Figure 3-11a   Figure 3-11b

Figure 3-11. PCR amplification using (a) Methanogenic archaeal primers,
146F/1324R; (b) Methanotroph primers, A189/mb661 (pMMO).
Lanes 1,6-DNA ladder, lane 20positive control, lane 3-Blake Ridge
sample, lane 4-Cascadia sample, lane 5-wastewater sample.

Table 3-1. PCR (polymerase chain reaction) primers used to analyze microbes in hydrate sediment.

Target	Primer	Reference
Universal Bacteria	27F / 1492R	Lane, 1991
Methanotroph type I	MethT1dF / MethT1bR	Wise, 1999
Methanotroph type II	27F / MetT2R	Wise, 1999
Methanotroph pMMO	A189 / mb661	Bourne, 2001
Methanogen	146F / 1324R	Marchesi, 2001
Sulfate-Reducing Bacteria	dsr1F / dsr4R	Karkhoff-Schweizer, 1995
Bacteria DGGE	b341GC / b758	Juck, 2000
Archea DGGE (nested)	PRA46F / PREA1100R PARCH340F / PARCH519R	Ovreas, 1997
Methanotroph type I DGGE	MethT1dF / MethT1bRGC	Wise, 1999 (modified)
Methanotroph type II DGGE	27FGC / 1492R	Wise, 1999 (modified)
Methanogen DGGE	146FGC / 1324R	Marchesi, 2001 (modified)
SRB DGGE	dsr1FGC / dsr4R	Karkhoff-Schweizer, 1995 (modified)

Effective protocols were identified to culture and analyze SRBs and were applied extensively in the investigation of microbial fuel cells described in the following section on Subsea Power Generation. To ensure viability, airtight vials containing Bactosulfate API broth, a liquid enrichment media, were inoculated with sediment samples immediately after collection, onboard the research vessels. A modified form of the media with the ammonium sulfate substituted for the ferrous component was also used. The composition of the Bactosulfate API broth is given in Table 3-2. Media components were filter sterilized. Inoculated media cultures were allowed to

grow for the duration of the research cruise. All cultures showed visual signs of sulfide production in the form of iron sulfide, a black precipitate. After transfer to the University of Hawaii, the cultures were used to inoculate fresh media, which was incubated at 37°C. After three generations these samples were genetically sequenced to identify the microbial species.

Table 3-2. Composition of Bactosulfate API Broth and the substitute media.

Component	Formula	Concentration, mg/L
Yeast Extract		1000
Ascorbic Acid	$C_6H_8O_6$	100
Sodium Lactate	$C_3H_5NaO_3$	5200
Magnesium sulfate heptahydrate	$MgSO_47H_2O$	410
Potassium Phosphate, dibasic	K_2HPO_4	100
Ferrous Ammonium Sulfate hexahydrate	$Fe(NH_4)_2(SO_4)_26H_2O$	140
*Ammonium Sulfate	$NH_4 SO_4$	200
Sodium Chlorate	$NaClO_3$	5000

*Ammonium sulfate component used to make the modified media

PCR techniques were used to identify bacteria in cultures producing sulfide that had been inoculated with the methane hydrate sediment samples. The bacterial cultures were sampled to obtain cell material for DNA analysis. 10 mL of one culture was centrifuged at 6,000 RPM to collect a solid cell pellet from which DNA was extracted with a soil extraction kit (MoBio). The DNA was serially diluted in ultrapure distilled, deionized and sterilized water, and used for the PCR reaction. The ribosomal DNA was amplified for 30 cycles (95° C for 1 min. denaturation, 55° C for 30 seconds annealing, and 72° C for 1 min. extension) using the universal primers 27F (5'–AGAGTTTGATCMTGGCTCAG-3') and 1492R (5'–TACGGYTACCTTGTTACGACTT-3') (Weisburg et al., 1991) and Invitrogen dNTPs and Taq polymerase. An approximately 1460 bp segment of the 16S rRNA gene was amplified. The PCR products were separated by electrophoresis on a 1.0% agarose gel and stained with ethidium bromide to confirm that the target gene was indeed amplified. Optimized conditions for the PCR cycle were utilized; however, nonspecific amplification could not be prevented. The target PCR product was purified by gel excision from a 1.0% agarose gel and extracted using a MoBio™ gel purification kit.

Fresh PCR product was used for cloning with an Invitrogen™ TOPO TA cloning kit and TOP10 cells. The transformation procedure was performed using the manufacturer's rapid protocol. Selective blue and white colony screening was performed on Luria Broth (10 g Bacto-Tryptone, 10 g Bacto-Yeast, 10 g NaCl, and 15 g agar pH 7.0 per liter) plates containing 50 µg ml-1 ampicillin and 40 mg ml-1 X-gal (40 µl spread on 37° C pre-warmed plates before inoculation), after incubation overnight at 37° C. Twenty of the picked colonies were incubated with a controlled temperature shaker overnight in 1.0 ml liquid LB media containing 50 µg ml-1 ampicillin at 37° C. *Escherichia coli* cells were collected by centrifugation. Plasmid DNA was extracted using a Quiagen™ Qiaprep spin mini prep kit. Plasmid DNA was serially diluted and

then amplified using the 16S primers and procedure previously described. Sequencing was performed on the gel purified product using an automated sequencer and primer 27F. Sequencing resulted in data for approximately 500 bps. The obtained sequences were aligned with those in the Ribosome Database Project by using BLAST (Altschul, 1990).

Subsea Power Generation

The primary accomplishment of this subtask was the completion of an experimental study to determine the potential and limitations of microbial fuel cells in methane hydrate sediments.

In areas of the deep ocean where hydrates are found, there is an abundance of methane which can serve as a source of carbon and energy to a microbial assemblage. In conventional fuel cells, methane is not used directly but needs to be converted to hydrogen via a high temperature catalytic reforming process. In microbial fuel cells, this reforming would be performed by a consortium of anaerobic bacteria which would metabolize the methane and other components of the sediment to produce chemical species that could be oxidized at low temperature on the fuel cell electrode. Such a microbial fuel cell could supply long-term power that may be used to replace batteries for seafloor instrumentation.

The specific objectives of this study were to demonstrate feasibility of the microbial fuel cell concept applied to representative methane hydrate sediment and the indigenous bacterial ensemble residing in this sediment; identify the most probable oxidation reactions that will occur on an anode exposed to the microbial metabolites and identify the bacteria that produce these reactants; quantify important system parameters including exchange current density and charge transfer coefficient; and establish baseline fuel cell power output, potential, and current density.

A host of bioreactors were designed and fabricated for this study, and were loaded with autoclaved synthetic seawater and sediment collected from methane hydrate zones on the Cascadia Margin, Blake Ridge, and the Gulf of Mexico to simulate the sediment-water interface on the ocean floor. Other bioreactors substituted liquid growth media inoculated with bacteria from the sediment samples for the sediment. During the tests, methane and other carbon sources and nutrients could be added to the bacterial cultures in the sediment and liquid media as a supplement, and oxygen or air could be bubbled into the seawater. Figures 3-12 and 3-13 present drawings and photographs of the bioreactors used in the experiments.

Cyclic voltammetry tests performed with graphite electrodes immersed in cultures of sediment bacteria from the Gulf of Mexico growing on Bactosulfate API media and a modified version of this media identified several oxidation peaks in curves of current vs. potential. The most probable reaction appears to be the oxidation of hydrogen sulfide to elemental sulfur with two electrons donated to electrode. At higher potentials, iron sulfide may also be oxidized. Linear potential scans of a graphite electrode immersed in oxygenated synthetic seawater suggest that oxygen reduction to water dominates the cathode reactions. The peak current observed for oxygen reduction was about 10 times the peak current observed for sulfide oxidation (20 mA versus less than 2 mA), suggesting that sulfide oxidation at the anode will be the current limiting electrode reaction in the microbial fuel cell.
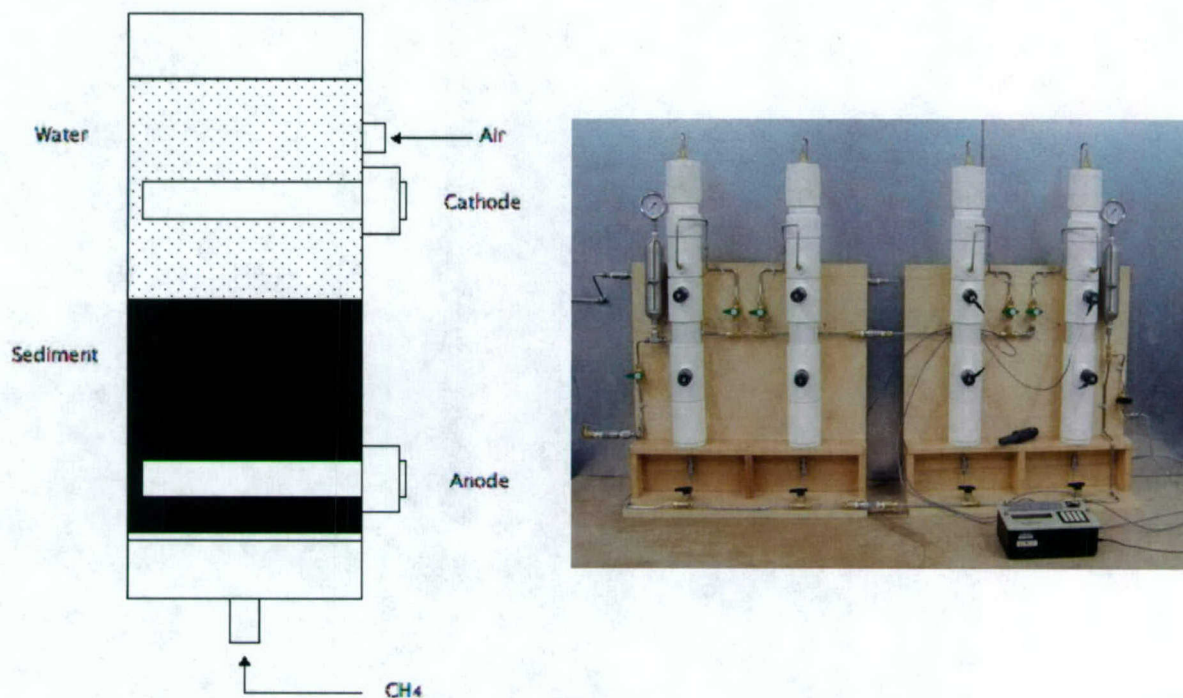
Figure 3-12. Drawing and photograph of bioreactor for testing two-electrode fuel cells in marine sediment and seawater.
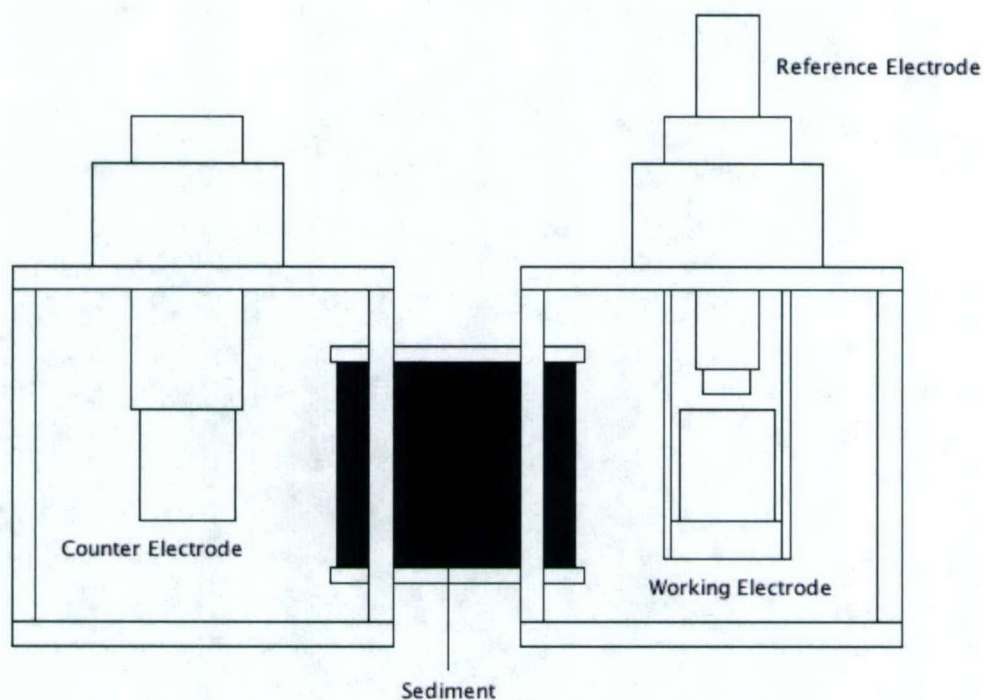

Figure 3-13. Two-compartment reactor joined by a 4 cm tube of sediment that was used in fuel cell and voltammetry experiments. The Plexiglas compartments are typically filled with liquid growth media inoculated with bacteria.

PCR amplified DNA sequences of sulfate-reducing bacteria from the genus *Desulfotomaculum* were found in anaerobic cultures inoculated with fresh sediment samples from the Gulf of Mexico. These microbes are the likely source of the sulfide metabolites that were oxidized on the fuel cell anode in the present study and are potentially one of the bacteria participating in the postulated anaerobic methane oxidation process.

Graphite fuel cells operated in synthetic seawater and sediment samples taken from the Gulf of Mexico confirmed the ability to exploit the indigenous microbial ensemble to generate electricity. In short-term fuel cell discharge experiments, sulfide generated from nutrients contained in the sediment reacted on the sediment electrode to produce a maximum power density of 10.3 mW/m^2. Addition of Bactosulfate API enrichment media containing lactate as the primary carbon source did not increase the power generated by the fuel cell, yielding 9.1 mW/m^2. These values of power density are comparable to the 10 mW/m^2 recorded for fuel cells deployed in estuarine sediment (Reimers *et al.*, 2001).

A graphite electrode fuel cell was also implemented using a liquid culture of sulfate-reducing bacteria in place of sediment and synthetic seawater separated from the liquid culture by a 4 cm diameter by 7 cm length tube filled with Gulf of Mexico sediment. The maximum power density of this fuel cell was 17.5 mW/m^2, which was 70% greater than in fuel cells where the anode was inserted directly into the sediment. Representative data are shown in Figures 3-14 and 3-15. The difference in power was due to increased current densities that can be supported by this system. Sulfide diffusion to the anode, where it is oxidized and donates two electrons to the fuel cell circuit, was enhanced by the significantly larger flux area of the liquid compared to the sediment pore water. These results demonstrate the importance of mass transport on the performance of seafloor sediment fuel cells.
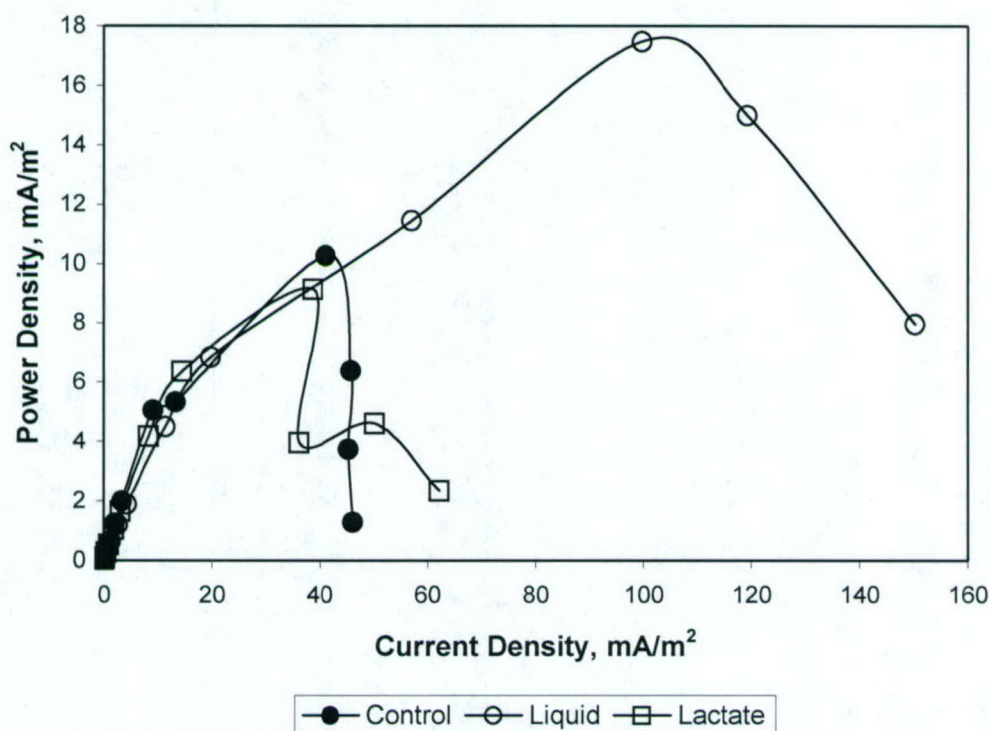

Figure 3-14. Power density vs. current density for the microbial fuel cells.
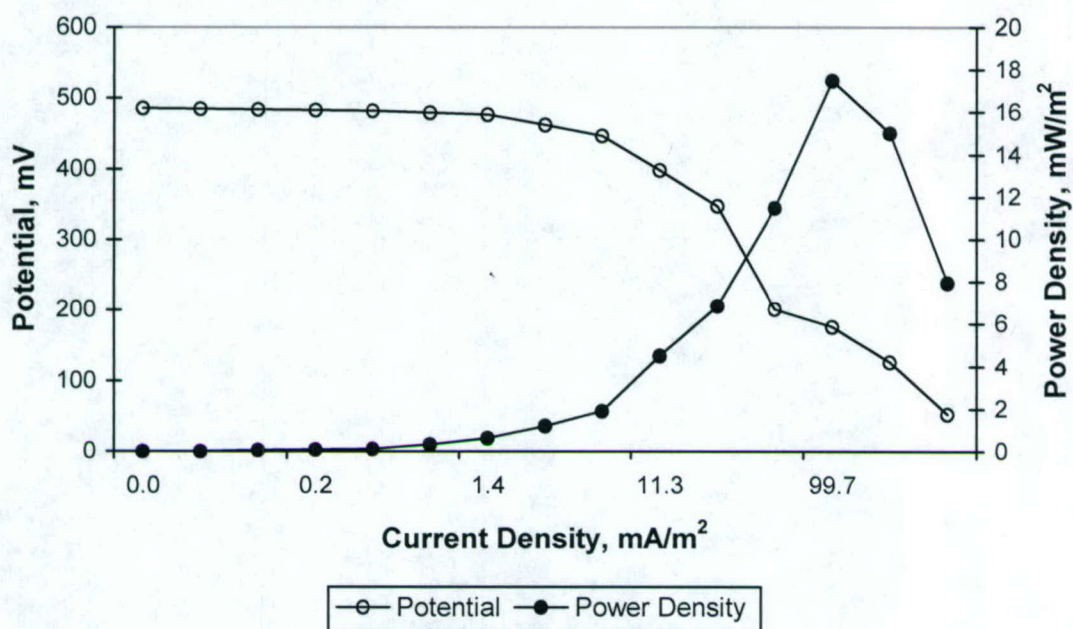
Figure 3-15. Potential and power density of a fuel cell operating in a liquid culture of sulfate-reducing bacteria separated from seawater by a tube of sediment.

Tafel plots of the fuel cell current-voltage data were employed to estimate the values of the exchange current density and charge transfer coefficient. The charge transfer coefficient was 0.98. The average value of the exchange current density was 5.75 mA/m^2. A typical Tafel plot is shown in Figure 3-16.

Figure 3-16. Tafel plot of current discharge from a laboratory fuel cell operating in Gulf of Mexico marine sediment.

The maximum power generation of about 0.01 W/m^2 observed in these tests implies that graphite electrodes with about 100 m^2 of external surf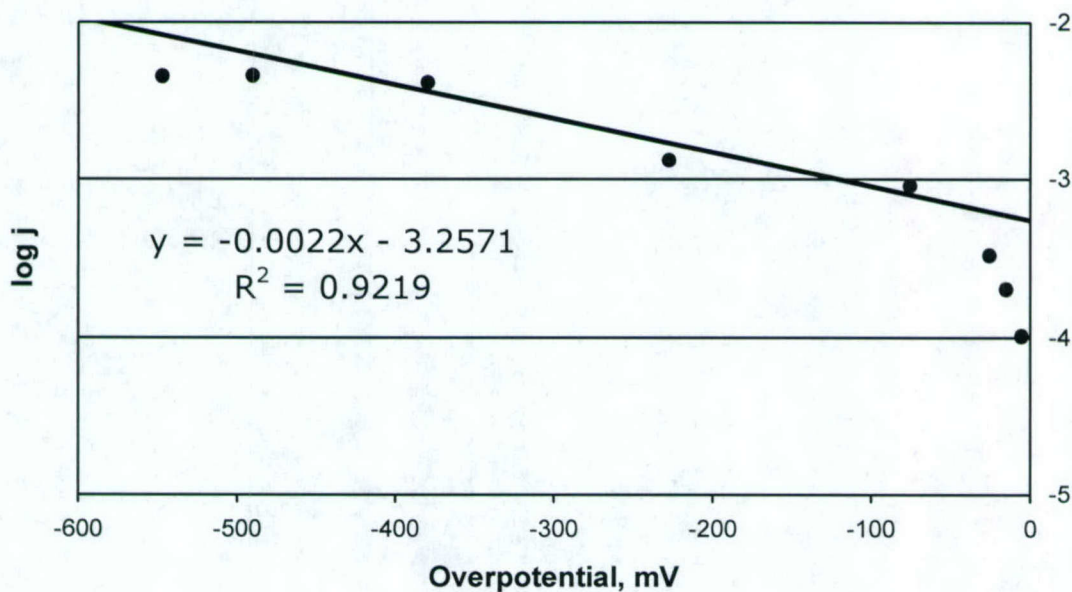ace area would be needed to produce 1 W of power, assuming that scaling effects are linear. A fuel cell with electrodes of this size is probably not feasible due to difficulties in deployment and the costs of the materials per unit of power generated. Significant technical breakthroughs are needed to increase current to a level required to realistically attain the target power.

While the open circuit potential of the fuel cell is fixed by the available reactants, potential drop during current flow can be decreased through improvements in sulfide transfer to the anode and proton transfer from the anode to the cathode. Introduction of artificial components such as immobilized biofilms on the anode and isolated electrolyte connecting the electrodes has the potential to substantially decrease voltage losses.

In conclusion, this investigation demonstrates the high probability that a sulfide/oxygen microbial fuel cell that previously has been successfully tested in estuarine sediment, can generate electricity in deep ocean sediments identified as methane hydrate sites. For short-term operation, the availability of methane is not required for power production. Prolonged power generation may, however, be limited by methane availability since there is evidence in the literature that a symbiotic oxidation of methane by *archea* or other species affects the vitality of the sulfate reducing bacteria, which produce the sulfide metabolites that are key to fuel cell operation. Further research appears to be warranted to determine the role that methane plays in the performance of the microbial fuel cell.

Modeling

A range of modeling activities were undertaken during Years 1 through 3, primarily to support and to complement the experimental work. As an example, a one-dimensional model was developed that considered heat and mass transfer effects from liquid reagents sprayed on the top of a cylindrical hydrate core to interpret gas evolution data from the destabilization experiments. Two of the modeling activities conducted to date have resulted in stand-alone publications and are described below.

Methane in the Oceanic Water Column

This effort was pursued to understand the behavior of methane in the oceanic water column. As a first step, a one dimensional model of transport, production, and oxidation of methane was devised and compared with concentration data from the literature. The rationale here was that, once verified, this simple model could be incorporated into a larger numerical code (e.g., OGCM) to investigate strong, localized leakage of methane from the seafloor that could occur as a result of inadvertent or purposeful destabilization of hydrates.

Measurements have indicated a consistent and widespread supersaturation of the surface ocean with methane relative to the atmosphere, and a substantial decline in dissolved methane with depth. As a result, the oceans are a net source of methane into the atmosphere. Since potential methanogenic processes in seawater are known to be anaerobic, an explanation for methane production in the oxygenated upper layer of the ocean has puzzled scientists. A credible theory rests on the existence of anaerobic microniches. Karl and Tilbrook (1994) and Tilbrook and Karl (1995) suggested that the most likely site for *in situ* methane generation are zooplankton guts, where high rates of oxygen consumption would promote methanogenesis. They also favored the

diffusive loss pathway from egested particulate matter to the water column as the most probable, while not excluding other mechanisms like particle disaggregation.

A one-dimensional advective-diffusion model to predict methane concentrations as a function of depth was developed which assumed particulate origin of surface methane. A constant eddy diffusion coefficient was considered below the mixed layer; vertical advection was either constant upwards, or varying with depth. Variable vertical advection rates allowed the representation of Ekman pumping (upper layer downwelling) and subduction.

As shown in Figure 3-17, the solution of the particulate problem provided a good match with available data, using model parameters that fell within expected orders of magnitude. The particulate methane production region appeared to be quite shallow (approximately 30 m thick), and well within the mixed layer. This would indicate that most particulate methane is transferred to the water column and to the atmosphere quite rapidly, with little effect on oceanic methane concentration profiles below the mixed layer.
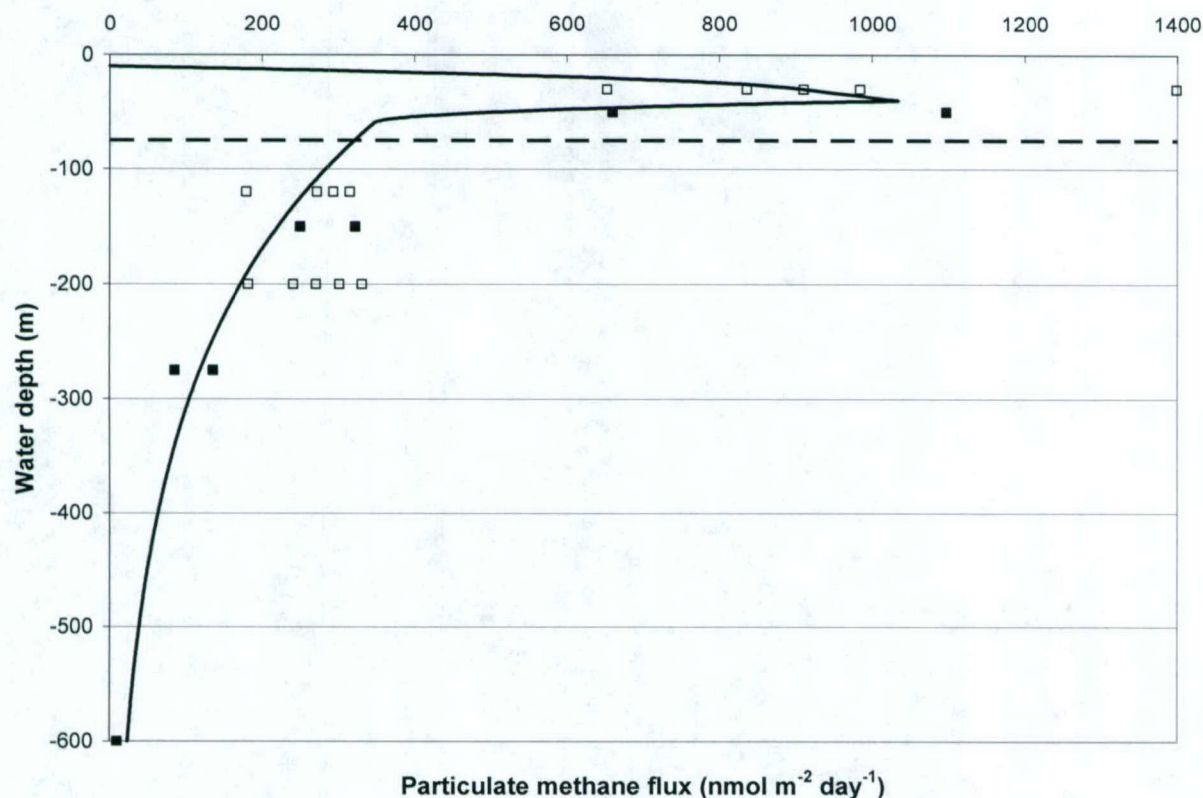
Figure 3-17. Particulate methane flux predictions (solid line) and data from Karl and Tilbrook (1994) and Tilbrook and Karl (1995) at Stations ADIOS (open squares) and VERTEX 4 (filled squares).

Even with the escape of most methane to the atmosphere, the water-column source proved to be quite strong below the mixed layer. Without methane oxidation, vertical advection rates that provided a good match with the data of Holmes *et al.* (2000) were always much larger than expected. As seen in Figure 3-18, the inclusion of first-order methane oxidation resolved this

problem, although oxidation rates reported in the literature seem exceedingly small with turnover times of several decades. The relative importance of methane oxidation stems from the considerable weakening of the available methane source, initially of particulate origin, below the mixed layer. Model details and predictions are included in the upcoming publication.
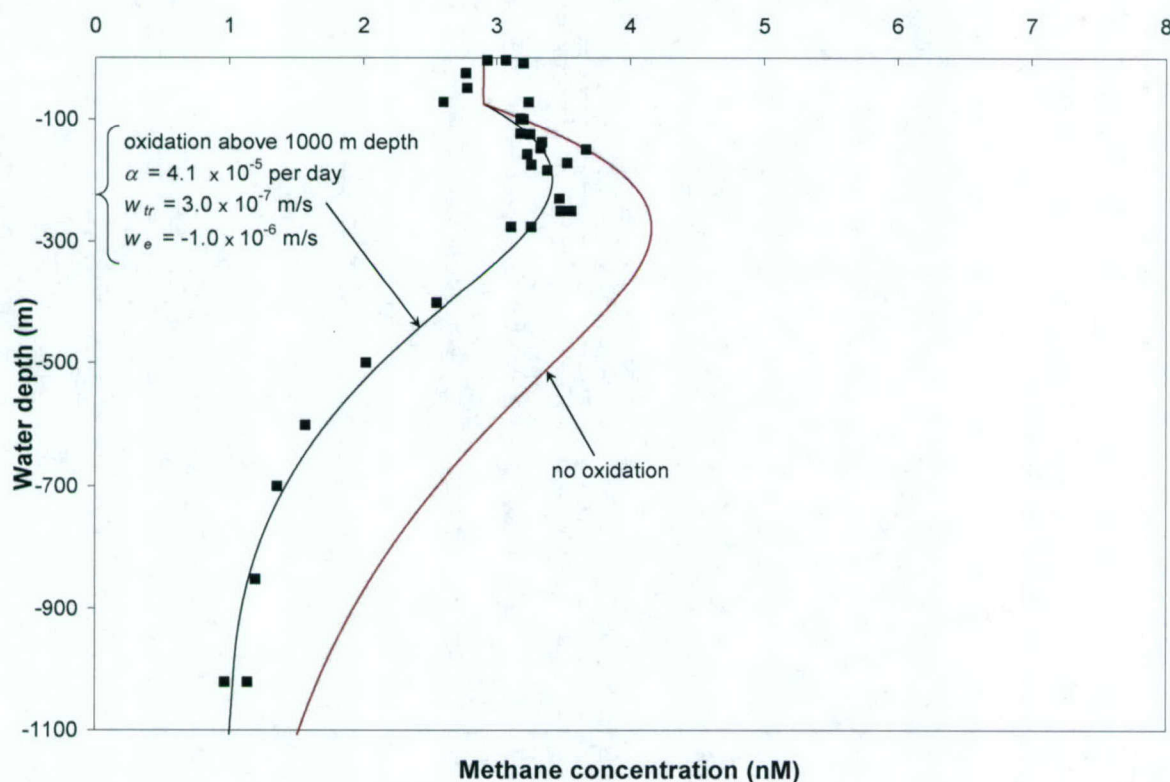

The chart contains the following labels:
- X-axis (top): 0, 1, 2, 3, 4, 5, 6, 7, 8
- Y-axis: Water depth (m): -100, -300, -500, -700, -900, -1100
- X-axis (bottom): Methane concentration (nM)
- Annotation: oxidation above 1000 m depth
- $\alpha = 4.1 \times 10^{-5}$ per day
- $w_{tr} = 3.0 \times 10^{-7}$ m/s
- $w_e = -1.0 \times 10^{-6}$ m/s
- no oxidation

Figure 3-18.   Influence of methane oxidation on methane concentration profiles (vertical advection rate at top of abyssal layer = 3.0×10^{-7} m/s).   October 1996 data (■ ; Holmes *et al.*, 2000) plotted for comparison.

In summary, the modeling protocol confirmed that methane of particulate origin is sufficient to explain observed methane open-ocean profiles and ocean-atmosphere fluxes. It also highlighted the significance of methane oxidation. Further model development is possible, for example by considering variable diffusion coefficients. Work is underway to extend the results to simulate the evolution of methane from a strong localized source on the seafloor.

Hydrate Dissolution in Undersaturated Water

Hydrate exposed to water that is not fully saturated with the hydrate-forming gas (e.g., methane) has been observed to decompose, even if the pressure and temperature falls within the stability regime. The fundamental thermodynamics of this effect have not, to date, been definitively addressed and are directly relevant to practical gas recovery scenarios and certain environmental issues.

Kim *et al.* (1987) introduced the concept of intrinsic decomposition rate to represent the breakdown of hydrate particles within a reaction-desorption layer at the solid-fluid boundary. In

a series of carefully designed experiments, Clarke and Bishnoi (2000, 2001, 2004, and 2005) were able to measure intrinsic hydrate decomposition and formation rates for different guest molecules (methane, ethane and carbon dioxide).

In this effort, the formalism describing the dissociation kinetics of hydrates as an intrinsic reaction was extended to cases when hydrates are immersed in undersaturated water. The model is based on the fact that two-phase equilibrium then governs hydrate dissociation, with the concentration of the hydrate-forming species in water playing a key role in providing the necessary fugacity gradient, beside temperature and pressure: in other words, and unlike instances of three-phase equilibrium, neither heating nor depressurization is necessary to trigger hydrate decomposition. Details of the mathematical development are provided in the manuscript.

An application of the model to the methane hydrate data of Rehder *et al*. (2003) established that the desorption layer itself should be undersaturated for hydrate dissolution to proceed (when pressure and temperature do not vary). This result contrasts with the current assumption of a saturated desorption layer. When applied to CO_2 hydrate data, however, the model suggested that the activation energy for hydrate decomposition measured by Clarke and Bishnoi (2004) for pressures corresponding to gaseous CO_2 may be excessive at higher pressures.

The results of this analysis have been incorporated into the code developed to interpret data from our hydrate destabilization experiments.

Field Studies

During Years 1 through 3, HNEI researchers and students participated in three NRL research cruises to offshore methane hydrate fields. In order to promote education and training under this grant for the next generation of hydrate researchers, Post Doctoral scholars and students were afforded preference. The participants included Mr. Ryan Kurasaki (graduate student), Dr. Thomas Gorgas (Post Doctoral scholar), and Dr. Brandon Yoza (Post Doctoral scholar). One cruise in July 2002 was conducted on the Blake Ridge located in the Atlantic Ocean about 400 km east from Charleston, South Carolina. The other two cruises took place in August 2003 and May 2004 on the Texas-Louisiana shelf in the Gulf of Mexico. Detailed reports are available from NRL. Seismic profiling and piston coring were performed during these cruises. Sediment and microbial samples were collected for subsequent testing at the University of Hawaii. Additional samples were obtained from the Cascadia Margin in the Pacific Ocean by NRL and transferred to the University of Hawaii.

International Collaboration

Through March 2005, three international workshops were organized by HNEI in cooperation with NRL and ONR GLOBAL, and two foreign graduate students were hosted by the University of Hawaii, to promote international R&D collaboration on methane hydrates. The first workshop was held in Honolulu, Hawaii on March 7-9, 2001. ONR GLOBAL and the National Energy Technology Laboratory of the Department of Energy provided additional funding support. Fifty-eight participants from the U.S., Japan, Korea, Canada, Norway, Russia, and the United Kingdom attended the workshop. Attendees included leading researchers in methane hydrates, and representatives from government agencies and the private sector.

The principal workshop objectives were: (1) review past, ongoing, and planned methane hydrate R&D projects and programs; (2) share information on budgets and research resources and priorities in different countries; and (3) establish linkages for domestic and international partnering. The program of the 2-1/2 day workshop included plenary lectures, panel discussions, small group breakout meetings, and a poster session. It was conducted as a working event where all participants conferred to develop a roadmap for future collaborative studies of methane hydrates. The workshop report is available online at:
http://www.hnei.hawaii.edu/Fiery_Ice_Wkshp.pdf

The second and third workshops followed a typical symposium format and included technical presentations and posters. The workshops were held in October 2002 and November 2004 in Washington, D.C. and Vina del Mar, Chile, respectively. Attendance increased to about 100 persons at the second workshop, but fell back to about 60 in Chile, probably due to the relatively remote venue. Among other achievements, the workshops served as catalysts for a joint exploratory research cruise off Chile and a planned joint investigation in 2006 on the Hikurangi Margin offshore New Zealand.

During Years 1 through 3, two foreign graduate students joined HNEI as visiting scholars to conduct research on methane hydrates. Between September 2003 and March 2004, Mr. Jose Lobos, a chemical engineering student from the Catholic University of Valparaiso in Chile, worked with HNEI staff and students to investigate hydrate dissociation kinetics. Mr. Lobos was supported by a grant from the ONR GLOBAL Visiting Scholar Program. He played a major role in the design of the evolved gas measurement apparatus.

Following the departure of Mr. Lobos, Ms. Kana Kuroda, an M.S. student from the Department of Marine System Engineering of Osaka Prefecture University in Japan joined HNEI to continue development of the hydrate dissociation experimental facility. Ms. Kuroda conducted joint research at HNEI from May 2004 through February 2005. She was sponsored by her university at no cost to the present grant. Ms. Kuroda is the first author of the paper on hydrate dissociation that was presented at the ISOPE 2005 conference in Seoul, Korea.

3.4. Summary of Papers and Presentations Resulting from Efforts

R&D conducted as part of the HEET Methane Hydrates Task has produced the following thesis, papers, and presentations.

THESIS

Kurasaki, R., "Investigation of a Biological Fuel Cell in Methane Hydrate Marine Sediment," M.S. Thesis, Bioengineering, Department of Molecular Biosciences and Bioengineering, University of Hawaii, December 2004.

PAPERS

Nihous, G.C. and S.M. Masutani, "Theoretical Considerations Concerning the Dissolution Rate of Gas Hydrates in Undersaturated Water," submitted to *Chem. Eng. Sci.*, June 2005, under review.

Nihous, G.C. and S.M. Masutani, "A Model of Methane Concentration Profiles in the Open Ocean," submitted to *Global Biogeochem. Cycles*, February 2005, under revision.

Masutani, S.M., "Greenhouse Gas Hydrates in the Ocean," in <u>Carbon Dioxide Utilization for Global Sustainability</u>, (S.E. Park, J.S. Chang, and K.W. Lee, eds.), pp. 487-494, Elsevier Science, 2005.

Masutani, S.M. and R.B. Coffin, "Laboratory and Field Studies of Marine Methane Hydrates," in <u>Proc. 5th International Symposium on CO_2 Fixation and Efficient Utilization of Energy</u>, pp. 78-82, Tokyo Institute of Technology, Tokyo, Japan, 2002.

Uchida, T., J.A. Ripmeester, S.M. Masutani, and E.D. Sloan, Jr., "Database on Hydrate Properties: Influence of Kinetic and Thermodynamic Parameters on Formation and Stability," in <u>Proc. 4th International Conference on Gas Hydrates</u>, 2002.

PRESENTATIONS

Kuroda, K., S.M. Masutani, and G.C. Nihous, "Laboratory Experiments to Investigate Hydrate Destabilization," accepted for presentation at ISOPE 2005, Seoul, Korea, 19-24 June 2005.

S.M. Masutani and R.B. Coffin, "Methane Hydrates," invited talk presented at the International Mechanical Engineering Congress and R&D Expo, Anaheim, California, November 2004.

Kurasaki, R.J., B.A. Yoza, and S.M. Masutani, "Benthic Methane Fuel Cells," presented at the 32nd International Geological Congress, Florence, Italy, August 2004.

3.5 References

Bourne, D.G., I.R. McDonald, and J.C. Murrell, "Comparison of pmoA PCR primer sets as tools for investigating methanotroph diversity in three Danish soils," *App. Environ. Microbiol.*, **67**(9), 3802-3809, 2001.

Circone, S., Stern, L.A., Kirby, S.H., Pinkston, J.C., and W.B. Durham, "Methane hydrate dissociation rates at 0.1 MPa and temperatures above 272 K," *New York Academy of Science*, 544-555, 2000a.

Circone, S., Kirby, S.H., Pinkston, J.C., and L.A. Stern, "Measurement of gas yield and flow rates using a custom flowmeter," *Rev Sci Instruments*, **72**(6), 2709-2716, 2000b.

Clarke, M. and P.R. Bishnoi, "Determination of the intrinsic rate of ethane gas hydrate decomposition," *Chem. Eng. Sci.*, **55**, 4869-4883, 2000.

Clarke, M. and P.R. Bishnoi, "Determination of the activation energy and intrinsic rate constant of methane gas hydrate decomposition," *Canadian Journal of Chemical Engineering*, **79**, 143-147, 2001.

Clarke, M. and P.R. Bishnoi, "Determination of the intrinsic rate constant and activation energy of CO_2 gas hydrate decomposition using in-situ particle size analysis," *Chem. Eng. Sci.*, **59**, 2983-2993, 2004.

Clarke, M. and P.R. Bishnoi, "Determination of the intrinsic kinetics of CO_2 gas hydrate formation using in-situ particle size analysis," *Chem. Eng. Sci.*, **60**, 695-709, 2005.

Englezos, P., Huang, Z., and P.R. Bishnoi, "Prediction of natural gas hydrate formation conditions in the presence of methanol using the Trebble-Bishnoi equation of state," *J Canadian Petr. Tech.*, **30**(2), 148-155, 1991.

Gao, S., "The decomposition of gas hydrates," http://www.owlnet.rice.edu/~sqgao/c602.pdf, 24 p., 2004.

Holmes, M.E., F.J. Sansone, T.M. Rust, and B.N. Popp, "Methane production, consumption, and air-sea exchange in the open ocean: An evaluation based on carbon isotopic ratios," *Global Biogeochem. Cycles*, **14**(1), 1-10, 2000.

Jamaluddin, A.K.M., Kalogerakis, N., and P.R. Bishnoi, "Modelling of decomposition of a synthetic core of methane gas hydrate by coupling intrinsic kinetics with heat transfer rates," *Canadian J Chem. Eng.*, **67**, 948-954, 1989.

Karl, D.M. and B.D. Tilbrook, "Production and transport of methane in oceanic particulate organic matter," *Nature*, **368**, 732-734, 1994.

Kim, H.C., Bishnoi, P.R., Heidemann, R.A., and S.S.H. Rizvi, "Kinetics of methane hydrate decomposition," *Chem. Eng. Sci.*, **42**, 1645-1653, 1987.

Komai, T., Kang, S.P., Yoon, J.H., Yamamoto, Y., and T. Kawamura, "In situ raman spectroscopy investigation of the dissociation of methane hydrate at temperatures just below the ice point," *J Phys. Chem.*, **108**, 8062-8068, 2004.

Marchesi, J.R., A.J. Weightman, B.A. Cragg, R.J. Parkes, and J.C. Fry, "Methanogen and bacterial diversity and distribution in deep gas hydrate sediments from the Cascadia Margin as revealed by 16S rRNA molecular analysis," *FEMS Microbiol. Ecol.*, **34**, 221-228, 2001.

Rehder, G., Kirby, S.H., Durham, W.B., Stern, L.A., Peltzer, E.T., Pinkston, J., and P.G. Brewer, "Dissolution rates of pure methane hydrate and carbon-dioxide hydrate in undersaturated seawater at 1000-m depth," *Geochimica et Cosmologica Acta*, **68**(2), 285-292, 2004.

Reimers, C.E., Tender, L.M., Fertig, S., and W. Wang, "Harvesting energy from the marine sediment-water interface," *Environ. Sci. Techno.*, **35**,192-195, 2001.

Sakamoto, Y., Komai, K., Kawabe, Y., Tenma, N., and T. Yamaguchi, "Gas hydrate extraction from marine sediments by heat stimulation method," *Proc 14th Int. Offshore Polar Eng. Conf.*, ISOPE, Toulon, Vol. 1, 52-55, 2004.

Sharma, G.D., Kamath, V.A., and S.L. Patil, "Natural gas hydrate resources of the Alaskan arctic and their recovery potential," *Proc 2nd Int. Offshore Polar Eng. Conf.*, ISOPE, San Francisco, Vol. 1, 652-659, 1992.

Sira, J.H., Patil, S.L., and V.A. Kamath,. "Study of hydrate dissociation by methanol and glycol injection," *Proc 65th Ann. Tech. Conf. Exh. Soc. Petr. Eng.*, SPE 20770, 977-984, 1990.

Stern, L.A., Kirby, S. H., Durham, W. B., Circone, S., and W.F. Waite, "Laboratory synthesis of pure methane hydrate suitable for measurement of physical properties and decomposition behavior," *In* Max, M.D. (ed.) Natural gas hydrate in oceanic and permafrost environments. Kluwer Academic Publishers, Netherlands, 245-261, 2000.

Svartas, T.M. and F.H. Fadnes, "Methane hydrate equilibrium data for the methane-water-methanol system up to 500 bars," *Proc 2nd Int. Offshore Polar Eng. Conf.*, ISOPE, San Francisco, Vol. 1, 614-619, 1992.

Tilbrook, B.D. and D.M. Karl, "Methane sources, distributions and sinks from California coastal waters to the oligotrophic north Pacific gyre," *Marine Chem.*, **49**, 51-64, 1995.

Ullerich, J.W., Selim, M.S., and E.D. Sloan, Jr., "Theory and measurement of hydrate dissociation," *AIChE J*, **33**(5), 747-752, 1987.

Wise, M.G., J.V. Mcarthur, and L.J. Shimkets, "Methanotroph diversity in landfill soil: Isolation of novel type I and type II methanotrophs whose presence was suggested by culture independent 16S ribosomal DNA analysis," *App.Eviron. Microbiol.*, **65**(11), 4887-4897, 1989.

4. The Hawaii Fuel Cell Test Facility

4.1. Objectives

The objective of this portion of the HEET program was to develop a state of the art test facility to evaluate fuel cell technologies for Navy applications. The focus of facility activities under this agreement was on performance and durability testing of fuel cells and components, development of cooperative testing programs with industry and government, and assessment of the effects of fuels contaminants on fuel cell performance.

This facility was designated the Hawaii Fuel Cell Test Facility (HFCTF). In addition to fuel cell testing, the facility houses portions of the facilities used for the methane hydrates task (Section 3).

The facility has served as a site for outreach to U.S. Navy personnel and the training of graduate students of the University of Hawaii. Visitors from academic institutions, businesses and the local community are also invited to tour the facility.

4.2. Scope of Work and Approach

The work conducted under this program included site selection and leasing, facility planning and design, contracting and construction, dedication and initiation of test operations. State and local permits were secured and applicable building and safety regulations and codes were followed to assure the construction and operation of a safe facility.

Three test stands were purchased from project partner, UTC Fuel Cells. These full-scale, single-cell test stands were installed and commissioned, and are in operation testing cells from various fuel cell manufacturers. In addition to providing test stands, UTC Fuel Cells provided pre-tested, full-scale fuel cells and test protocols that enabled the facility to begin productive testing with minimal delay.

The facility can support an additional five to seven test stands. Two subscale test stands for characterization of the effects of fuel and air contaminants, along with a test stand for Hardware-in-Loop testing and one for evaluation of fuel cell stacks, are being installed under follow-on funding.

The facility infrastructure includes a Stuart Energy electrolyser, Barnstead de-ionized water maker, oiless scroll air compressor and purification system, a hydrogen storage and distribution system, nitrogen, oxygen, carbon dioxide, carbon monoxide, and compressed air supply system, a Varian 3800 Gas Chromatograph, a Hewlett Packard GC - Mass Spectrometer, a cooling water loop, calibration instruments and tools, and nine workstations and related work benches, tools, materials and supplies.

In parallel with construction and installation of facility hardware, facility operations manuals and test protocols have been developed for safe operation and gas/fluids analysis. Functional PC models for operation of the test stands have been programmed, which allow researchers and operators to visually track each test function and parameter in real time.

The facility currently houses five full time research personnel. Additional staff will be added as needed. Facility staff are working closely with personnel from the Naval Undersea Warfare Center Keyport Pacific Detachment (NUWC) to develop documentation, protocols and procedures that will enable the facility to be in compliance with ISO 17025 requirements for

management, testing and calibration test procedures and quality standards, and fuel cell testing for the U.S. Navy.

The facility has also been the site of educational and outreach seminars for personnel from the U.S. Navy, Air Force, and Coast Guard. Facility personnel have conducted numerous tours for representatives from government, academic institutions and the local community.

The facility is managed by the Hawaii Natural Energy Institute (HNEI) at the University of Hawaii. Figure 4-1 shows the founding partners of this facility. Three full-scale fuel cell test stands were purchased by HNEI from UTC Fuels Cells Division of United Technologies. UTC Fuel Cells supplied pre-tested fuel cells and testing protocols, and facility safety system design criteria and guidelines. Hawaiian Electric Company (HECO) provided the site, site improvements and utility hook-ups, and 24-hour security for the facility at minimal cost to the project. The U.S. Navy's Office of Naval Research has provided the program funding.

Figure 4-1. Founding partners.

The highlights of work accomplished during the past three years include:

- Facility siting, design and construction.
- Installation of test stands, instrumentation, and associated support equipment.
- Four long-term (2000-hr) fuel cell tests to characterize fuel cell durability.
- Demonstration of accelerated fuel cell degradation protocols.
- Development and documentation of testing protocols and safe operating procedures.

Figure 4-2 presents a drawing of the overall site layout, showing the various fuel cell testing and methane hydrates project elements. Elaboration of the aforementioned accomplishments are summarized in the following section of this report.

4.3. HFCTF Planning, Design and Construction

Initial planning for the test facility was begun in the fall of 2001, with occupancy beginning in December of 2002. The development of the test facility represented a coordinated effort of experienced staff members at HNEI, UH Facilities Office, UTC Fuel Cells, HECO, the project architect and construction contractors. In August of 2004, the facility received the Project Outstanding Meritorious Award from the Hawaii Section of the American Society of Mechanical Engineers.
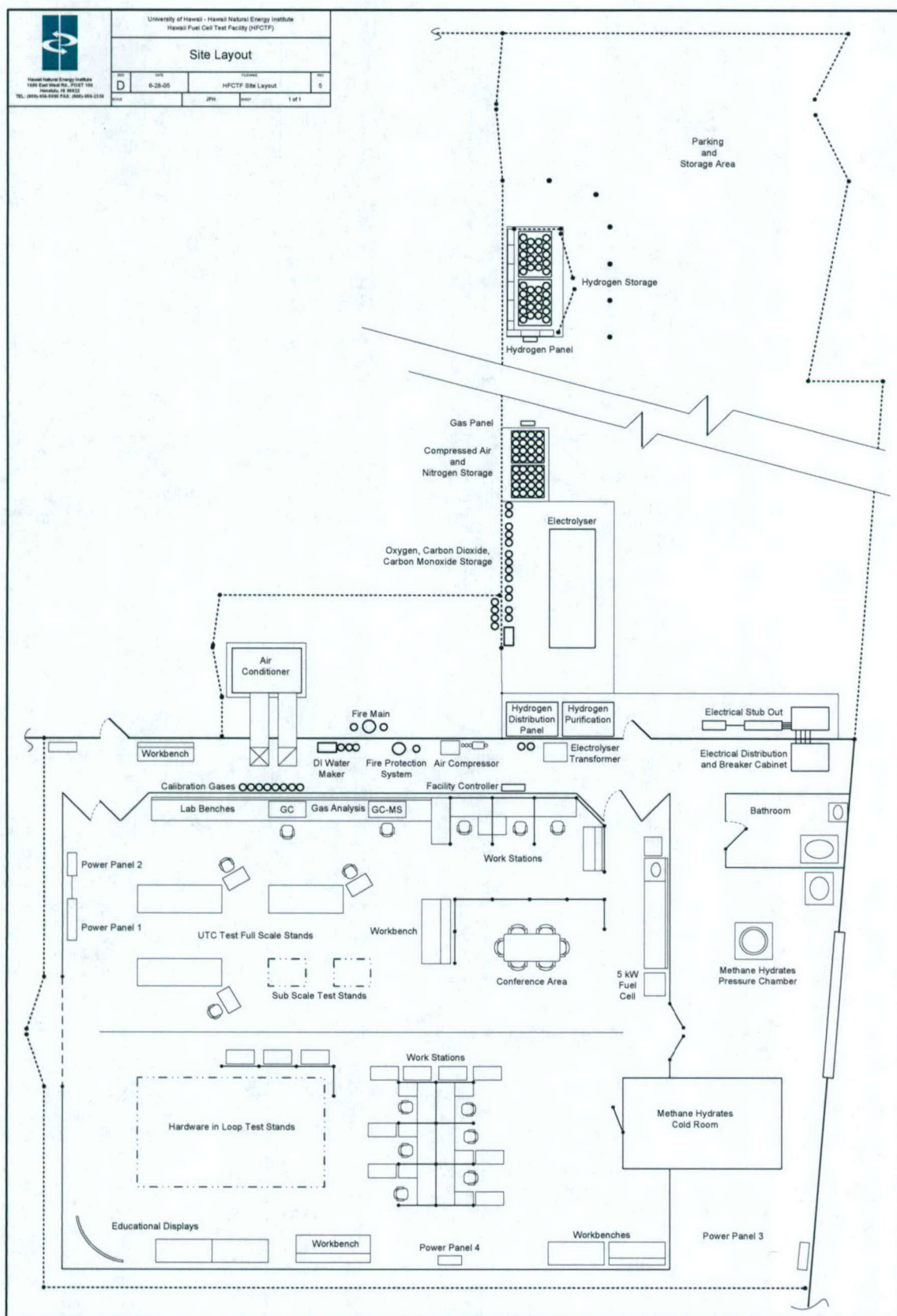
Figure 4-2. Overall site layout drawing

4.3.1. Site Selection

In the fall of 2001, over 20 potential sites were investigated, including ones at the University of Hawaii, U.S. Navy – Pearl Harbor, and commercial buildings in the Honolulu area. Project partner Hawaii Electric Company (HECO) was also contacted and it offered space in one of its warehouses located in downtown Honolulu, approximately five miles from the University of Hawaii at Manoa campus. The HECO site was selected based on meeting the overall program objectives. The site has 24-hour security provided by HECO's security staff. The site was leased from HECO in December 2001 at a nominal annual rate.

4.3.2. Permitting

With the assistance of a local architectural firm, several informational and pre-permit briefings were held with state and local agencies during the summer of 2002. In these meetings, HNEI project plans, conceptual drawings, building and fire code considerations were reviewed. This was followed by submission of contractor design drawings to the City and County of Honolulu, in mid October 2002. The building permit was issued on December 2, 2002 and construction commenced immediately. Final completion of construction approval was issued on April 20, 2003, roughly six (6) months from the submission of the project construction plans.

HECO is a regulated public utility. Use of their property and expenditures made by HECO required approval by the Hawaii Public Utilities Commission (PUC). The required use request, lease documents and proposed site improvements were submitted to the PUC in January 2002, with final approval granted in May 2002.

4.3.3. Contracting

Early in 2002, a request for proposal (RFP) was prepared and issued for the detailed design of the facility. Unfortunately, all of the bids submitted were beyond the funding HNEI had budgeted for the project, so alternative approaches were explored. An alternative design-and-build RFP also met with bids well beyond the amount of funding available for the project.

As a result, an agreement was negotiated allowing HNEI to provide project management services and substantial support to the prime construction contractor. The electrical, mechanical, and fire protection construction elements were bid as separate contracts. HNEI, with the assistance of UTC Fuel Cells, HECO and the prime contractor, prepared basic specifications, schematic drawings, and RFPs for each of the construction areas. With the assistance of the University's Facilities Planning and Management Office, the architect, and HNEI staff, contractors for each construction area were selected and contracted during the months of June, July and August 2002. HNEI elected to design and construct the gas and fluid delivery systems itself.

The facility was designed, constructed, permitted and dedicated over a nine (9) month period beginning with contracting the construction and ending with final completion approval by the City and County of Honolulu on April 20, 2003. The overall cost (less HNEI labor), including construction of the gas and fluid storage and supply systems, was $450,000. HECO also contributed approximately $440,000 in site improvements and warehouse upgrades at no cost to the project.

4.3.4 Design

As discussed in earlier paragraphs, the design of the facility involved a number of experienced persons at UTC Fuel Cells, HECO, UH Facilities Planning, the project architect, contractors, equipment and gas suppliers, and HNEI. In light of the emerging nature of hydrogen research and limited published information available on facility design, considerable time and effort was expended to employ conservative safety margins in the design.

In response to the concern of installing permanent and costly wall and ceiling renovations in a leased warehouse, HNEI elected to install a portable, tension-membrane (Sprung) structure inside the warehouse, following a "building inside a building" approach as shown on Figure 4-3. This internal structure was installed at a cost of $65,000, paid for by the University of Hawaii. The flexibility of this building permits the staff to make timely changes and modifications with minimal costs and disruption to ongoing work.
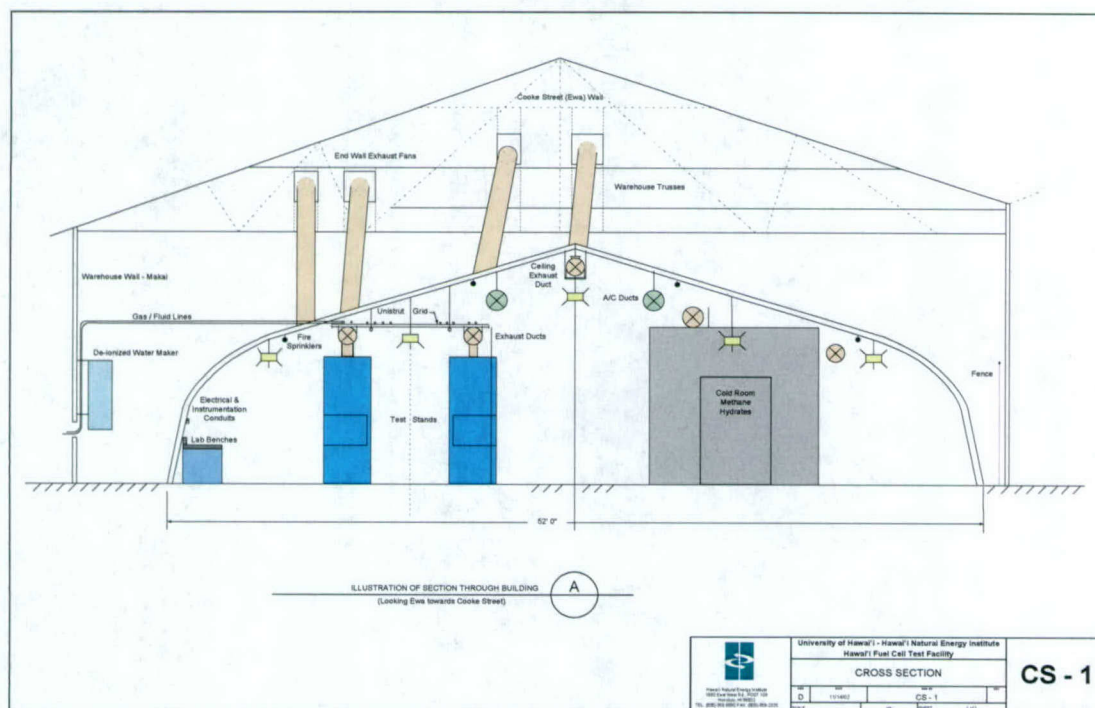

Figure 4-3. Cross section of facility.

HNEI designs and specifications call for stainless steel tubing, Swagelok fittings and valves that are compatible with fuel cell testing. The as-built floor plan pictured in Figure 4-4 illustrates the layout of equipment and test stands in the test facility.

In August 2004, the facility was honored to receive the Outstanding Project Meritorious Award from the Hawaii Section of the American Society of Mechanical Engineers (ASME) -- see Figure 4-5. The award is given to mechanical engineering type projects or designs in Hawaii, Guam and American Samoa that have been completed in the past five years.
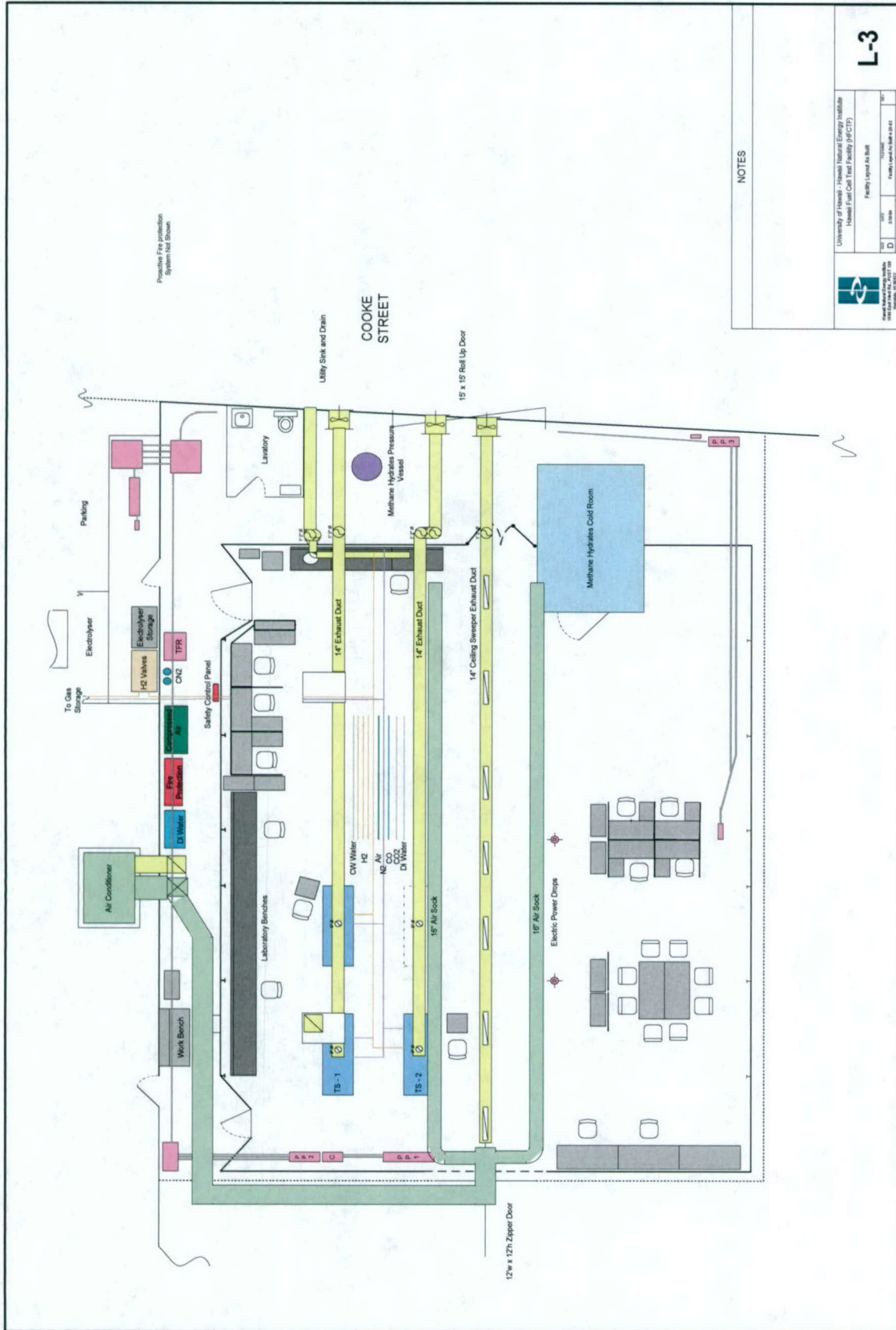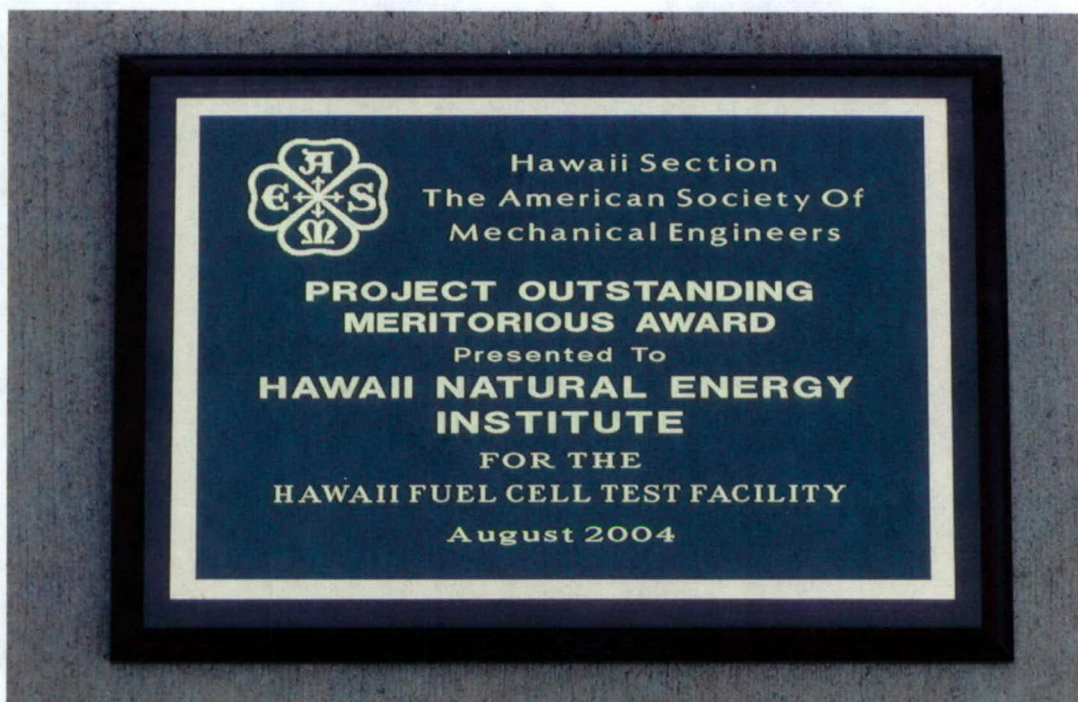
Figure 4-4. Facility floor plan.

Figure 4-5. ASME award.

Electrical   Conceptual and schematic level designs for the facility electrical system were prepared as part of the RFP documents and pre-project permitting briefings. An electrical power stub-out and main circuit breaker providing 1,600 amps of 208/120 volt three phase electrical power was installed at the site by HECO at no cost to the project. The electrical contractor prepared the final design for distributing the power throughout the facility. A distribution switch board and breakers distribute the power to four primary breaker panels and to a separate transformer serving the electrolyser (an element of the overall facility). Power is then distributed from each power/breaker panel to nearby equipment and instruments.

Mechanical   The mechanical system includes the exhaust ventilation system and air conditioning system. The exhaust ventilation system is key to operating a safe facility that uses hydrogen on a daily basis. Basic design requirements and schematic drawings were prepared by HNEI staff using NFPA, UFC, CGA and local standards for storing and transporting hydrogen and related gases. Project partner UTC Fuel Cells also provided safety design protocols and experience based on their operation of fuel cell test facilities for over 40 years. Final construction drawings, air conditioning, and system balancing specifications were prepared by the mechanical contractor.

Exhaust ventilation is provided to each individual test stand as well as the entire facility. Should a hydrogen line break in a test stand, the ventilation flow, which is provided continuously to each test stand, is designed to dilute the escaping hydrogen to less than 10% of the lower explosive limit (LEL) for hydrogen. The facility itself is ventilated by a ceiling sweeper exhaust duct (running all the time) located at the ridgeline. The hour-glass cross section of the facility and tendency of hydrogen to rise provide ideal conditions to remove hydrogen from the facility. Hydrogen sensors installed throughout the facility trigger audio and visual alarms at 10% of the LEL for hydrogen, and complete shutdown of hydrogen flow at 25% of the LEL. Multiple hydrogen flow shutdowns occur at the test stands, at the entry to the facility, and at the hydrogen storage pad.

Fire Protection   The fire protection system includes a sprinkler system above the internal membrane building which was installed by HECO, and a pre-active fire sprinkler system installed inside the membrane structure. The interior system was coordinated with the warehouse system and is integrated into HECO's security office fire alarm system. The system is designed to Uniform Fire Code and local Honolulu Fire Department codes and requirements. In the event of a fire, heat detectors mounted on the ceiling of the facility trigger water flow into the piping, and the melt down of heat sensitive plugs in the sprinkler heads actuates the release of water.

Gas and Fluid Supply   The gas and fluid delivery system was designed by HNEI staff. The design complies with NPFA, UFC, and CGA standards, and is consistent with guidelines and protocols provided by UTC Fuel Cells. Hydrogen is stored in pressurized cylinders in pallet racks of 18 cylinders. Pallet racks and loose cylinders are stored in a protected storage area outside the warehouse. The primary hydrogen delivery line is split into separate, dedicated lines that run to each test stand. This manifold is located in a ventilated cabinet outside the warehouse structure. This assures that should a line leak or break inside the facility, the leakage will be limited to the flow to the individual test stand. Each gas line is also equipped with a mechanically triggered flow limiter which reacts and shuts off the flow if any sudden excess flow is detected. The flow limiter is triggered by any change in differential pressure across the limiter.

The distribution panel also houses pneumatically actuated valves that close upon receiving a hydrogen detection alarm or a major facility power failure.

The hydrogen supply system is also designed to deliver hydrogen produced by the on-site electrolyser. Hydrogen produced by the electrolyser is stored in the cylinder racks in the hydrogen storage pad. The design incorporates various pressure relief valves, pressure regulators, sampling ports, exhaust vents, and manual shutoff valves.

In response to a request from HECO, HNEI designed and installed a quick-shutoff, nitrogen purge and disconnect system for the hydrogen supply and delivery lines located between the hydrogen storage area and the warehouse. This system was required to permit HECO to quickly trench and repair underground power lines that are buried in a narrow corridor that runs through that area of the property.

In addition to hydrogen, pallet racks of nitrogen and compressed air are also stored on-site and provide purge gas and backup air to the facility. Loose cylinders of O_2, CO_2, CO, N_2, and compressed air are also plumbed to the facility from a cylinder rack located outside the facility. Each gas is manifolded to a primary delivery line and pressure regulated to the specified delivery pressure. During periods of high nitrogen usage, liquid nitrogen is brought on site and connected to the nitrogen delivery system.

Compressed air is provided by an oiless scroll compressor. The air is then processed through a refrigerated dryer, two coalescing filters, an activated carbon filter, a regenerative dryer with mole sieve desiccant, and fine particle filter before delivery to the test stands. De-ionized (DI) water is also processed on-site. City water is distilled and processed through de-ionizing resin beds. The DI water is used to humidify the test gases and as a cooling media in the test stands.

4.3.5. Construction

Site Preparation   Construction began with site preparation, involving cleaning and coating the warehouse floor and installation of a tensioned-membrane (Sprung) structure inside the warehouse building, creating the "building inside a building" (see Figure 4-6). This portable

Sprung structure was installed in 3 to 4 days with end panels in place. The structure provides a clean, air conditioned space for housing research personnel, test stands, and related equipment. Project partner HECO installed electric power service, a warehouse fire protection system, security fencing and a bathroom at no cost to the project.

A series of photographs documenting construction phases is included in Appendix A.

Figure 4-6. "The building inside a building."

Electrical   As noted, HECO provided 1,600 amps of three phase 208/120 volt power to a main circuit breaker power cabinet and meter located outside the warehouse. HNEI assumed responsibility for the power distribution system from this panel into the warehouse and all interior installations. The electrical contractor installed the main distribution switch and breaker board inside the warehouse. Power was then distributed to four smaller distribution/breaker panels located throughout the facility. The test stands, air conditioners, electrolyser, exhaust fans/motors, and drop-down and strip receptacles are hard wired directly to those panels. Workstations, instruments, computers, analyzers, hand tools, etc. are plugged into drop down and strip outlets.

Mechanical   The mechanical contractor installed the facility air conditioning system, three exhaust ventilation fans/motors and ducts, and fume hood ducting. The test stands and ceiling sweeper ducts extend through the end walls of the Sprung structure to fans/motors located high on the warehouse wall. The fans/motors exhaust 600-700 cfm on a continuous basis. The facility air conditioning and ceiling sweeper exhaust system has run continuously since the dedication of the facility in April 2002. The fans/motors are serviced quarterly and the air conditioner bi-monthly. The layout of the ventilation system is also shown in Figure 4-4.

Fire Protection   The fire protection system inside the facility is comprised of high-strength, lightweight steel tubing and press-fit sprinkler heads and fittings. Four sprinkler lines run the length of the facility with crossover headers at each end. A main distribution line runs to the pre-action system which continuously charges the system with low pressure air. Four heat detectors are mounted on the ceiling. Upon detection of heat at the set-point, the primary clapper valve is

tripped and water flows into the overhead piping. Upon melting of the heat sensitive plugs in the sprinkler heads, water deluges the fire. The heat detectors and overall system are tested and certified annually by the Honolulu Fire Department. HNEI staff also periodically tests the heat detection and hydrogen detection systems between certifications.

Gas & Fluid Supply HNEI staff designed and installed the gas and fluid supply systems. The gas lines are installed on an overhead grid structure and drop down to valve panels and test stands. In the case of cooling water, return lines recirculate the water to the heat exchanger and pumping system. Control valves, mass flow controllers, pressure regulators, and gages are mounted in protective housings and cabinets.

Staff personnel were trained and certified by Swagelok in tube fabrication and fitting assembly. Stainless steel tubing, Swagelok fittings and valves were used throughout the facility. Upon assembly, all connections are leak tested at appropriate test pressures. All lines are also color coded with respect to the gas or fluid being delivered.

Since dedication in April 2003, the facility has performed beyond expectations and without incident. Minor upgrades and improvements are a continuing activity. Figure 4-7 below pictures the three UTC test stands which occupy about one quarter of the facility. Plans and designs are underway to expand the exhaust ventilation system, gas and fluid delivery system, and test stand cooling system to accommodate four to six additional test stands that will be used for durability and cycle tests, including fuel cell stacks.

Figure 4-7. Interior of test facility.

4.3.6. Safety Systems

Approach Since this program required the storage and handling of significant quantities of hydrogen, a conservative approach to operational safety was followed. This included:

- Follow all available existing codes and guidelines.

- Adapt UTC Fuel Cell facility guidelines where appropriate.
- Install redundant safety and shutoff systems where practical.
- Set lowest possible alert/alarm limits on the gas detectors.
- Upon any event, provide redundant automatic and manual shut-off of the hydrogen flow to the facility.
- Design for continuous ventilation using conservative estimates of gas concentration.
- Establish procedures to routinely test, calibrate and maintain the safety systems.

Facility Control System   All key facility operation, detection sensor, and emergency stop buttons are hard wired to a central facility control system located just outside the Sprung structure. Reports from the hydrogen gas detectors, heat sensors, emergency stop buttons, and electric power failures are relayed to the facility controller. The facility controller is programmed to continually monitor these reports and trigger any required action.

If status or detection levels are outside the preset conditions programmed into the facility control system, a series of visual and audio alarms and possible shut downs are triggered. For example, in the case of a hydrogen leak, the facility controller actuates visual and audio alarms when detecting hydrogen at 10% of the LEL and shuts down all hydrogen flow to the entire facility when detecting 25% LEL. Alarms are also triggered should a sensor wire break or a power failure occur that extends beyond the reserve available in the facility backup power supply.

In the case of a fire, heat sensors report to the facility controller which actuates visual and audio alarms, shuts down the flow of hydrogen to the facility, and triggers the fire protection system.

In addition to automatically actuated reactions, the facility has manually operated Emergency Stop Buttons, located both inside and outside the facility. If any of these buttons are pushed, the facility controller sets off visual and audio alarms and shuts down the flow of hydrogen.

Gas Safety   Facility hydrogen and fuel gases are stored in pressurized cylinders housed in a cinder block and fenced concrete pad located outside the facility and approximately 50 feet from the warehouse. As summarized in the design section, the main hydrogen line from the hydrogen storage cylinder banks is split into single delivery lines for each test stand before the hydrogen enters the test facility. This safety precaution significantly reduces the amount of hydrogen that can escape should a delivery line break inside the facility. In addition, each delivery line has an in-line hydrogen flow limiter and automatic mechanical shutdown triggered by pressure differential should the flow increase beyond the preset operating limits.

Hydrogen gas detectors have been installed at critical locations throughout the facility. These locations include:
- Facility ceiling at multiple locations.
- Exhaust ducts at test stands and ceiling sweeper.
- Hydrogen valve panel cabinet -- outside the facility.

In addition to the facility gas detectors, each test stand and the electrolyser have hydrogen detectors that when actuated will shut-down the equipment. The test stands also have carbon monoxide and oxygen gas detectors and exhaust ventilation detectors that trigger audio alarms and corrective actions to maintain a safe operating environment.

The facility safety system is comprised of a series of pneumatically-operated hydrogen valves that require approximately 80 psig pressure to remain open. If an order is received from the facility controller or a major power failure occurs, the pressure from the nitrogen control system is reduced to zero and the valves automatically go to their normally closed position, effectively shutting down the flow of hydrogen to the entire facility.

Fire   As noted, a pre-active fire protection system has been installed in the facility. The sprinkler system is normally filled with air maintained at low positive pressure. In the event of a fire, the ceiling-mounted heat detectors trigger water flows into the overhead sprinkler system piping. The heat generated also melts the heat sensitive plugs in the sprinkler heads and water deluges the fire.

In parallel with triggering water fill of the sprinkler system, the heat detectors signal the facility controller and visual and audio alarms are set off. The facility controller also alerts the HECO security office and personnel from that office notify the Honolulu Fire Department.

If the fire persists, the warehouse fire protection system will be activated and release water on the fire.

The heat detectors and overall system is tested and certified annually by the Honolulu Fire Department. HNEI staff also periodically test the heat detection and hydrogen detection systems between certifications.

The air conditioner system also has a smoke detector mounted in the return air duct. Upon detection of smoke, the air conditioner shuts down to prevent circulating additional air to the fire.

Ventilation   As noted, the ceiling sweeper exhaust ventilation system operates at all times, sweeping air from the top of the facility ceiling. The ducting also has a hydrogen detector mounted inside the duct to warn of a hydrogen leak inside the facility. The test stands are serviced by separate exhaust ducts, typically two to five test stands per duct, depending on individual test stand requirements. The test stands are instrumented with ventilation flow meters that trigger low flow and no-flow alarms should the exhaust flow be reduced below preset velocities.

At this time, the exhaust ventilation system is operated manually. With the installation of additional exhaust ducts required to support the new test stands, plans are to further integrate the ventilation system into the facility control system. All exhaust fans/motors will automatically adjust to full flow upon detection of hydrogen in the facility and/or receipt of a signal from the facility controller.

4.4. Fuel Cell Test Program

Initial testing was designed to validate test protocols, confirm performance of equipment, and provide data on fuel cell performance. Highlights of the fuel test program under this agreement include:

- Installation and commissioning of three full-size fuel cell test stands.
- Development of a fuel cell assembly laboratory.
- Development of fuel cell test protocols.
- Training of HNEI personnel.
- Testing of full-scale fuel cells:
    - Long-term tests (approx. 2000 hr) using simulated reformate fuel.
    - Accelerated degradation testing.
- Design and purchase of two subscale test stations.

4.4.1. Full-Size Test Stands

The facility took delivery of its first test stand in August 2002 and its second in December 2002. They were installed in concert with facility construction and followed by installation of the third test stand in March 2003.

These three UTC X-811 test stands are designed to characterize full-size (up to 600 cm²), single-cell, atmospheric pressure, proton exchange membrane (PEM) fuel cells. The test stands can perform long-term life testing and cell performance characterization over a wide range of operating conditions, including hydrogen or reformate fuel, air or oxygen as oxidants, and temperatures to 100°C. Trace contaminants can be introduced after the humidification to characterize fuel or oxidant contamination effects.

Each test stand provides the fluid and electrical interface conditions required to start, operate, shutdown, and evaluate the fuel cells under test. The test stand controls the flow, temperature, pressure, and dew point of fluids into the fuel cells, and accepts the electrical output, heat, and waste gases. The test stands can run experiments automatically or manually, and have the capability to provide automatic alarm and shutdown signals for personnel and equipment protection.

In the 3rd Quarter of 2004, test stand No. 3 was modified to allow testing of subscale, pressurized fuel cells and new software was developed to allow for full automation of the new hardware components. Figure 4-8 shows the three UTC X-811 test stands following installation. Figure 4-9 shows shows the interior view of one of the test stands. Specifications of these test stands are detailed in Table 4-1.
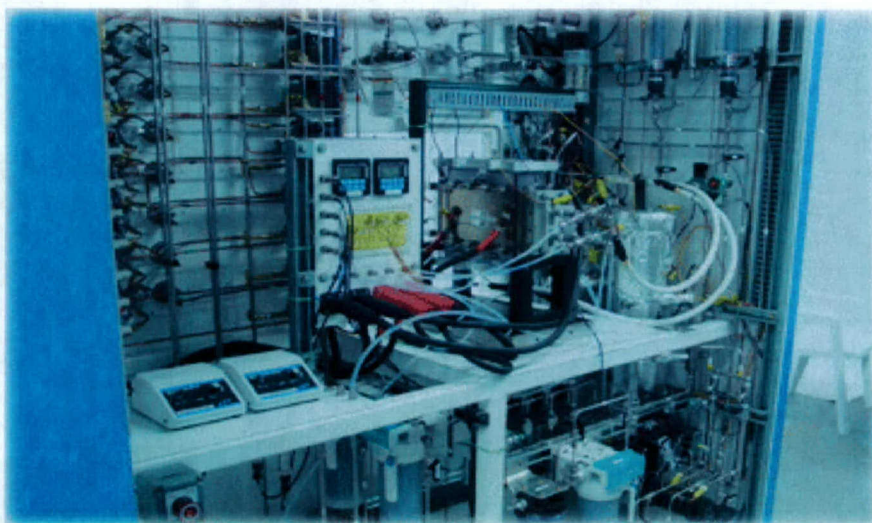

Figure 4-8. Three UTC fuel cell test stands.

Figure 4-9. UTC test stand components (rear view of stand).

Table 4-1. Overview of UTC test stand specifications.

Reactant Gas Flow	Anode flow controllers (thermal mass flow controllers) Hydrogen (up to 10.5 LPM) Nitrogen (up to 48 LPM) Carbon dioxide (up to 4.9 LPM) Carbon monoxide (using 1000 ppm CO in Nitrogen, up to 1 LPM) Cathode flow controllers (thermal mass flow controllers) Air (up to 48 LPM) Oxygen (up to 10 LPM) Nitrogen (up to 48 LPM) Flow controllers ensure 3% flow rate accuracy over required ranges for each cell type/size/test condition.
Humidification System	Bubbler type humidifiers Dew point range from 25° - 90°C w/ +/- 2°C control accuracy Gas temperature control up to 110°C

Pressure Control	All test stands are designed for ambient pressure at the fuel cell exit
	Test stand 3 has been modified with an automated back pressure
	    control system with the following characteristics:
	        Pressure control range: $0 - 207$ kPag ($0 - 30$ psig)
	        Pressure control (steady state): +/- 1.4 kPa

Heater Control Zones	Heater controls: +/- 1C stability 8 independent heater controllers on each test stand
Coolant System	Coolant flow range: 0-1000 cc/m Designed to control coolant pressure below atmosphere for UTC cells Maximum temperature: 90°C Conductivity is maintained in-situ polishing loops Conductivity monitored at the exit of the cell
Load System	Automated cycling in constant current and constant voltage mode Multiple current ranges: 0-100 A and 0-1000A Ability to operate at < 0.1V using power booster
Miscellaneous	Minimum sample rate of the data acquisition system: 1 sec Measure cell high freq. resistance (HFR) with milliohm meter at 1kHz Ability to sample water from the exhaust gas stream condensate and/or coolant flows for chemical analysis

4.4.2. Fuel Cell Assembly Laboratory

In spring 2005, HNEI initiated development of a fuel cell assembly laboratory located on campus at the University of Hawaii at Manoa. The primary objective of the laboratory is to facilitate the assembly of single-cell test hardware for testing to be performed at the fuel cell test facility. The assembly lab was located on the campus of the University of Hawaii to prevent proprietary fuel cell components from being viewed by other manufacturers who may be visiting or using the testing facility. Once assembled, the fuel cells are transported to the facility for testing.

The current capabilities of the fuel cell assembly lab allow for cutting and preparation of membrane electrode assemblies and gas diffusion layers and appropriate equipment for stacking the gas flow fields, current collectors, and pressure plates according to OEM specifications. The laboratory houses a large crane for maneuvering UTC full-scale cells, a Carver 12" x 12" hot press for component cutting and compression of electrode material onto a membrane for Ballard, GM, and UTC cells, a vacuum chamber for pretreatment of cells during assembly, and laminar flow hood for a particulate-free air flow for assembling delicate components. Future expansion of the laboratory to allow fabrication of fuel cell electrodes and membrane electrode assemblies from raw materials is planned.

4.4.3. Development of Fuel Cell Test Protocols

As part of the partnership with UTC Fuel Cells, test protocols for performance, durability, and accelerated degradation testing were transferred to HNEI. This involved transfer of proprietary test plans, visits by UTC engineers and technicians to the facility, and open consultations by telephone and email. Protocols provided to HNEI include:

- cell startup and conditioning,
- cell polarization behavior (current vs. voltage) at varying oxygen concentrations and reformate fuel mixtures,
- fuel and oxidant utilization sweeps,
- hydrogen crossover evaluation techniques,
- electrochemical area determination techniques, and
- durability/life testing protocols and accelerated degradation techniques.

HNEI is continuing to work with other fuel cell manufacturers including General Motors and Ballard Power Systems to expand the testing protocols available at the facility including protocols for subscale and pressurized PEM fuel cells. Further details of testing and test plans adopted by HNEI are covered in the following sections.

4.4.4. Training and Testing with Full-Size Fuel Cells

In January 2003 with the assistance of engineers and technicians from UTC Fuel Cells, HNEI test engineers were trained in the operation of the test stands and installation of UTC fuel cells. Testing with hydrogen fuel using two fuel cells from UTC began in April 2003, shortly after receiving the facility construction completion permit. Tests to validate the test stands and HNEI operation continued through May of 2003, allowing HNEI engineers to gain experience while receiving direct feedback from UTC.

In June 2003, two HNEI researchers traveled to UTC for additional training. Cell assembly, testing protocols, procedures, and test plans were addressed. Shortly after, the first round of 2,000-hour endurance tests using UTC fuel cells was initiated.

Between July and November 2003, UTC Series 400 (400 cm^2) and Series 600 (600 cm^2) fuel cells were operated continuously with simulated reformate fuels at constant current holds (200

and 300 Amps, respectively) with periodic diagnostic sweeps every 100-200 hrs to evaluate the long-term effects of operating on the simulated reformate mixtures. The simulated reformate mixture compositions contained 18 or 42% hydrogen, up to 20% carbon dioxide, and up to 10 ppm carbon monoxide, with the balance being nitrogen. Over 160 individual experiments were conducted on the Series 400 cells and 130 individual tests on the Series 600 cells during this extended test period. The facility's initial year culminated with the successful demonstration of automated 24-hour, 7 days/week life/endurance testing. Comparison with UTC Fuel Cells data validated the HNEI protocol implementation and equipment operation. Examples of data produced during this initial round of testing are present in Figures 4-10 to 4-12. Figure 4-10 shows hydrogen/oxygen polarization curves taken at different times over the first 1,300 hrs of operation of the Series 400 cell. The top two overlapping curves represent the validation of the initial data taken at the fuel cell test facility with data produced at UTC on the same cell prior to shipment. The other curves in the figure show decay as the cell ages. Figure 4-11 shows examples of the 100 hr constant current holds on the UTC series 600 fuel cell between 300 and 600 hrs. Figure 4-12 shows polarization curves of the UTC Series 400 fuel cell under different test conditions following 1,600 hrs of operation. Test conditions include pure hydrogen and oxygen, pure hydrogen and air, simulated reformate fuel (with 2% air injection) and air, and simulated reformate fuel (with 1% air injection) and air.
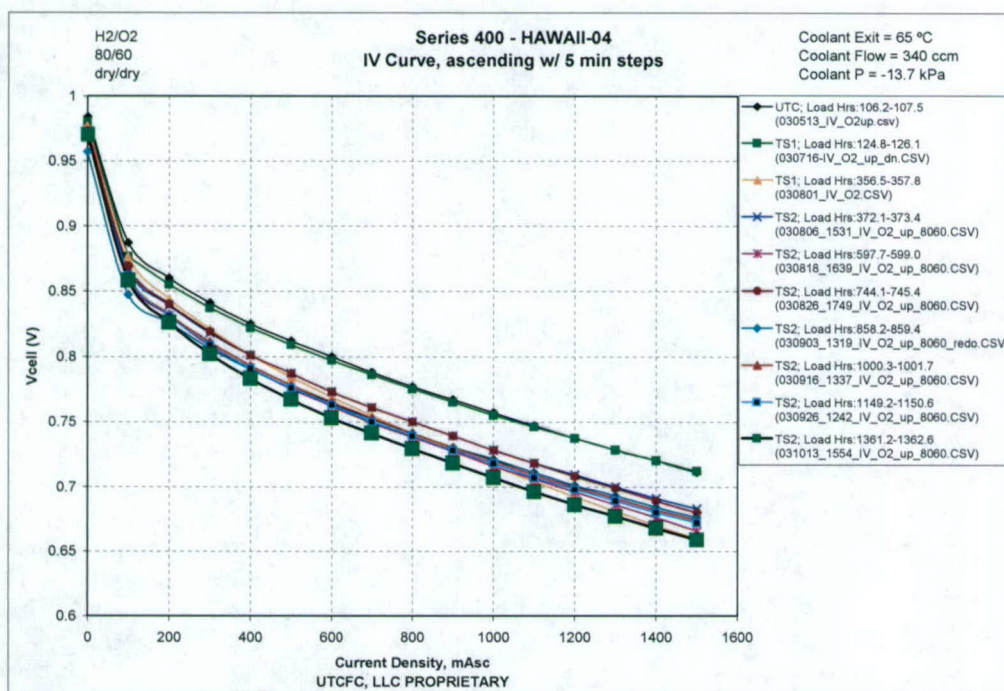

Figure 4-10. Hydrogen/oxygen performance curves using UTC Series 400 test cell during the first 1,300 hrs of operation.
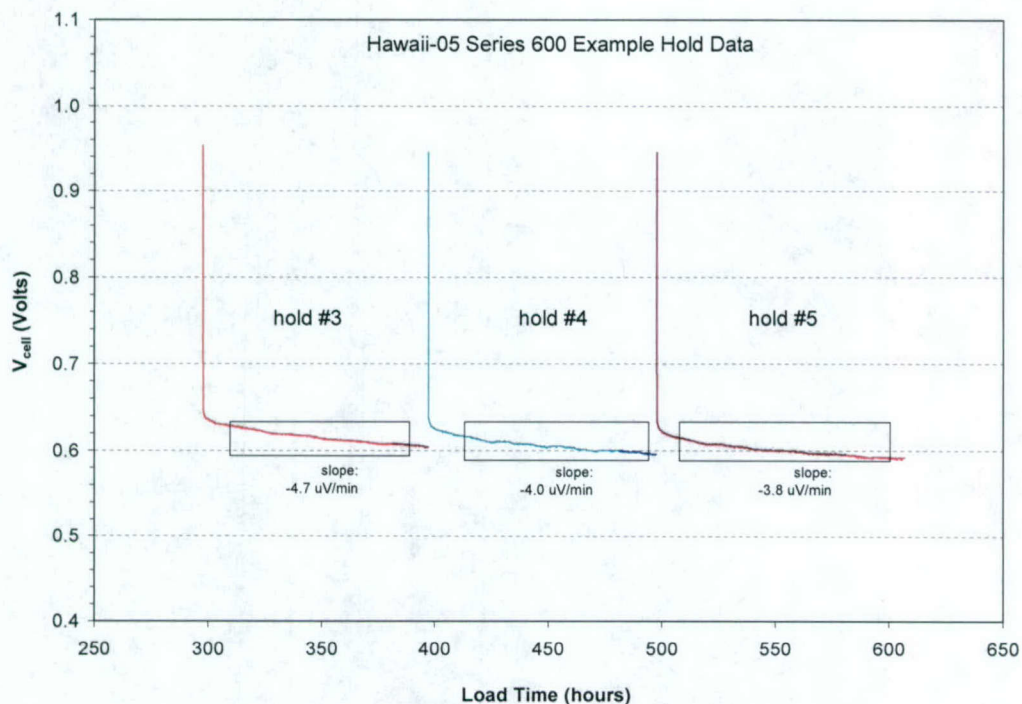
Figure 4-11. Example of constant current hold data on UTC Series 600 fuel cell at 300 Amps running on simulated reformate fuel.
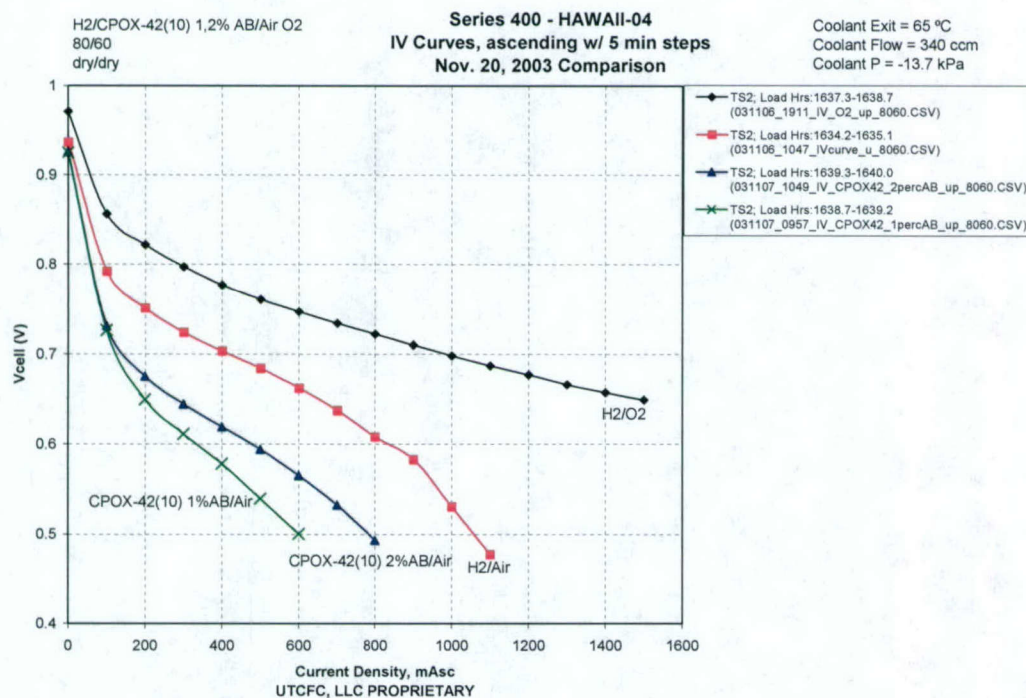

Figure 4-12. UTC Series 400 fuel cell performance curves operating on various fuel and oxidant compositions.

In January 2004, HNEI initiated a second round of 2,000-hr testing implementing accelerated degradation mechanisms on two UTC Series 300 (400 cm²) fuel cells. Parallel testing using

identical test protocols were conducted. The tests were conducted using hydrogen and oxygen with 10% air injection on the anode (to induce hydrogen peroxide formation, a known cause of membrane degradation). Other elements of the testing included elevated temperatures (affecting seal integrity), and load current cycling with constant flow rates (causing hydration and dehydration of the membrane, inducing mechanical degradation). Over 180 individual experiments were conducted on each cell. A limited amount of diagnostics were performed every 50 hrs, with a full suite of diagnostics every 200 hrs. This series of tests was completed in August of 2004. Figure 4-13 shows an example of the data produced during the first 1,500 hrs of the accelerated degradation testing. The top curve of the average voltage, Vavg, represents the data at 100 mA/cm^2 during cycling, while the lower portion represents the data at 800 mA/cm^2 during cycling. The average voltage difference, dVavg, is shown to increase with time, indicating some form of degradation was occurring. It should be noted that at 700 hrs the temperature was decreased from 80°C to 65°C due to higher decay rates than anticipated. Following completion of testing it was found that a seal adhesive material had a softening temperature near 80°C, thus when the temperature was lowered the rate of decay of the cell performance decreased.
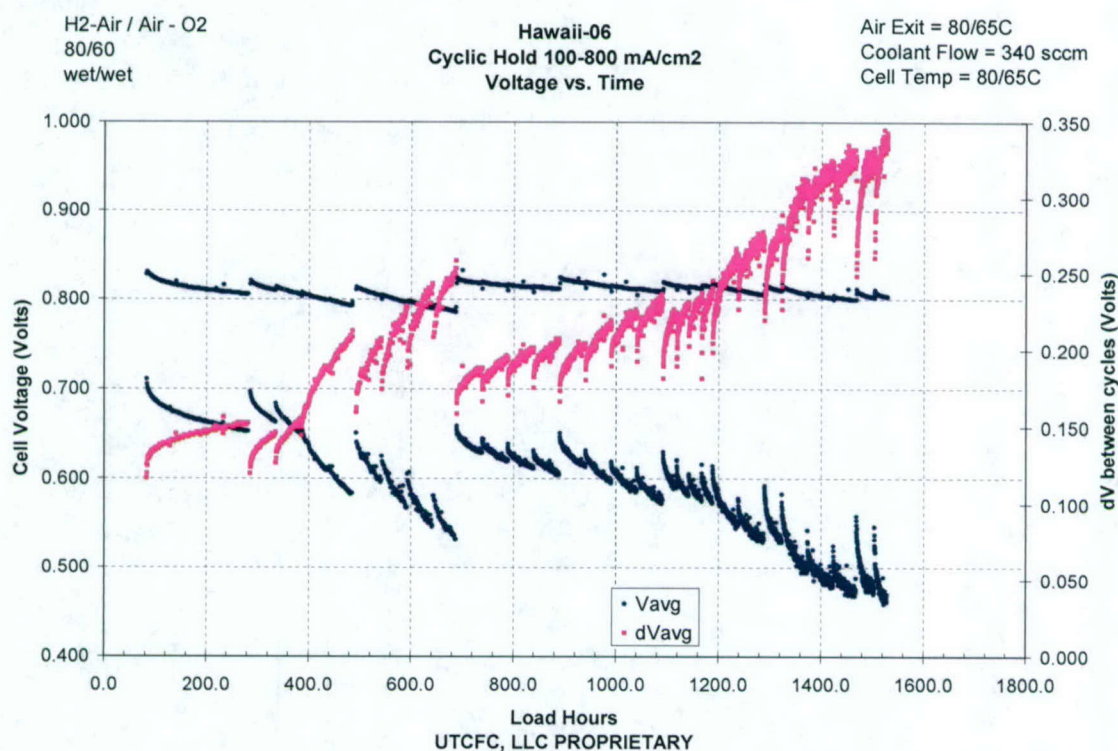

Figure 4-13. Cell voltage vs. load hours during accelerated degradation testing.

4.4.5. Training and Testing with Subscale Fuel Cells

In October 2004, the Fuel Cell Development Center of General Motors transferred two 50 cm^2 pressurized single-cell fuel cell test hardware assemblies to HNEI for use in fuels purity work to be conducted with funding from the U.S. Department of Energy (DOE). GM also provided on-site training on test protocols and fuel cell assembly (see Figure 4-14) for HNEI researchers and test engineers. Several preliminary 10 to 20 hour fuels purity tests were run on the GM cells assembled by HNEI staff.
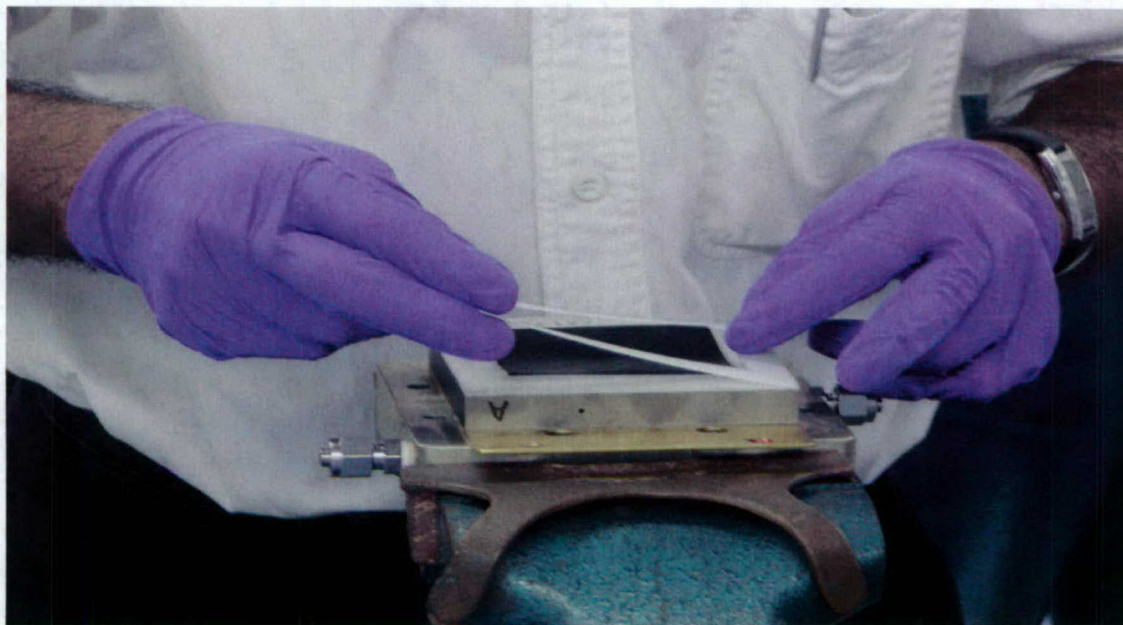
Figure 4-14. Assembly of 50 cm^2 fuel cell (step displayed: alignment of the Teflon gasket onto the membrane electrode assembly).

In November, Ballard Power Systems provided two new 50 cm^2 fuel cell test hardware assemblies to HNEI for testing. Ballard also sent one of their test engineers to train HNEI test staff on cell builds and Ballard test protocols. Similar to the GM visit, a week of preliminary testing followed, using fuels of varying purity.

4.4.6. Subscale Test Stands

Expansion of the testing capabilities following the initial installation of the three UTC stands (and upgrade of one of the UTC stands) began in late 2004 with the development of specifications for two custom-designed Greenlight Power (GLP) G50 test stands. The test stands are scheduled to be delivered to the facility in July 2005. The GLP test stands are designed to test subscale (50-100 cm^2) pressurized single-cell PEM fuel cells from manufacturers including General Motors and Ballard Power Systems.

Like the UTC test stands, the GLP stands provide a complete set of electronic monitoring and automated functions to fully control and monitor gas flows, coolant, and humidification. Gas flow rates are metered and controlled through the use of highly accurate mass flow controllers. Humidification of these gases is achieved through the use of a proprietary contact humidification technique, which fully saturates the gases to an adjustable dew point. Stack pressure is maintained through the use of highly accurate and extremely responsive back pressure regulators. The G Series feature a fully controlled coolant loop for the pre-heating and control of stack temperature. This system can accept either de-ionized water or a combinations of water and ethylene glycol to cool the cells during testing. The G50 Series features include numerous safety interlocks, nitrogen purge capability, and an independent hydrogen sensor to place the test station in a safe mode in the event of a hydrogen leak. Figure 4-15 shows a front view of the GLP test stands. An overview of the test stand specifications is provided in Table 4-2.

Figure 4-15. Front view of Greenlight Power G50 test stand.

Table 4-2. Overview of GLP 50 test stand specifications

Reactant Gas Flow	Anode flow controllers (thermal mass flow controllers) Hydrogen (up to 4 LPM) Nitrogen (up to 5 LPM) 2 spare anode channels w/ no flow controller installed (future use) Cathode flow controllers (thermal mass flow controllers) Air (up to 13 LPM) Oxygen (up to 13 LPM) Nitrogen (up to 5 LPM) Hydrogen (up to 1 LPM) 2 spare cathode channels w/ no flow controller installed (future use) Flow controllers ensure 3% flow rate accuracy over required ranges for each cell type/size/test condition.
Humidification System	Proprietary contact humidification Automated humidifier bypass Dew point control range from 35° - 90°C w/ +/- 2°C control accuracy Humidifiers designed with heat exchangers for fast cooling
Pressure Control	Automated back pressure control system with the following characteristics: Pressure control range: 0 – 300 kPag (0 – 43 psig) Pressure control (steady state): +/- 2 kPa
Heater Control Zones	Heater controls: +/- 1°C stability 4 independent heater controllers on each test stand.

Coolant System	Coolant flow range: 0-2000 cc/m Maximum coolant pressure: 400 kPag (43 psig) for Ballard cells Conductivity is maintained by replenishment
Load System	Automated cycling in constant current and constant voltage mode Current range: 0-150A Ability to operate at < 0.1V using power booster
Miscellaneous	Minimum sample rate of the data acquisition system: 0.1 sec Measurement of cell high frequency resistance (HFR) at 4 frequencies using Electrochemical Impedance Spectroscopy techniques Ability to sample water from the exhaust gas stream condensate and/or coolant flows for chemical analysis Water balance measurement system for analyzing fuel cell exhaust water volumes

4.5. Selected Papers, Presentations, Meetings, and Outreach Resulting from Efforts

PAPERS/PRESENTATIONS/MEETINGS

"Hydrogen Fuel Purity – Effect on Fuel Cell Performance," University of DE Seminar Series, Newark DE, April 2005

"HNEI FC Research Overview," presented to staff of PMS 403, Washington DC, April 2005

"Fuel Cells for UUV Applications," poster at DARPA BAA Workshop, Endicott MD, April 2005

"HNEI FC Research Overview," presented to Captain Greg Vaughn, Washington DC, February 2005

"HNEI Research Overview – Fuel Cells," presented to staff of Pacific Northwest Laboratories, Richland WA, January 2005

"Fuel Cell Research at our Nation's Universities," presented at Senate Hydrogen and Fuel Cell Caucus, Washington DC, November 2004

"Full Scale PEM Testing at the Hawaii Fuel Cell Test Facility," presented at 2004 Joint International Meeting, The Electrochemical Society Inc., Honolulu HI, November 2004

"Hawaii Fuel Cell Test Facility," presented to Hawaii Section of the American Society of Mechanical Engineers, Honolulu HI, August 2004

"Hydrogen, Fuel Cell and Methane Hydrates Research," presented to Naval Research Advisory Council, Honolulu HI, March 2004

"Hydrogen and Fuel Cell Research," presented to staff of National Renewable Energy Laboratory, Golden CO, January 2004

"Hydrogen and Fuel Cell Research," presented to DuPont Corp, Wilmington DE, September 2003

"Future Energy Development," briefing to Secretary of the Navy, Washington DC, March 2003

"Hydrogen/Fuel Cell Projects at HNEI," presented at Aerospace Fuel Cell Application & Technology Meeting, Boeing Phantom Works, Seattle WA, July 2002

"Hydrogen – Fueling the Future," presented at DOD/HECO Energy Partnership Meeting, Honolulu HI, July 2002

"Fuel Cell Technology: Global Climate Change," presented at AIChE Spring Meeting, March 2002.

"Hawaii Natural Energy Institute: HEET Project," presented to Naval Air Systems Command, Patuxent River MD, October 2001

LABORATORY VISITORS

HNEI staff have conducted educational and informational seminars and tours for numerous military, academic, public and private company personnel. A partial list of attendees and visitors includes personnel from the following organizations:

- U.S. Navy - Office of Naval Research
- U.S. Coast Guard - Naval Engineering Support Unit - Honolulu
- U.S. Air Force - Warner Robins AFB
- U.S. Army – ERDC-CERL
- U.S. Department of Energy - Energy Efficiency and Renewable Energy
- U.S. Department of Transportation - Research & Innovation Technology Administration
- Los Alamos National Laboratory
- National Renewable Energy Laboratory
- Air Products and Chemicals Inc.
- Dupont Corporation
- Johnson Matthey
- General Motors
- Toyota Motor Corporation
- Daimler Chrysler
- Nissan
- Ballard Power Systems
- Hydrogen Research Institute
- Asia Pacific Economic Council
- Asia Pacific Center for Security Studies
- Yokohama National University
- Hawaii Community Development Authority
- Women In Technology Club - Waiakea High School

Over 1,000 people have visited the facility since its dedication in April 2003. The facility can be visited by appointment and non-interference basis.

5. Fuel Processing and Gas Conditioning for Hydrogen Production

5.1. Objectives

The objectives of this task were to develop an experimental setup and to perform research on fuel processing and gas conditioning for hydrogen production. Eventually the hydrogen from the fuel processing unit is expected to be tested at the Hawaii Fuel Cell Test Facility, as a step forward from pure bottle hydrogen and hydrogen produced via electrolysis.

5.2. Scope of Work and Approach

Due to the lack of naturally occurring hydrogen (H_2), successful fuel cell implementation will require H_2 production based on highly efficient fuel processing in which fuels are converted to H_2, and contaminants and pollutants are removed.

In the near term, conventional hydrocarbon fuels can be potential sources of H_2, serving as transition fuels toward future production of H_2 from renewable sources. Liquefied petroleum gas (LPG) is a mixture of ethane to butane hydrocarbons that exist as liquids under modest pressures at ambient temperatures (Falkiner, 2003). LPG is easily transported and stored on-site (Ahmed et al., 2002) and may be attractive in remote areas or for residential use. In Hawaii, the majority of electricity is generated from fossil fuels. There are ample supplies of LPG and its price is competitive with that of gasoline. Being safe and non-toxic, LPG is a promising source of H_2 for off-grid applications in Hawaii.

Fuel processing converts LPG into H_2 and carbon dioxide. Small amounts of methane, carbon monoxide, and potential contaminants for polymer electrolyte membrane (PEM) fuel cells, such as sulfur compounds, are removed. Reforming is the key step to convert fuels to H_2, CO_2, and CO. Autothermal reforming is likely the most suitable reforming method for LPG fueled PEM fuel cells utilized for residential use. Compared with steam reforming, autothermal reforming is easily operated for small systems, offers better temperature control, and has less tendency to coke (Rostrup-Nielsen, 2001).

A ranking of activity for metal-supported catalysts in autothermal reforming of methane and steam reforming of ethane are reportedly Rh>Pd>Ni>Co (Rostrup-Nielsen, 1984; Ayabe et al., 2003). Despite differences in activity, Ni is less expensive than precious metals and greater amounts of Ni can be loaded to provide the same overall activity as Rh catalyst (Ahmed et al., 2002).

LPG vapor can be used like natural gas but some adjustment of conditions, e. g., air/fuel ratio, are needed (Falkiner, 2003). Comparing with methane, larger molecules of LPG usually require higher temperature to obtain complete conversion to hydrogen, carbon dioxide and carbon monoxide. As expected due to the greater carbon number, propane fuel was found to cause more carbon deposition than methane fuel (Ayabe et al., 2003). Another source of catalyst deactivation is sulfur poisoning by odorant, such as ethyl mercaptan, which is commonly added to LPG.

Under this agreement, the following work was carried out:

- development of an automated lab-scale fuel processing system,
- fuels characterization,
- thermodynamic study to calculate operating conditions at optimal processing efficiency,
- parametric study of autothermal reforming conditions of LPG,

- and catalyst deactivation study.

The experimental results were evaluated and modeled by multivariate data analysis method.

5.3. Technical Accomplishments

Automated test bench

An automated fuel processing testbed was designed, fabricated, and is currently in use. As shown in Figure 5-1, it consists of a lab-scale fixed-bed reactor, gas sampling and analysis capability, a control and data acquisition system, and a safety system. LabVIEW is used for control and data acquisition. Feed rates of fuel, oxidizer, and steam, processing conditions, gas conditioning, and gas analysis are automated. Safety measures are installed so that the system can be run unattended. The system can also be accessed and controlled remotely.
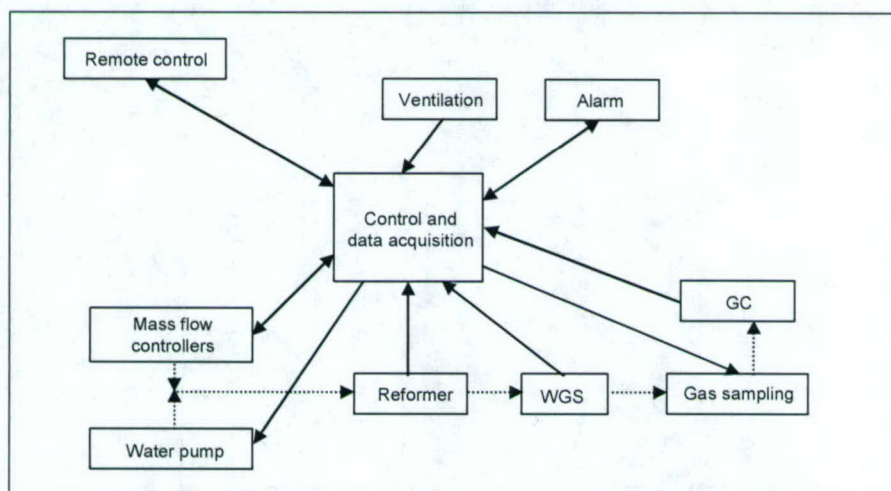

Figure 5-1. Conceptual design of the automated fuel processing testbed (WGS = water gas shift; GC = gas chromatograph).

The fuel processing system has been used to:
1) convert gas (LPG) to hydrogen,
2) evaluate catalyst performance,
3) study catalyst deactivation,
4) and perform parametric testing of optimized reforming conditions.

Figure 5-2 provides details of the automated fuel processing testbed. The reforming reactor containing a catalyst bed was heated by an electrical furnace with a heating length of 30.5 cm. Temperatures within the reactor were measured at two locations upstream of the catalyst bed and at one location immediately following the catalyst bed as indicated in Figure 5-2. Air and LPG were introduced from gas bottles and were metered into the reactor by mass flow controllers. Water was introduced to a vaporizer unit prior to entering the reactor. After the reactor, water was separated from product gas in a condenser, then further dried using silica gel or a coalescing filter. A Shimadzu GC 14A equipped with a thermal conductivity detector (TCD) was used to quantify the concentrations of H_2, N_2, CO, CH_4, CO_2, C_2H_4, C_2H_6, C_3H_6 and C_3H_8.in the dry reformate gas. Test durations ranged from 3.6 to 43.5 hours. Reactor operating conditions were monitored and recorded on one minute intervals. Composition of the gas exiting the reactor was usually determined every 30-35 minutes by GC.
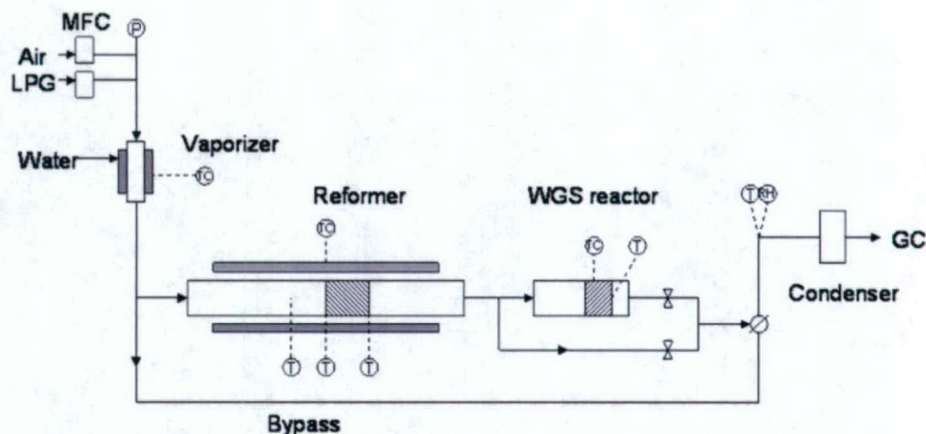
Figure 5-2. Schematic diagram of the fuel processing testbed (WGS = water gas shift; GC = gas chromatograph).

Fuel characterization: LPG vapor composition

The composition of LPG vapor is determined by the equilibrium of liquid and vapor in the LPG vessel. Lighter hydrocarbons (i.e., propane) with higher saturated vapor pressures vaporize in greater proportion to their concentration in the liquid phase. As vapor is withdrawn from the bottle, the amount and composition of the liquid remaining in the bottle changes. The vapor pressure in the bottle gradually decreases, and the fractions of higher hydrocarbons in the liquid and gas phases increase. As a result, the composition of vapor obtained from the head space of an LPG bottle depends on the composition of liquid in the bottle, the amount of liquid left in the bottle, and the bottle's refill history. In the experiments, three propane-based fuels were tested; (1) LPG in an 8.3 kg tank (Tank A) that had been refilled several times, i.e., history undocumented; (2) LPG in newly purchased, 8.2 kg tanks (Tanks B and C); and (3) Grade 5.0 propane (Propane). The LPG is a commercial product from GasPro Hawaii sold as an engine-grade or high-octane propane. In all tests, vapor was withdrawn from the head space of the tank. LPG was analyzed using the Shimadzu GC equipped with an Alltech HayeSep D 100/120 (3.05 m × 0.32 mm) packed column and TCD. Sulfur concentrations in the fuels were determined on a Varian 3800 GC equipped with a Varian CP-Sil 5 CB capillary column (50 m × 0.32 mm) and a pulsed flame photometric detector (PFPD).

During the experiments, compositions of vapor from Tank A and Tank C were monitored by the GC with TCD. Results of the analysis are presented in Figure 5-3. As shown, the LPG vapor composition varied with time, the result of differing vapor pressures of the constituent species. Generally the lighter components (ethane, propylene, and propane) were in higher concentration when the bottle was full. As gas was withdrawn from the bottle, the concentration of these components was reduced and the heavier component, butane, increased. Although the liquids in the two tanks were not sampled and analyzed, by integrating the discharged gas composition curve it is evident that Tank A, that had been refilled several times, had more butane and less propane than the new Tank C that had only been filled once. Tank C was pressurized with N_2 before filling with LPG, and this is evident in Figure 5-3. N_2 concentration decreased rapidly at the beginning of usage (Figure 5-3). Since the LPG contained mostly propane, the vapor composition of hydrocarbons was nearly constant, except for the first and the last kilogram of LPG in the bottle.

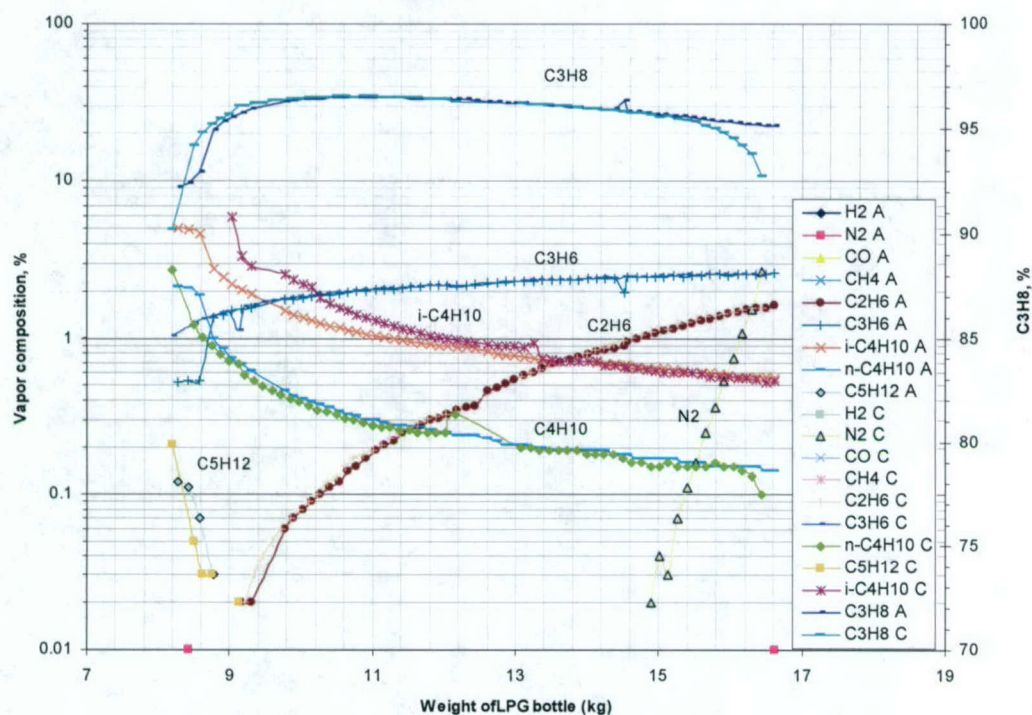**Old bottle A and New bottle C refilled on 040907**

Figure 5-3. Gas compositions of vapor from tank A and tank C.

The sulfur content in LPG tanks was measured by the GC/PFPD at three points, full tank, half tank, and near empty (Table 5-1). The difference between a new bottle and used bottle was not found to be significant. It was interesting to discover that even though the LPG was reportedly dosed with 40 ppm ethyl mercaptan on average, mercaptan found in the vapor varied greatly. The concentration of mercaptan in vapor increased drastically when the bottle was close to be emptied.

Table 5-1. Sulfur in LPG vapor.

Tank	Condition	Weight (kg)	Ethyl mercaptan (ppm)
A	full	16.7	6.9
A	half	12.5	14
A	empty	8.7	140
C	full	16.5	1.5
C	half	12.2	14
C	empty	8.5	170

Thermodynamic analysis

Thermodynamic analysis of autothermal reforming (ATR) of light hydrocarbons was performed with consideration of global mass balances, chemical equilibrium, and changes in enthalpy in the process. Process parameters, oxygen to carbon ratio (O/C) and steam to carbon ratio (S/C), were optimized at maximum fuel processing efficiency under a thermo-neutral condition.

The reforming process studied is shown in Figure 5-4. Light hydrocarbon fuels, air and water are introduced at 298 K, 1 atm. The inlet stream is heated by heat exchange with hot gases from downstream components. Above light-off temperature, the hydrocarbons start to react. Autothermal reforming is carried out at high temperature, T_R. After the ATR, the gases are cooled and undergo water-gas shift at T_w to reduce CO. ATR and water-gas shift are included in the analysis. Further removal of CO is not included and will be discussed later. Overall heat loss in about 20%. The energy balance is based on a unit amount of fuel. Thermodynamic data are obtained from FACTSage software and the NIST Chemistry WebBook (NIST, 2004).
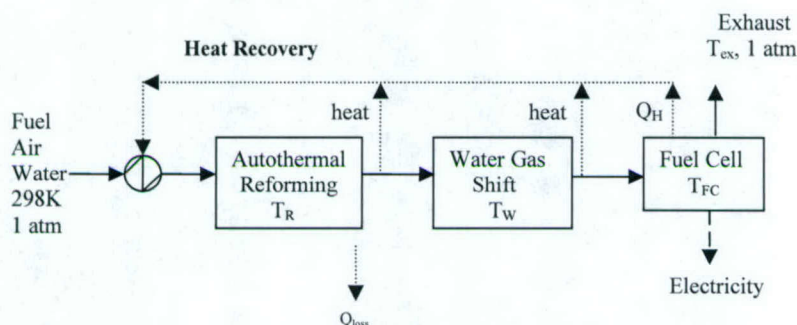
Figure 5-4. Schematic diagram of the reforming process.

Figure 5-5 gives an example of energy distribution in autothermal reforming of 1 mole of propane, with the resultant H_2 used in a fuel cell (FC), most being utilized by the cell but some being rejected. CO is assumed to be completely converted to H_2. The fuel processing efficiency of the process is 85.5%. Up to 4% efficiency improvement can be achieved by recovering sensible and latent heat in the exhaust gas. Combusting the rejected hydrogen (18% of the total in Figure 5-5) can considerably improve fuel utilization.
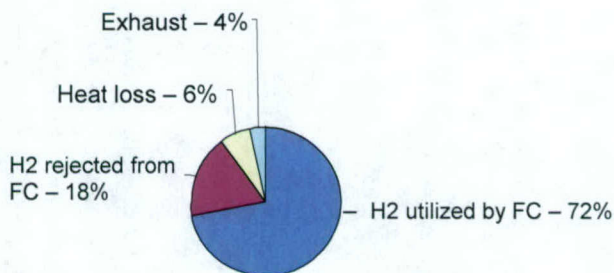
Figure 5-5. Distribution of energy in autothermal reforming of 1 mole of propane.

Figure 5-6 shows changes in enthalpy for each step and cumulative enthalpy changes in fuel processing. Raising temperatures of the inlet stream requires heat in the first three steps. Then, ATR and WGS reactions and cooling of the hot exit stream release heat for heat exchange. Note that in real situation, inlet gases only need to be heated to light-off temperatures of hydrocarbons to start ATR. In that case, step 3 will be less negative and step 4 (ATR) will be less positive, but the net sum of step 3 and 4 will be the same. If the heat loss of the process can be maintained at

or below the small positive enthalpy value shown at the end of cumulative enthalpy change (Figure 5-6), then the process does not require external supplemental heat addition.
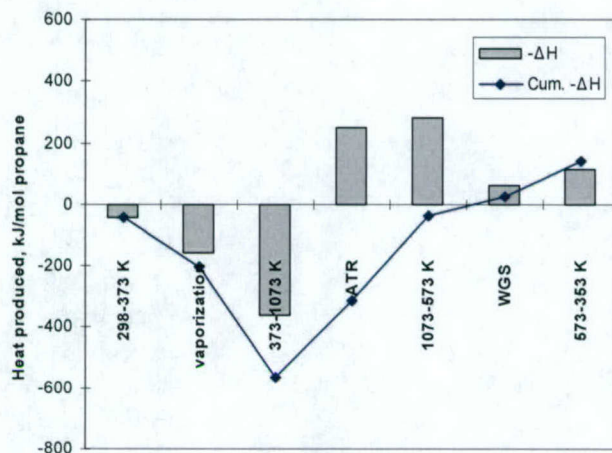

Figure 5-6. Heat budget for steps in the reforming process.

Results of optimization for hydrocarbons with 20% heat loss show that the differences between hydrocarbons are small, except for propylene. Fuel processing efficiencies were around 85% to 87%. Hydrogen in the reformate gas was about 40%. O/C is around 1.0 and S/C is about 1.3. Operating at an S/C ratio this low could cause coking on catalyst surfaces. Combusting the rejected hydrogen from the fuel cell will lead to a higher optimal value of S/C and improve the conversion conditions.

The simple analysis provided good understanding of autothermal reforming of light hydrocarbons. Thermal integration and insulation were of design importance. Operating parameters, S/C and O/C, were optimized with no external heat input. The optimal values for hydrocarbons are similar, except for propylene. Heat recovered from the fuel cell exhaust gas will provide small improvement in the fuel processing efficiency. Combusting hydrogen rejected by the fuel cell is favored for the overall fuel utilization, as well as for avoiding the coking problem due to low S/C.

Parametric study of reaction conditions: multivariate analysis and modeling

Effects of experimental parameters (Table 5-2 below) on autothermal reforming of LPG were studied over a total of 17 tests with durations falling into two groups: shorter duration tests of about 4 hours and longer tests of about 40 hours. Temperature was found to be the most important parameter. Complete conversion of LPG was achieved at 800°C (*T3*) at an *S/C* = 1.5 and *O/C* = 1.0. More details can be found else where (Wang *et al.*, 2004). The composition of reformate gas from a typical autothermal reforming test is presented in Figure 5-7. Equilibrium gas compositions were calculated using FACTSage[TM] 5.1, and Partial Least-Square Regression (PLSR) was used for predicted compositions. Equilibrium and predicted values are shown as lines in the figure. The gas concentrations for hydrogen, nitrogen, carbon monoxide and carbon dioxide approached equilibrium because the water-gas shift reaction was not rate limited at the reaction temperature, nominally 800°C. Methane was higher than the equilibrium value, indicating methane reforming was kinetically controlled. The observed trend of increasing methane concentration implies decreasing catalyst activity over time.

Table 5-2. Experimental ranges.

	Variables	Abbreviation	Unit	Min	Max
Descriptor variables – X block					
1	Catalyst	*Cat*		C11-NK	G91-EW
2	Furnace set point	*Tsp*	°C	620	770
3	Gas hourly space velocity v/Vcat	*GHSV*	1/h	7000	18,500
4	Steam to carbon ratio	*S/C*		0.30	1.93
5	Oxygen to carbon ratio	*O/C*		0.64	1.38
6	Sulfur in LPG	*Sulf*	ppm	Low (1-15)	High (15-150)
7	C_2H_6 in LPG	*C2H6*	%	0	4.19
8	C_3H_6 in LPG	*C3H6*	%	0	3.33
9	C_3H_8 in LPG	*C3H8*	%	87.5	100
10	C_4H_{10} in LPG	*C4Ht*	%	0	10.9
11	CH_4 from previous step	*CH40*	%	0	3.29
12	Difference of reaction time	*dt*	hour	0.05	5.83
	Time on stream	*TOS*	hour	0.05	43.5
Response variables – Y block					
1	T1	*T1*	°C	414	912
2	T2	*T2*	°C	575	963
3	T3	*T3*	°C	676	818
	Product gas composition on dry basis				
4	H_2	*H2*	%	19.1	44.5
5	N_2	*N2*	%	30.8	63.2
6	CO	*CO*	%	4.32	15.3
7	CH_4	*CH4*	%	0	3.29
8	CO_2	*CO2*	%	4.56	14.5
9	C_2H_4	*C2H4*	%	0	4.55
10	Mass balance of carbon	*MBC*	%	54.1	109

A multivariate data analysis method, PLS regression, was used to evaluate the experimental results. From the analysis, the significance of each parameter and the correlations between variables were clearly revealed. A predictive, three-component PLSR model was developed for product gases and mass balance of carbon based on 190 experiment points. The PLSR models accounted for about 70% of the variance in the data set.

In comparison with the equilibrium calculation in Figure 5-7a, the PLSR model (Figure 5-7b) yielded good predictions for CO and CO_2 concentrations, but poorer results for H_2 and N_2. Prediction of methane concentrations were much improved by the PLSR model. The observed methane concentration was, however, nonlinear over time and the linear regression model could not accurately predict the shape of the curve. but was able to provide a close approximation of the average line. The effects of fuel compositions were considered quantitatively for hydrocarbons and qualitatively for sulfur. The model can be used to predict autothermal reforming under similar conditions.
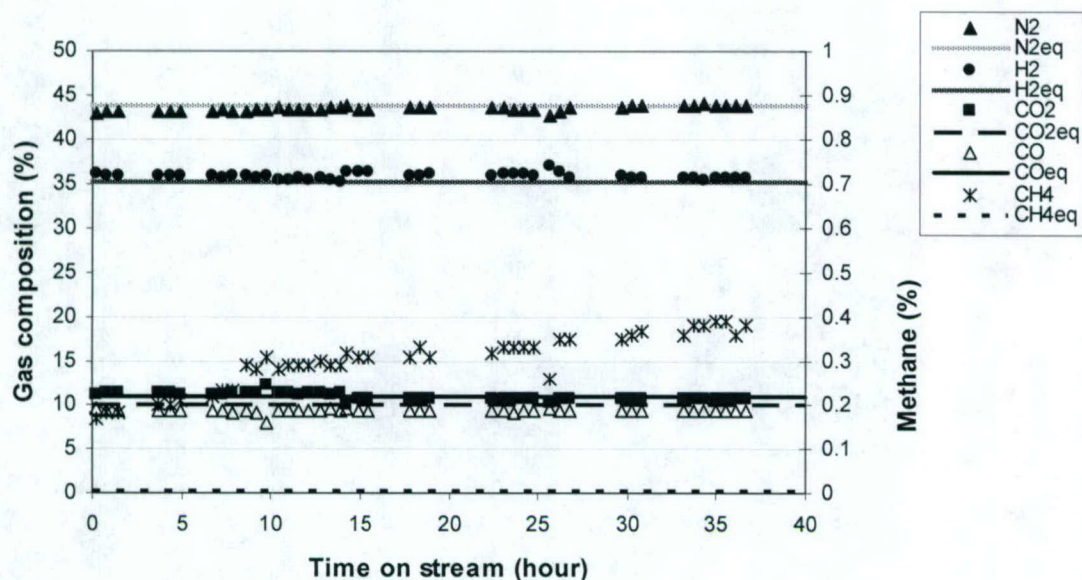
(a)
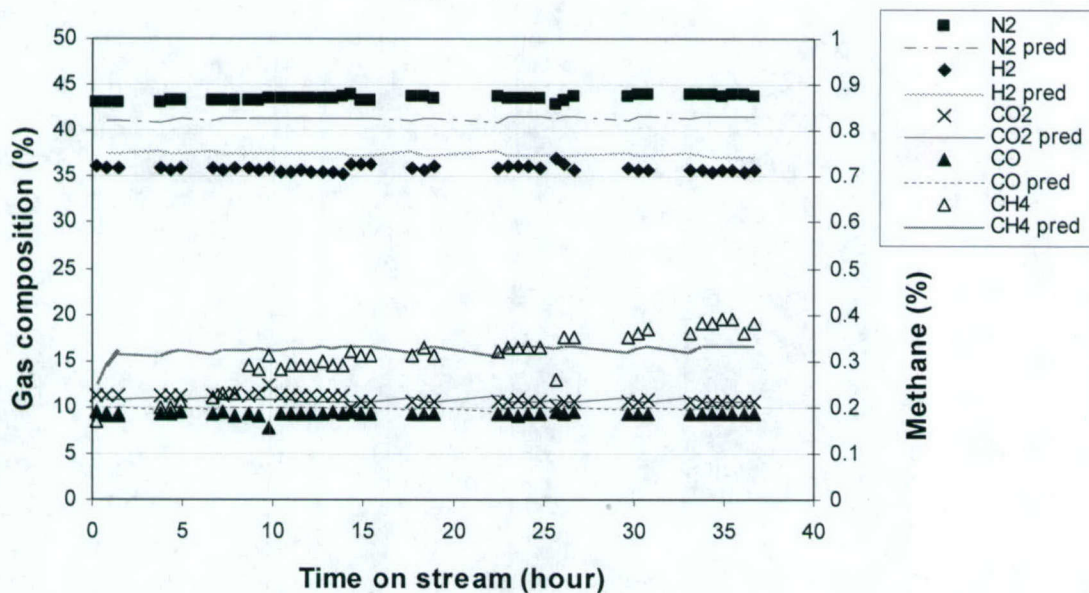
(b)

Figure 5-7. Comparison of gas compositions obtained by experiments, PLSR prediction and equilibrium. Gas composition (dry basis) from autothermal reforming of LPG from Tank B. Test conditions: catalyst – 20g of G91-EW, temperature 800°C, S/C = 1.76, and 0/C = 1.13.
(a) Equilibrium gas compositions are calculated by FACTSage and are shown as lines.
(b) Lines are predicted by a 3-component PLSR model.

The PLS method was advantageous in that it statistically analyzed the data points and provided quantitative relations between the response variables and the descriptor variables for a limited amount of experiments. The PLSR model took into account the LPG vapor composition and could predict kinetically controlled variables, e.g., methane concentration over the test range. Based on the present results, more experiments and analysis are planned to confirm the multivariate analysis results and to improve the accuracy of the PLS regression model.

Catalyst deactivation under the test conditions

Coking is a main cause of catalyst failure in hydrocarbon reforming. Carbonaceous deposits on catalyst surfaces block active sites, leading to catalyst deactivation. Ethyl mercaptan is commonly added to LPG as an odorant. Ethyl mercaptan will mainly be converted to hydrogen sulfide in autothermal reforming. For reforming catalysts, sulfur will readily bind with nickel, causing severe deactivation.

Experiments performed over ~40 hours time on stream were plotted to study catalyst activity (Figure 5-8). Propane, LPG from Tank A, and LPG from Tank B were tested. Autothermal reforming was conducted on ~20 g samples of G91-EW, at 800°C, S/C = 1.75-1.80 and O/C = 0.90-1.13. The experiment with LPG from Tank B was repeated. As shown in Figure 5-8, initial concentrations of methane and ethylene were almost the same, indicating rate of reactions on fresh catalyst were nearly identical regardless of fuel sources. Both methane and ethylene concentrations increased with increasing time on stream. The rate differed for different fuel sources. The weight of Tank A in the test shown in Figure 5-3 began at 11.5 kg and ended at 8.6 kg. By GC analysis (Table 5-1), vapor from Tank A could contain sulfur as high as ~100 ppm, while vapor from Tank B had sulfur below 15 ppm. In addition, over the range of fuel use from the two bottles, Tank B had more light hydrocarbons and Tank A had more heavy hydrocarbons (Figure 5-3). By examining the results in Figure 5-8, it seemed that catalyst deactivation was mainly caused by sulfur poisoning. However, heavy components in LPG might also contribute to the increases in methane and ethylene.
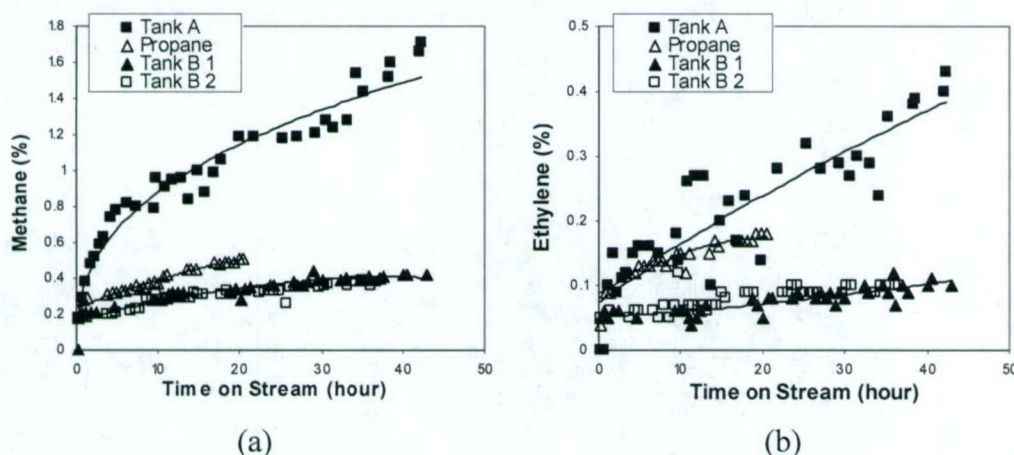

Figure 5-8. Methane (a) and ethylene (b) concentrations after autothermal reforming of different fuels. G91-EW, 20 g, 800°C, S/C = 1.75-1.80, O/C = 0.90-1.13.

By the PLS analysis, the significance of each parameter on catalyst activity and hydrocarbon conversion efficiency was clearly revealed.

- Catalyst G91-EW performed better in reducing methane and ethylene. Carbon deposition was more likely to occur at low temperature.
- Over the range of conditions tested, the main effect of S/C was to shift CO to CO_2 through the water gas shift. Increasing S/C also contribute to CH_4 reduction. At high O/C, H_2 decreased due to oxidation reactions and dilution by nitrogen.

- A lower concentration of methane in the reformate gas was found to be dependent on temperature, catalyst type, catalyst activity, and sulfur in the fuel. Ethylene removal was related to temperature, oxygen, and catalyst activity.
- Sulfur poisoning was the main reason for catalyst deactivation under test conditions.

5.4. Summary of Papers and Presentations Resulting from Efforts

PAPERS/PRESENTATIONS

Wang, W., S.Q. Turn, V. Keffer, and A. Douette, "Parametric Study of Autothermal Reforming of LPG Using Multivariate Analysis," submitted to *Ind. & Engg. Chem. Res.*, May 2005, under review.

Wang, W., S.Q. Turn, V. Keffer, and A. Douette, "Thermodynamic Analysis of Autothermal Reforming of Light Hydrocarbons for Hydrogen," in Preprint Paper, 229th ACS National Meeting, *Am. Chem. Soc., Div. Fuel Chem.*, **50**(1), 110-111, 2005.`

Wang, W., S.Q. Turn, V. Keffer, and A. Douette, "Parametric Study of Autothermal Reforming of LPG," in Preprint Paper, 227th ACS National Meeting, *Am. Chem. Soc., Div. Fuel Chem.*, **49**(1), 142-143, 2004.

5.5. References

Ahmed, K., Gamman, J., and Foger, K. "Demonstration of LPG-fueled solid oxide fuel cell systems," *Solid State Ionics*, **152-153**, 485-492, 2002.

Ayabe, S., Omoto, H., Utaka, T., Kikuchi, R., Sasaki, K., Teraoka, Y., and Eguchi, K., "Catalytic autothermal reforming of methane and propane over supported metal catalysts," *Applied Catalysis, A: General*, **241**(1-2), 261-269, 2003.

Falkiner, R.J., "Liquefied petroleum gas," *ASTM International*, Glen Burnie, MD, 2003.

NIST Chemistry Webbook, *National Institute of Standards and Technology*, http://webbook.nist.gov/chemistry/, 2004.

Rostrup-Nielsen, J.R., "Catalytic steam reforming," in Catalysis - Science and Technology, **5** (J. R. Anderson and M. Boudart, eds.), Springer-Verlag, Berlin, Heidelberg, 66 p., 1984.

Rostrup-Nielsen, J.R., "Conversion of hydrocarbons and alcohols for fuel cells," *Phys. Chem. Chem. Phys.*, **3**, 283-288, 2001.

Wang, W., S.Q. Turn, V. Keffer, and A. Douette, "Parametric Study of Autothermal reforming of LPG," in Preprint Paper, 227th ACS National Meeting, *Am. Chem. Soc., Div. Fuel Chem.*, **49**(1), 142-143, 2004.

6. Novel Fuel Cell Components

6.1. Objectives

The effort to develop novel fuel cell components included two major activities: a) biocarbons for use in fuel cell bipolar plates, and b) enzymatic bio-fuel cells. Both of these topics are addressed in the following paragraphs.

Biocarbons for use in fuel cell bipolar plates

Graphite is an important component of the bipolar plate assembly that is employed in many fuel cells. Graphite also plays a critical role in many batteries and capacitors. Graphite is desired for these applications because it is an excellent conductor of electricity and it is inert. Unfortunately, because it is inert it is not a good support for catalysts. Likewise, it has a very low porosity and surface area. High surface areas can be desirable for some catalytic applications.

The electrical conductivity of many biocarbons (carbonized charcoal produced from biomass) approaches that of graphite. These biocarbons can be inert. Unlike graphite, biocarbons can possess very high surface areas and easily can be loaded with catalysts. In spite of these attractive features, virtually no attention has been given to the use of biocarbons as replacements for graphite in fuel cell bipolar plates, capacitors, and batteries.

The objective of this work was to characterize the electrical and physical properties of a wide range of biocarbons in order to facilitate their use in improved fuel cell bipolar plates, capacitors, and batteries.

Enzymatic bio-fuel cells

Enzymatic bio-fuel cells (EBFC) are interesting and attractive alternatives that can complement the conventional fuel cell technologies which traditionally use transitional metal oxides or noble metal catalysts for conversion of chemical energy, typically stored in hydrogen, to useful electrical energy. Some of the more promising aspects of the EBFC include:

- Reproduction (via chemical or biological means) – a unique characteristic that conventional Pt-based counterparts lack and a significant advantage for potentially low cost production and unlimited supply. It also promises a solution to overcome degradation on system performance for long-duration applications, especially at remote locations (covert operations, deep ocean deployment, or space travel), where catalysts might be repaired or replenished on site;
- Selectivity – can be designed to react with only certain types of species, and thus, simplify fuel logistics or cell design;
- Tolerance to contaminants – potentially better than Pt;
- Adaptability – can adapt to different environments (e.g., temperature extremes) for optimal operation; and
- Self-assembly. – possibly *in situ* in a biological system to simplify fabrication processes for micro-devices.

This work has been focused on elucidating the fundamentals underlying charge transfer limitations in biological catalysts, and transferring this knowledge into the engineering design of practical *bio-fuel cells*. To reach this goal, the following specific tasks have been pursued for systems employing both gas and liquid phase fuels:

- To establish an array of quantitative characterization techniques, test cells, and modeling capabilities to determine the limitations in the bioelectrocatalysis, and to construct a bio-electrochemical test bed that will allow us to refine such techniques in microbial or enzyme based bioelectrocatalysis operation, and
- To develop a technology base with know-how to improve performance (e.g., catalyst lifetime, current density) with respect to important process variables such as choice of catalyst, choice of mediators, fuel purity, and mode of immobilization (e.g., direct attachment versus entrapment of enzyme).

6.2. Scope of Work and Approach

Biocarbons for use in fuel cell bipolar plates

- Biocarbons were produced by Flash Carbonization™ (FC) from a variety of biomass feedstocks. Dopants and catalytic materials were added to some biomass feedstocks prior to carbonization.
- The electrical resistivity of compact packed beds of the biocarbons was measured as a function of compaction pressure.
- Other properties of the biocarbons were measured by gas sorption analysis, XRD, FTIR, elemental analysis, etc. The effects of these properties on the electrical resistivity of the biocarbons were inferred.
- Small samples of biocarbons were distributed to interested parties for testing and evaluation.

Enzymatic bio-fuel cells

To execute the specific objectives, four specific tasks have been pursued. In *task 1* we developed a number of prototype test cells to characterize negative electrode (anode) performance with or without biological catalysts. The approach taken was to develop a prototype and then to trial it with experiments that used various metal supports and immobilization techniques. In *task 2* we developed a strategy to combine electrochemical characterization and spectrophotometric techniques to evaluate bioelectrocatalytic performance of the negative electrode configurations. The approach taken was to couple the electrochemical measurements with spectrophotometric detection of chemical mediators to measure rates for both electron transfer as well as chemical consumption of fuel. In this manner we were able to characterize the electron transfer efficiency in terms of bound enzyme. In *task 3* we executed trials on a model system using hydrogenase enzyme as the catalyst and compared the performance of our cell against others who have reported similar work with hydrogenase. The approach taken was to immobilize hydrogenase enzyme on various types of carbon and metal supports. The enzyme was sourced from the laboratory of Dr. Michael Adams, a well-established researcher on high temperature hydrogenase enzymes. In *task 4* we applied the results to assist with the design and construction of future test beds for applications using alcohol dehydrogenase. The approach taken in this work was to develop cell designs that continue to improve the use of liquid fuels and permit *in-situ* immobilization of enzyme catalyst in conductive polymers, as well as the full suite of electrochemical and spectrophotometric characterization techniques developed in task 2. In addition, with recognition of the need to improve electrode microstructure in order to enhance catalytic performance, we developed additional *in-situ* materials characterization techniques to allow us to monitor and control the microstructure of the electrode configuration to assist immobilization efficiency. These include the application of high-resolution imaging techniques of scanning electron microscopy (SEM) and Imaging Elipsometry (IE). With respect to the

latter, we believe we are one of the first groups to use IE for the analysis of electrode pore structure.

6.3. Technical Accomplishments

Biocarbons for use in fuel cell bipolar plates

- Our accomplishments prior to 2004 are detailed in a recent paper (Mochidzuki *et al.*, 2003) that is included in Appendix B to this report. In summary we found that many carbonized charcoals conduct electricity nearly as well as graphite powder. These carbonized charcoals can have surface areas that approach 500 m^2/g.

- Carbon materials cannot be shipped by air unless they have been tested and certified according to certain UN test procedures. During 2004 we purchased a furnace and other equipment needed to execute the UN tests, and we developed the necessary procedures to accomplish the tests. Because our biocarbons failed one of the tests, there are some restrictions placed on their shipment by air. Fortunately, because our biocarbons passed all the other tests, these restrictions are not onerous.

- We shipped a dense, non-porous biocarbon to Dr. Ian Towle with Technology Interface in the UK for use in fabricating bipolar plates for PEM fuel cells. Unfortunately, his company is suffering financial problems and will not be able to test our biocarbon sample in the near future. We also shipped a porous, high-surface area biocarbon to Prof. Don Baird (Virginia Polytechnic University) for use in fabricating bipolar plates. He indicated to us that the biocarbon did not perform as well as graphite powder. He was not able to tell us exactly what carbon properties would be desired to improve upon the performance of graphite powder in a bipolar plate.

- We prepared a doped (catalytic) biocarbon by ion exchanging boron (boric acid) into corn cob biomass, and carbonizing the cob. Tests indicate successful ion exchange and the cob carbon was loaded with boron. Further tests are planned. The boron dopant did not change the electrical conductivity of the cob biocarbon (already very high).

- We prepared a very high purity (ash-free) biocarbon from sucrose that may be suitable for use as a high-value carbon "riser" in metallurgical applications.

- We prepared a boron doped (catalytic) biocarbon by mixing boric acid powder with sucrose powder and then carbonizing the sucrose/boric acid mixture. Likewise, we plan to prepare a phosphorous-doped biocarbon by a similar procedure. This procedure easily lends itself to the preparation of biocarbons that include other dopants/catalysts. Further tests are planned to learn about the properties of these doped/catalytic biocarbons.

- We are keenly interested in determining the chemical structure of charcoal and carbonized charcoal biocarbons. Recent literature suggests that biocarbons may include diamond-like regions and/or fullerenes as well as graphitic regions. To gain insight into the structure of biocarbons, we prepared model biocarbons from sugars (e.g., glucose, fructose, inulin) and a Kraft lignin, as well as representative biocarbons from typical biomass (e.g., oak wood, corn cob, and macadamia nut shell). We plan to accomplish detailed analyses of these model biocarbons in collaboration with the Hungarian Academy of Sciences in Budapest and the University of Waikato in New Zealand.

Enzymatic bio-fuel cells

Task 1: Several prototype cells were constructed to deliver gas fuels. Figure 6-1 shows the final version. The mini-gas diffusion cell was designed for immobilization and post-immobilization electrochemical characterization in one vessel, and also for gas diffusive fuel supply (i.e., fto improve hydrogen mass transfer). Hence, it combined the function of previous designs including

both the micro-immobilization and mini cells (not shown). Complete details on the cell can be found in Johnson *et al.* (2005a). The cell was used to characterize performance of a hydrogen fuel cell in which a high temperature hydrogenase was used to oxidize soluble hydrogen.
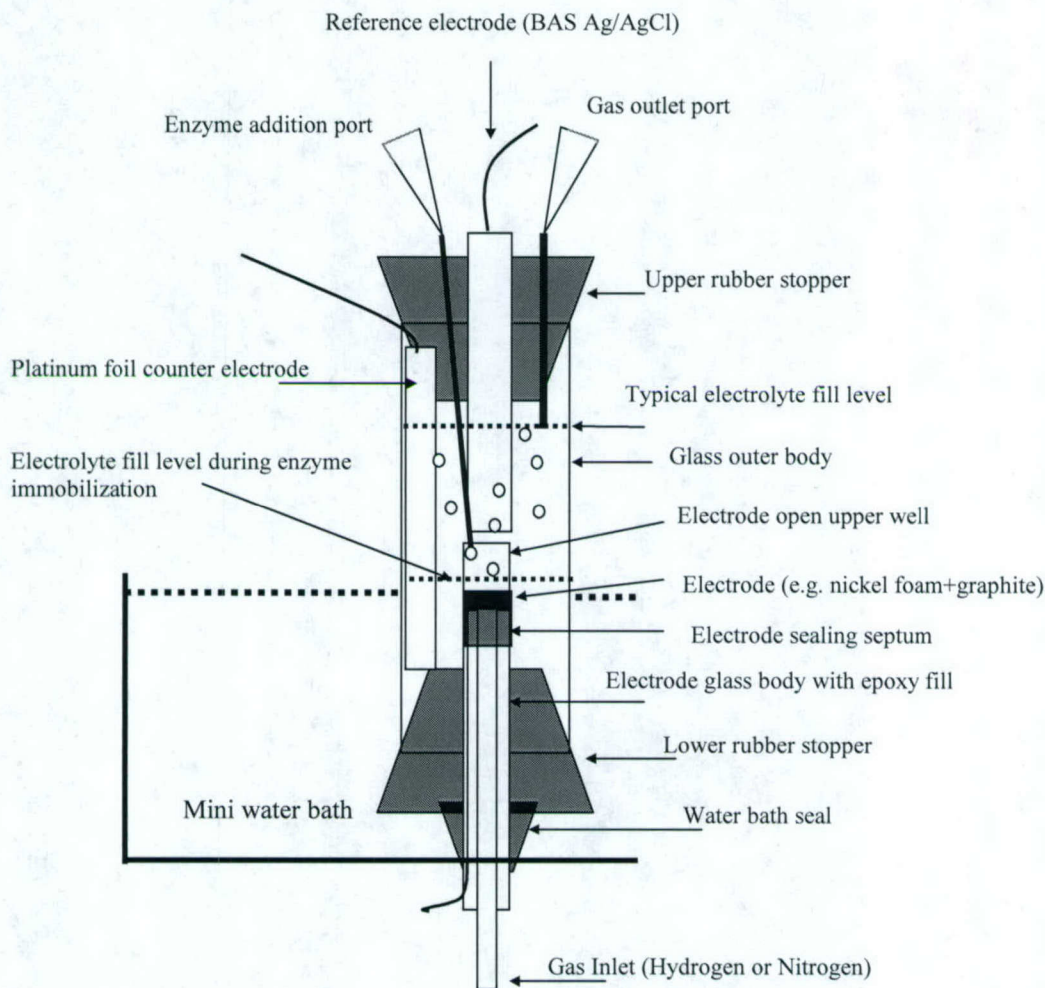
Reference electrode (BAS Ag/AgCl)

Enzyme addition port

Gas outlet port

Upper rubber stopper

Platinum foil counter electrode

Typical electrolyte fill level

Glass outer body

Electrolyte fill level during enzyme immobilization

Electrode open upper well

Electrode (e.g. nickel foam+graphite)

Electrode sealing septum

Electrode glass body with epoxy fill

Lower rubber stopper

Mini water bath

Water bath seal

Gas Inlet (Hydrogen or Nitrogen)

Figure 6-1. Final version of the prototype cell.

Task 2: Potentiostatic DC polarization, dynamic potentiometry, and electrochemical impedance spectroscopy (EIS) were combined with spectrophotometric detection of enzyme activity in order to characterize the electrodes and to differentiate between the relative contributions from enzyme loading, charge transfer, and mass transport to the limiting current density, which we found to be a critical consideration for fuel cell application. In particular, we believe we were one of the first groups to report charge transfer efficiency for bound enzyme. Detailed description of the data and results can be found in Johnson *et al.* (2005a).

Task 3: Through the combined utilization of spectrophotometric detection of enzyme activity, mass transport modeling, and electrochemical characterizations (e.g., potentiometry, DC polarization and electrochemical impedance spectroscopy), a good understanding and characterization of redox enzyme electrode performance (in particular the limits to current density) could be obtained. In particular, we were able to determine immobilization efficiencies, loading density and charge transfer efficiency of bound enzyme, thus elucidating possible mechanisms limiting electrode performance. For example, we were able to distinguish between

total immobilized enzyme (spectrophotometric determination) and that percentage of enzyme that was suitably placed for successful charge transfer (DC polarization, EIS), thus permitting the determination of charge transfer per bound enzyme. This calculation showed, for our systems, that the charge transfer efficiency of bound enzyme was relatively efficient even in the absence of charge mediators, therefore greater bulk enzyme loading immobilization efficiencies were needed to increase current density. Additionally, mass transport modeling combined with DC-polarization data indicated that the current densities achieved were well below the threshold for hydrogen mass transport limitation for the system, suggesting that future electrode development should emphasize the enhancement of immobilization efficiency to increase the current density of the immobilized thermostable hydrogenase electrode. A complete analysis of the hydrogenase fuel cell can be found in Johnson *et al.* (2005a).

Task 4: In task 4 we began the work of developing test cells that permitted *in situ* electrochemical deposition of conductive polymers to metal supports. This switch accommodated liquid fuels and was made because outcomes from *task 3* had highlighted limitations due to gas solubility that questioned the further development of a hydrogen fuel cell using non-metal catalysts. This required the use of enzymes that are not known for their ability to directly transfer electrons to the metal support (as does hydrogenase). As such, conductive polymers that can be electrochemically deposited from solution were embraced as a technique to immobilize the enzyme within a framework that could facilitate the transfer of charge to the metal support. The cell we designed is presented in Figure 6-2. Its key feature is its modular plate design that permits a precise geometry for the working, reference and counter electrodes, as well the potential for continuous flow of fuel into and out of the cell. A full description of this work can be found elsewhere (Johnson *et al.*, 2005b).

Supporting this work, one more characterization technique for estimating the effective diffusion coefficient, to permit estimation of porosity of the immobilization matrix, was developed (Johnson *et al.*, 2005b). Specifically, a mass balance model was developed to estimate reactant concentration at the enzyme surface using bulk concentrations, which could then be measured *in situ* by spectrophotometric detection or *ex situ* by HPLC analysis of acetaldehyde. With this technique the mass transfer characteristics of the porous electrode can be estimated by comparison of experimental data against model predictions of system performance for continuous flow of flow through the system. In practice, an effective diffusion coefficient is calculated and the enzyme kinetic parameters are also evaluated and compared against their values in free solution.
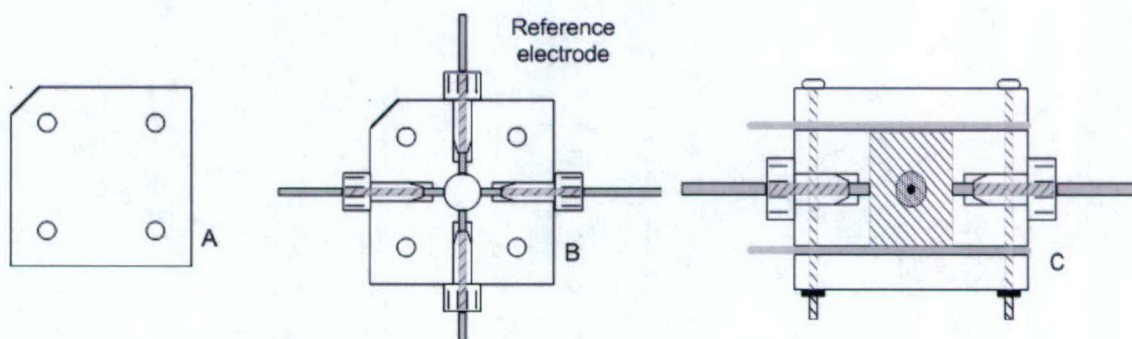

Figure 6-2. Schematic of the micro enzyme fuel cell.

We propose that the technique can be used to quickly screen immobilization protocols and to provide some insight to mass transport of reactants, metabolic byproducts, and electrons. For example, it is possible to estimate the actual V_{max} of the electrode, and hence to quantify the amount of active enzyme available for bioelectrocatalysis. When comparing results between immobilization protocols, the technique also provides a mechanism to test films of different thickness and porosity (as modified through the immobilized technique), provided the films are immobilized with an equal concentration of enzyme and on an electrode of equal surface area.

A paper describing a complete treatment of the method as well as an example application using alcohol dehydrogenase immobilized in the conductive polymer polypyrrole has now been submitted to the journal Enzyme and Microbial Technology (Johnson *et al,*. 2005b).

6.4. Summary of Papers and Presentations Resulting from Efforts

Biocarbons for use in fuel cell bipolar plates

PAPERS

Mochidzuki, K., F. Soutric, K. Tadokoro, and M.J. Antal, Jr., "Electrical and Physical Properties of Carbonized Charcoals," *Ind. Eng. Chem. Res,.* **42**, 5140-5151, 2003. This paper is included in Appendix B.

At least two other papers are now in preparation and will be submitted for publication during 2005 or early 2006.

PRESENTATIONS

Dr. Kazuhiro Mochidzuki presented the material contained in his paper listed above at the 2003 Annual Meeting of the American Institute of Chemical Engineers in Indianapolis.

Enzymatic bio-fuel cells

PAPERS

Cooney, M. J., W.J. Johnston, and B. Y. Liaw, "In situ measurement of effective diffusion coefficients in enzyme immobilized electrodes," submitted to Enzyme and Microbial Technology, 2005.

Johnston, W.A., B.Y. Liaw, R. Sapra, M.W.W. Adams, and M.J. Cooney, "Design and Characterization of Redox Enzyme Electrodes: New Perspectives on Established Techniques with Application to An Extremeophilic Hydrogenase," *Enzyme and Microbial Technology*, **36**: 540 – 549, 2005.

PRESENTATIONS

Liaw, B.Y. F Quinlan, and M.J. Cooney, "Polypyrrole Deposition in Aqueous Solutions: Film Characteristic Dependence on Deposition Conditions," 208th Meeting of the Electrochemical Society, Los Angeles, California, Oct. 16-21, 2005.

Liaw, B.Y., V. Svoboda, and M.J. Cooney, "Morphological Study of Conducting Polymer via Electrochemical Deposition Using Imaging Ellipsometry and RQCM Technique," 208th Meeting of the Electrochemical Society, Los Angeles, California, Oct. 16-21,2005.

Cooney, M.J., B.Y. Liaw, W. Johnston, V. Svoboda, F. Quinlan, and N. Maynard, "Design of macropore structure for enzyme fuel cells operation," Fuel Division: Biofuel cells, 230th ACS National Meeting, Washington, DC, Aug 28-Sept 1, 2005.

Liaw, B.Y., V. Svoboda, F. Quinlan, and M.J. Cooney, "Understanding Conductive Polypyrrole Deposition Via Micro- and Nano-Scale Observations," Division of Colloid and Surface Chemistry, 230th ACS National Meeting, Washington, DC, Aug 28-Sept 1, 2005.

Cooney, M.J., B.Y. Liaw, and W. Johnston, "Comparative effects of reaction kinetics and mass transfer limitation in micro enzyme fuel cell bioreactors," Biochemical Engineering XIV: Frontiers and Advances in Biotechnology, Biological and Biomolecular Engineering, Harrison Hot Springs, BC, Canada, July 10-14, 2005.

Liaw, B.Y., M.J. Cooney, F. Quinlan, V. Svoboda, and N. Maynard, "Engineering Effective Bioelectrocatalysis Electrodes for Power Generation," Second International Conference on Polymer Batteries and Fuel Cells (Fuel Cells), Las Vegas, Nevada, June 12-17, 2005.

Cooney, M.J., W. Johnston, and B.Y. Liaw, "Modeling the relative contribution of mass transfer limitation on performance in enzyme fuel cells," 207th Meeting of the Electrochemical Society, Quebec City, Canada, May 15-20, 2005.

Quinlan, F., M.J. Cooney, and B.Y. Liaw, "Investigation of polypyrrole morphology with different deposition conditions," 207th Meeting of the Electrochemical Society, Quebec City, Canada, May 15-20, 2005.

Johnston, W. A., M.J. Cooney, and B. Y. Liaw, "Evaluating adsorption and charge transfer of redox enzymes bound to carbon support," 204th Meeting of the Electrochemical Society, Orlando, Florida, July, 2003.

6.5. References

Biocarbons for use in fuel cell bipolar plates

Mochidzuki, K., F. Soutric, K. Tadokoro, and M.J. Antal, Jr., "Electrical and Physical Properties of Carbonized Charcoals," *Ind. Eng. Chem. Res.,* **42**, 5140-5151, 2003. This reference is included in Appendix B.

Enzymatic bio-fuel cells

Johnston, W., M.J. Cooney, B.Y. Liaw, R. Sapra, and M.W.W. Adams, "Design and characterization of redox enzyme electrodes: new perspectives on established techniques with application to an extremophilic hydrogenase," *Enzyme and Microbial Technology*, **36**: p. 540 - 549, 2005a.

Johnston, W., M.J. Cooney, and B.Y. Liaw, "Modeling the relative contribution of mass transfer limitation on performance in enzyme fuel cells," 207th meeting of the Electrochemical Society, Quebec City, Canada, 2005b.

APPENDIX A

HFCTF Phases of Construction

The following pages present a series of photographs documenting phases of construction of the Hawaii Fuel Cell Test Facility.
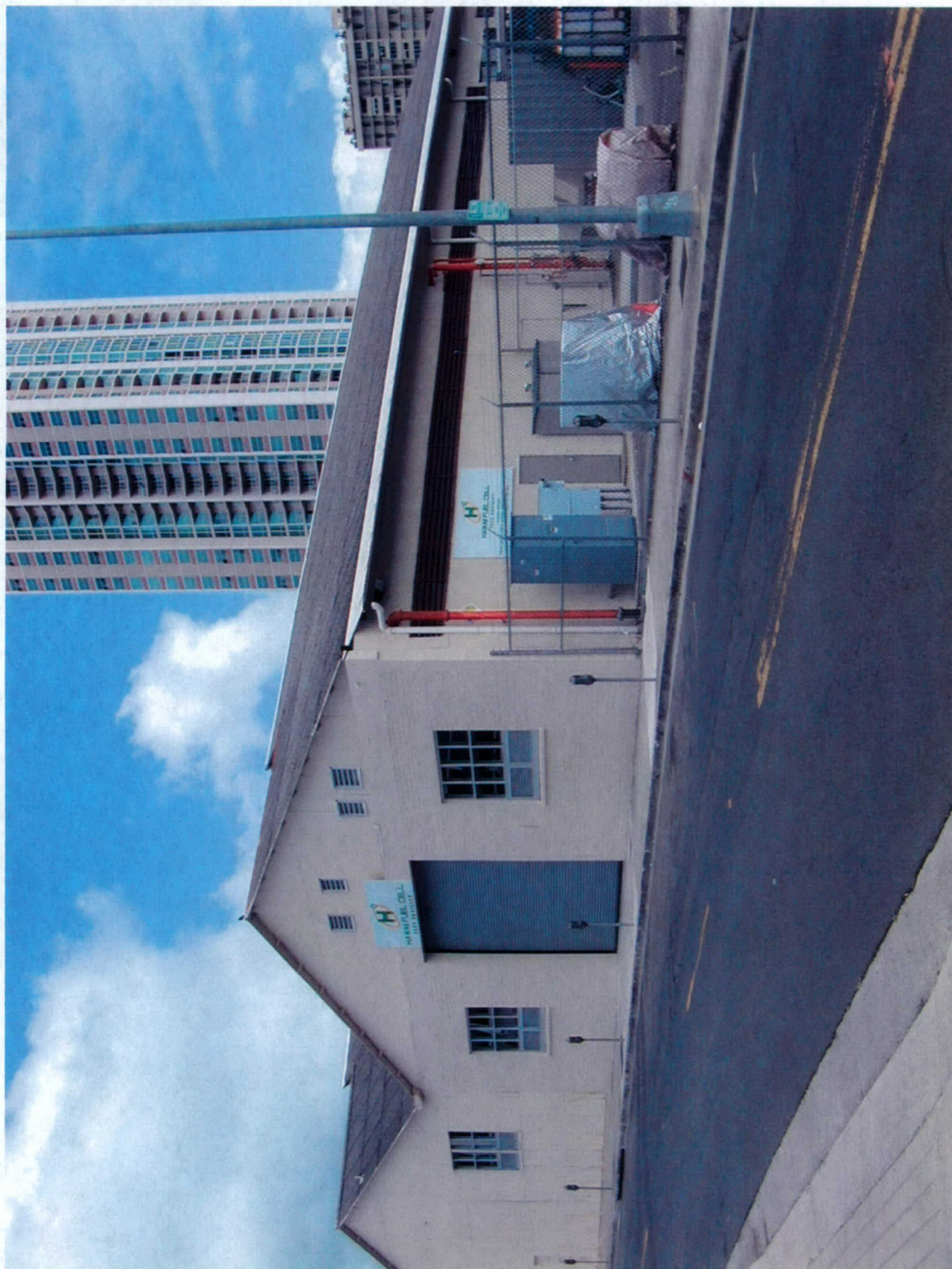
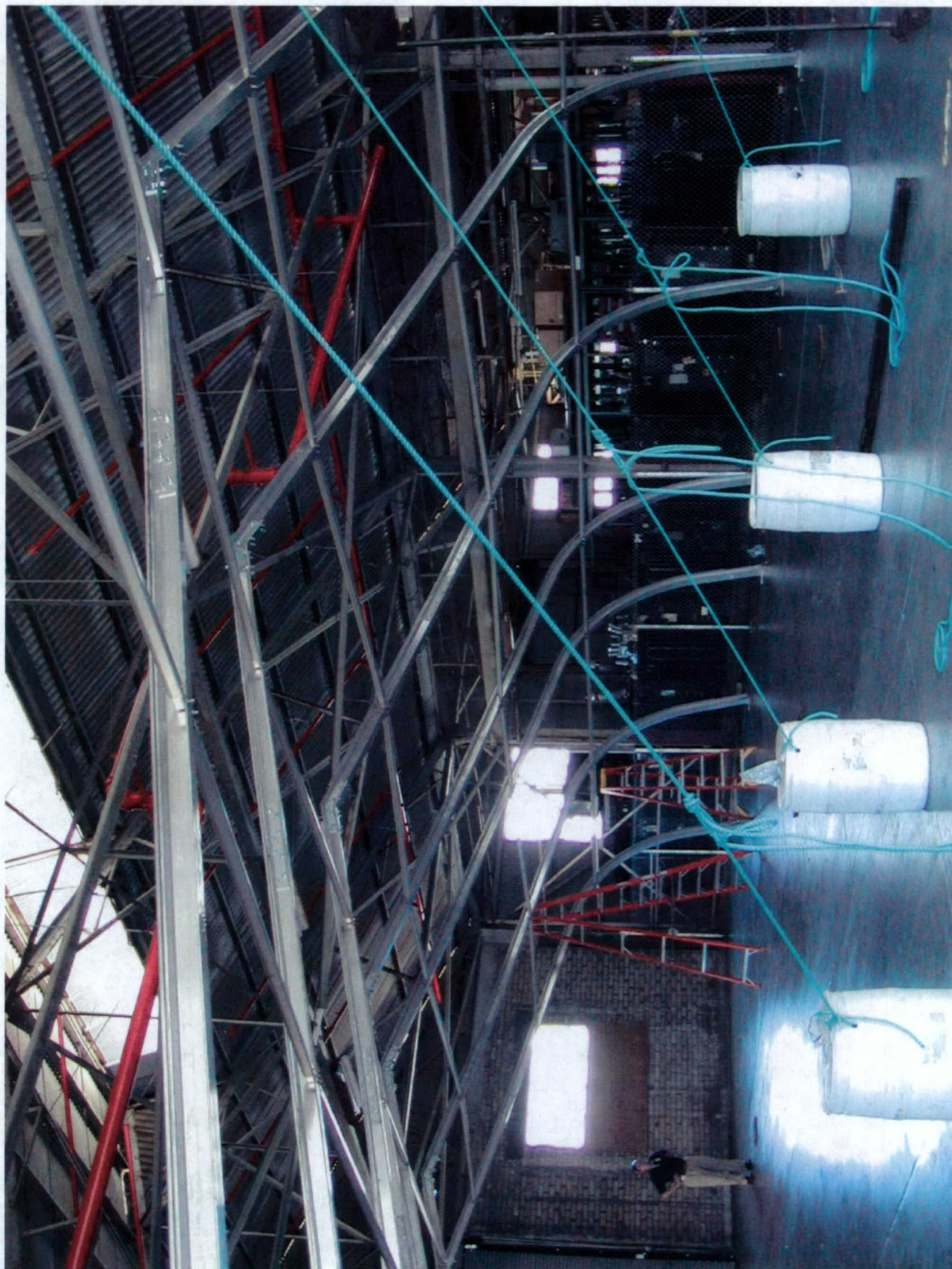Figure A-1. External view of facility from Cooke Street.

HNEI

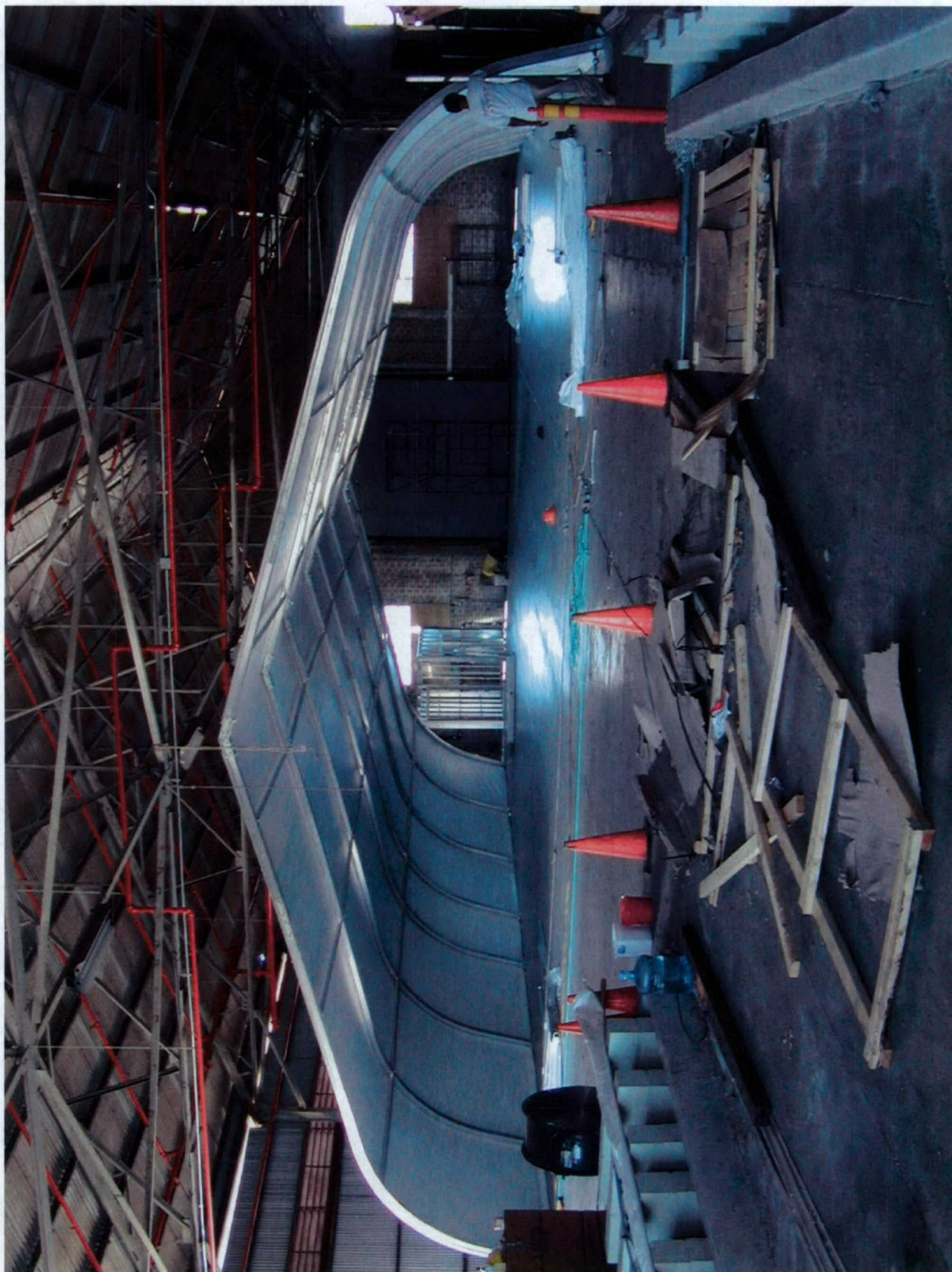Figure A-2. Framing the sprung structure within the warehouse.

HNEI

Figure A-3. The 'building inside the building' taking shape.

75

Figure A-4. Gas storage area outside the facility.

HNEI

Figure A-5. Secured hydrogen storage area outside the facility.

77

HNEI

Figure A-6. Stuart Energy electrolyser outside the facility.
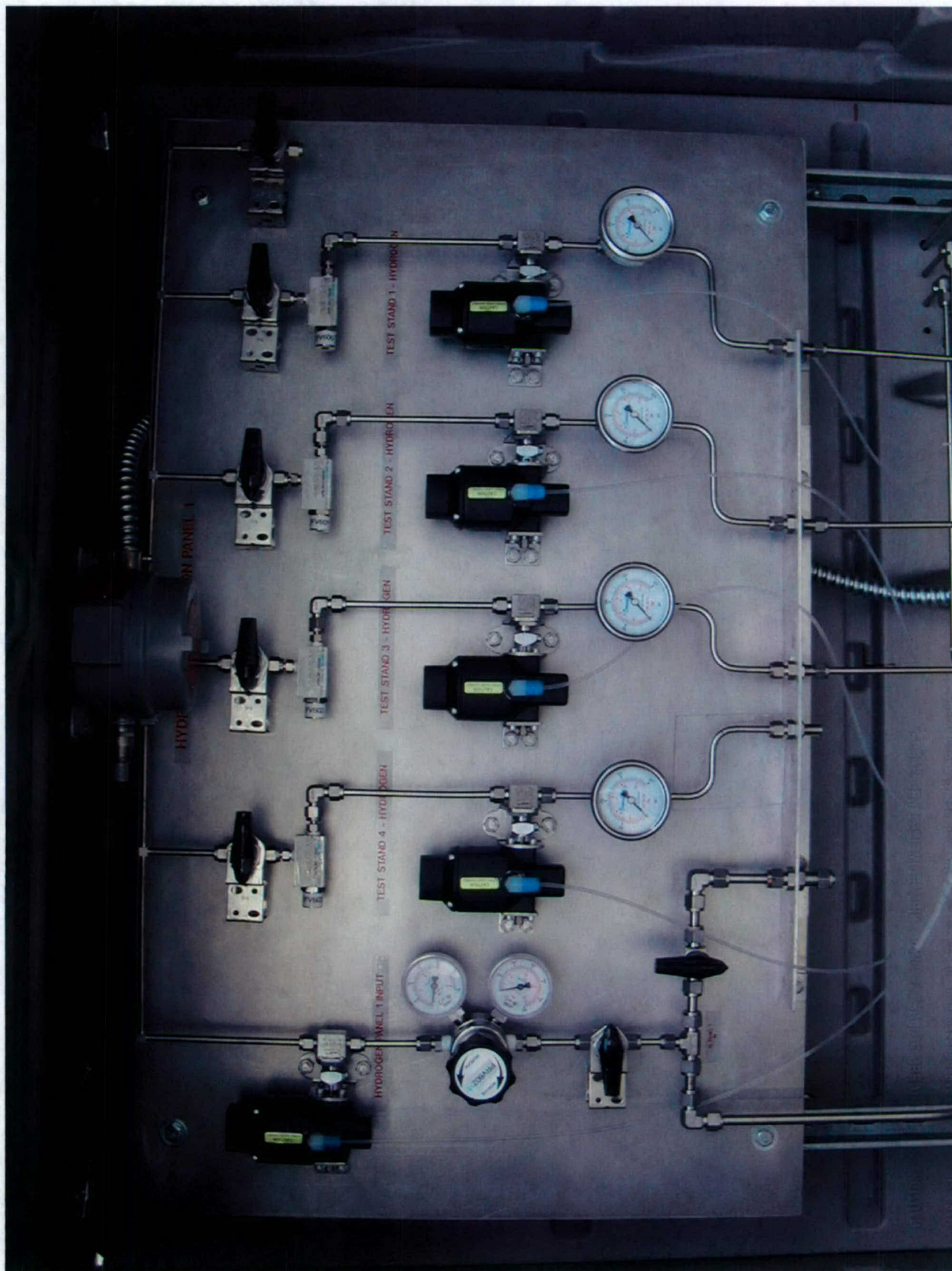
78

HNEI

Figure A-7. Hydrogen gas control panel.

79

HNEI

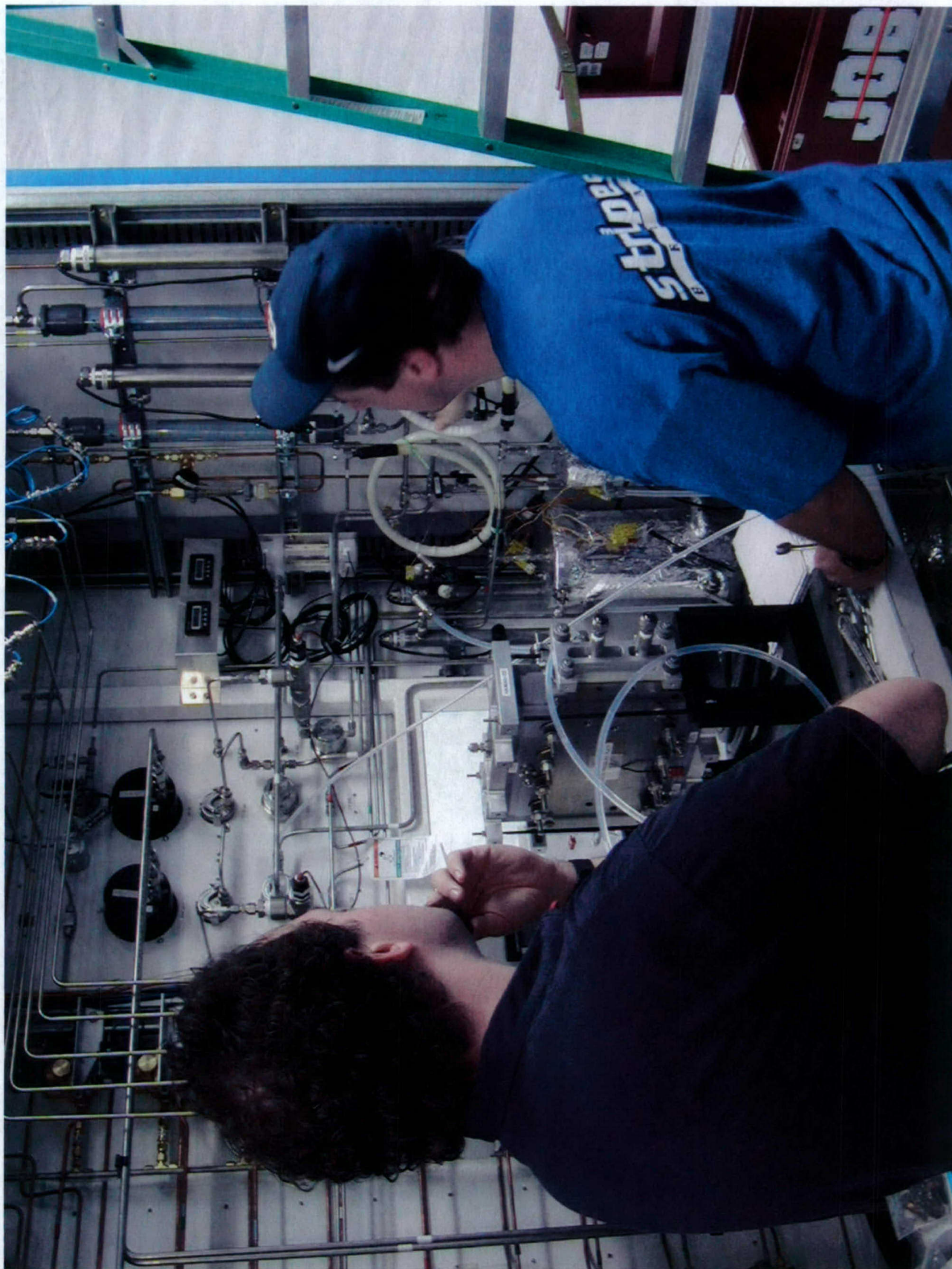Figure A-8. Fuel cell test stand entering the facility.

HNEI

Figure A-9. Installation checkout of fuel cell test stand.

81

HNEI

Figure A-10. Outreach activity: display of facility to tour group.

HNEI

APPENDIX B

Reference: Mochidzuki *et al.*, 2003

The following pages present the complete reference for Section 6. Novel Fuel Cell Components, Subsection on Biocarbons for use in fuel cell bipolar plates:

Mochidzuki, K., F. Soutric, K. Tadokoro, and M.J. Antal, Jr., "Electrical and Physical Properties of Carbonized Charcoals," *Ind. Eng. Chem. Res.* **42**, 5140-5151, 2003.

Electrical and Physical Properties of Carbonized Charcoals

Kazuhiro Mochidzuki, Florence Soutric, Katsuaki Tadokoro, and
Michael Jerry Antal, Jr.*
Hawaii Natural Energy Institute, University of Hawaii at Manoa, Honolulu, Hawaii 96822

Ma´ria To´th
*Research Center for Earth Sciences, Laboratory for Geochemical Research, Hungarian Academy of Sciences,
Budao¨rsi u´t 45, Budapest 1112, Hungary*

Borba´la Zelei and Ga´bor Va´rhegyi
*Chemical Research Center, Research Laboratory of Materials and Environmental Chemistry,
Hungarian Academy of Sciences, P.O. Box 17, Budapest 1525, Hungary*

Because coal does not conduct electricity and graphite is costly and inert, little attention has been given to the development of a carbon fuel cell (i.e., a battery that utilizes a consumable carbon anode to generate electrical power). In this work we show that a packed bed of carbonized charcoal particles subject to a compressive pressure (ca. 8 MPa) can be a good electrical conductor $\sigma < 0.2$ Ωcm). Low electrical resistivities σ are manifest by many different charcoals after carbonization at a heat treatment temperature (HTT) of 950 °C. The 5 orders of magnitude decrease in the electrical resistivity of charcoal with increasing HTT from 650 to 1050 °C is not associated with any dramatic change in the carbons' X-ray diffraction spectrum, its Fourier transform infrared spectrum, or its elemental analysis. Our findings cause us to visualize carbonized charcoal to be a macromolecular, cross-linked, three-dimensional, aromatic structure replete with conjugation and π bonds that facilitate the movement of electrons, as well as nanopores, and micromolecular cracks. Because charcoal powder is competitive in price with fossil fuels and because carbonized charcoal is extremely reactive with a volumetric energy density (in a compacted packed bed) comparable to conventional liquid fuels, compact packed beds of carbonized charcoal hold promise for use as electrodes and consumable anodes in fuel cells. The packed-bed apparatus we describe is a prototype anode for use in a biocarbon fuel cell.

Introduction

Carbon batteries played an important role in the history of fuel cell research. Sixteen years after Grove[1] demonstrated an "electrolyte gas cell" that gave an open-circuit EMF of about 1 V between H_2 and O_2, Becquerel attempted to build a fuel cell that consumed coal.[2,3]

Unfortunately, the electrolyte contained a nitrate that attacked the carbon without producing a current. Later Jablockoff[2,3] tested an apparatus modeled on a similar concept. By the end of the 19th century, the increasing demand for electric power began to consume considerable amounts of coal because the conversion efficiency was low (3%).[1] Contemplating this problem, in 1894 Ostwald[1] called for development of a fuel cell that would react carbon with oxygen to produce electricity more efficiently than thermomechanical equipment. Two years later in Boston, Jacques[1] demonstrated a 1.5-kW battery that employed a consumable carbon anode, an iron cathode, and an air-bubbled alkali hydroxide electrolyte to generate 0.9 V at 400-500 °C. Operating intermittently, this battery delivered power with an overall efficiency of 32% during a 6-month period. The experiment failed because carbonates accumulated in the electrolyte that halted the electrochemistry.[1] In 1904 Haber and Bruner[1] showed that the Jacques carbon fuel cell actually involved the production of hydrogen as an intermediate in the electrochemistry. However, Haber was unable to build a practical carbon fuel cell. In 1937 Baur and Preis[3] tested a fuel cell that used a coke anode and an electrolyte composed of zirconia stabilized with magnesia or yttria at >1000 °C. Vielstich explains that the high temperature was needed because of the low

reactivity of the carbon fuel.[1] No practical carbon fuel cells resulted from the work of Baur and Preis.

Interest in carbon fuel cells resurfaced during the 1970s, when the Stanford Research Institute (SRI) attempted to develop a coal-based fuel cell that employed molten lead at temperatures of 500-900 °C.[4,5] This work was abandoned in 1981. Recently, Scientific Applications and Research Associates[6] reported progress in further developing the SRI concept. At Stanford University, Gur and Huggins[7] demonstrated a high temperature (725-955 °C) fuel cell that employed stabilized zirconia as a solid electrolyte and a graphite anode. To the best of our knowledge, these recent developments have not led to the demonstration of a practical carbon fuel cell. Summarizing the status of carbon fuel cells, Bockris and Srinivasan[3] concluded that carbon fuel cells are impractical because (i) coal is not an electrical conductor and (ii) graphite is too scarce and expensive to be used as a fuel. Thus, the history of carbon fuel cell research suggests that the chief obstacles to the development of a biocarbon fuel cell are the electrical conductivity of the biocarbon, its cost, and its reactivity.

It has been known for centuries that biocarbons can possess very high electrical conductivities. In 1810 carbonized charcoal electrodes were used in an arc lamp, and in 1830 carbonized charcoal was used as an electrode for primary batteries. These electrodes were made from powdered charcoal or coke bonded with sugar syrup or coal tar, pressed, and carbonized.[8] Recently, Coutinho, Luengo, and their co-workers[9-11] reported extensive studies of biocarbon electrodes

manufactured from charcoal particles bonded together by wood tar and subsequently carbonized. The measured electrical re-sistivity of the electrode fell to 10^{-2} Ωcm for carboniza-tion at temperatures above 900 °C. This background suggests that carbonized charcoal could be used to fabricate the consumable anode of a carbon battery. Furthermore, we remark that charcoal can be produced from biomass inexpensively in yields that approach the theoretical limit.[12-15] Carbonized charcoal is also easy to store, and an established infrastructure exists to deliver charcoal to consumers worldwide. Moreover, carbonized charcoal, unlike graphite, is extremely reactive.[14,16-19] For these reasons we have a keen interest in the development of biocarbon fuel cells. The first step is to establish baseline data for the electrical properties of carbonized charcoal electrodes. In this paper we present data that describe the effects of increasing carbonization temperature on the properties of carbonized charcoal particles, including their electrical resistivity in a packed bed subject to compressive force, their chemical and physical composition as determined by elemental analysis, Fourier transform infrared (FTIR), and X-ray diffraction (XRD) spectra, and their surface area. We focus on a carbonization temperature of 950 °C because earlier work has proven the high reactivity of this biocarbon.[16-19] The packed-bed apparatus employed in this work is now being used as the anode of a biocarbon fuel cell, whose performance will be the subject of future papers.

Apparatus and Experimental Procedures

The raw biomass materials that served as substrates to produce the high-yield charcoals employed in this study were obtained as representative grab samples in Hawaii. The high-yield[12-14] and flash carbonization[15] charcoals were produced according to procedures described in earlier publications.[13,15]

Carbonization Procedures. A tubular furnace (Applied Test Systems 3210) with temperature control (Applied Test Systems XT-16), which can reach temperatures as high as 1200 °C, was employed to carbonize the high-yield charcoal samples. A quartz tube (122 cm length and 1.99 cm i.d.) was placed within the furnace and used to carbonize a measured amount of charcoal in a ceramic boat. By location of type K thermocouples in the boat, it was possible to accurately measure the heat treatment temperature (HTT) of the charcoal. UHP nitrogen gas was delivered at 1.0 L/min to the tube during the carbonization process, thereby ensuring that the carbonization process, including the heat-up and cool-down steps, occurred in an inert environment. In a few cases, charcoals were carbonized within a closed crucible in a muffle furnace (Barnstead Themolyne FB1215M). This procedure was employed in our earlier work[13] and is able to carbonize larger quantities of charcoal more conveniently than the tubular furnace. Unfortunately, several weaknesses accompany the use of a muffle furnace. First (and perhaps foremost), the muffle furnace thermocouple (TC) reports its own tem perature, which is neither the temperature of the furnace nor the temperature of the carbon within the closed crucible. Our studies indicate that the muffle furnace TC reports a temperature about 30-40 °C higher than the temperature of the outer surface of the ceramic crucible.

The measurement of the carbon temperature within the closed crucible is not easy; consequently, we do not know how large of a temperature gradient exists between the outer surface of the crucible and the center of the carbon bed in the closed crucible. Second, the lid of the crucible leaks a little air; consequently, the carbonization is not accomplished in a truly inert environment.

FTIR Analyses. The FTIR spectra were measured by a FTIR spectrometer system (Perkin-Elmer 1710), including a DTGS (deuterated triglycine sulfate) detector, DRIFT accessory, and microsampling. The specimens were examined in powder form, using KBr as the reference material. The spectra were recorded from 4400 to 400 cm^{-1} by averaging 100 scans at 4-cm^{-1} resolution.

XRD Analyses. XRD measurements were carried out for phase and crystal structure identification with a Philips PW1710 diffractometer using Cu KR radiation and a graphite monochromator (45 kV, 35 mA, and divergence 1°). Average crystallite size (L_{002}) and deformation (lattice strain, ε) were determined from singleline profile Fourier (Voigt method) analysis.[20-22]

Brunauer-Emmett-Teller (BET) Surface Area and Total Pore-Volume Analyses. An automatic gas sorption analyzer (Quantachrome Aurosorb-1) was used to determine the specific surface area and total pore volume of the carbonized charcoals. After a vacuum outgas step at 483 K for 4 h, the nitrogen-adsorption isotherm was measured at liquid-nitrogen temperature (77 K). The BET method was employed to determine the surface area from a limited linear region of the adsorption isotherm, usually $0.05 < P/P_0 < 0.35$. The total pore volume was calculated from the amount of nitrogen adsorbed at a relative pressure close to unity ($P/P_0 > 0.99$). To validate our surface area determinations, we measured the surface area of a commercial Barnebey and Sutcliffe (B&S) coconut shell activated carbon (AC). Our result (1201 m^2/g) was close to the value reported by B&S (1106 m^2/g) for bulk samples.

Electrical Resistivity. The electrical resistivity of the biocarbon samples was determined by a two-probe packed-bed technique at room temperature (ca. 20 °C). As shown in Figure 1, the nickel electrodes at the top and bottom of the 1.9-cm-diameter packed bed, contained in an alumina tube, enable measurement of the electrical resistance of the bed. The packed bed is compressed by the upper electrode, which is forced against the bed by a pneumatic piston. Note that the electrodes are insulated from the apparatus by Teflon and alumina. The electrical resistance of the packed bed is measured with a precision, hand-held milliohmmeter (ISOTK M210). This meter has a resolution of 0.001 Ω from 0 to 1.990 Ω, a resolution of 0.01 Ω from 1.99 to 19.90 Ω, and a resolution of 0.1 Ω from 19.9 to 199.9 Ω. Our setup mimics the apparatus originally employed by Mrozowski[23] in his pioneering work but was designed to enable its future use as the anode of a carbon fuel cell. The resistivity, ρ in ohm centimeters, is given by the equation $\rho = RA/l$, where R, A, and l are the measured resistance in ohms, cross-sectional area of the bed in square centimeters, and length between the probes in centimeters, respectively. Note that the measured length (i.e., the offset of the piston in Figure 1 relative to its
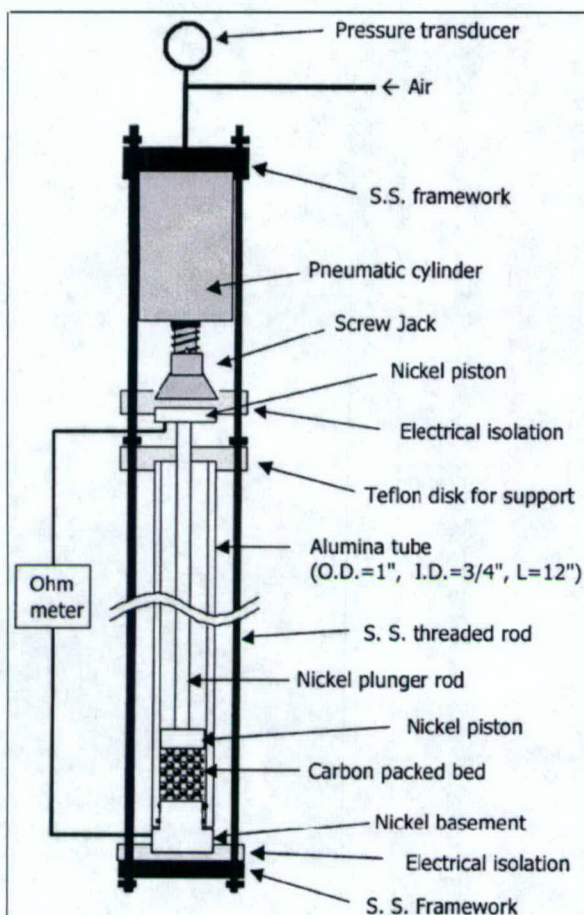
Figure 1. Apparatus employed to measure the electrical resistivity of a packed bed of carbonized charcoal.

empty bed position) is not the exact length l of the bed because of the compression of the nickel electrode and the stretching of the stainless steel threaded rods that results from the compressive force applied to the packed bed. To account for these effects, we measured the change in the apparent length of an empty bed (i.e., zero offset length) over the range of applied pressures used in this work (see Figure 2). After an initial small, nonlinear change in length (due to slack in the system), the change in the zero offset length was linear with pressure. The Hook's law slope of the line (-3.23 $\times$ 10⁻³ cm/MPa) displayed in Figure 2 is nearly identical with the theoretical value (-3.34 $\times$ 10⁻³ cm/MPa) calculated using Young's moduli of Ni 200 and SUS 316 and the appropriate geometric factors for the elements of the cell under compression and tension. We used the Hook's law formula to correct the zero offset value of the instrument, and this correction resulted in a decrease in the calculated values of the packed bed's resistivity and its bulk density. Higher compressive pressures and shorter bed lengths had a bigger impact on this correction. In the case of a compressive pressure of 9.5 MPa and a bed length of 0.1 cm, the correction resulted in a ca. 35% decrease of the measured resistivity and the apparent bulk density of the packed bed.

Finally, we remark that we easily detected the Seebeck voltage (created by temperature differences between the two biocarbon-nickel interfaces[24-26]) when the ceramic tube, containing compressed carbonized charcoal, was heated to temperatures above 29 °C. As expected, no
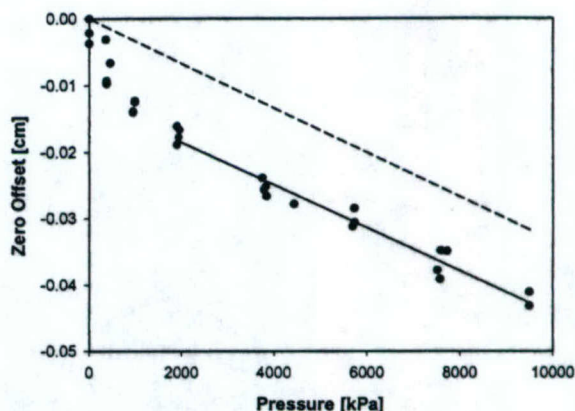

Figure 2. Effect of compressive pressure on the zero offset of the measured bed height. Zero offset values calculated by Hook's law (- -). Measured zero offset values (b).

thermoelectric effect was observed when the apparatus was unheated and in thermal equilibrium at room temperature.

Results

Unless noted otherwise, the carbons listed in Table 1 were prepared in the tubular furnace at the indicated HTT with a soak time of 10 min. Typically two to three boat lots were needed to produce enough carbonized charcoal for subsequent analyses. As expected, the mass loss of the macadamia nut shell (macshell) charcoal increased monotonically with increasing HTT, except for the 1050 °C sample that was produced from a sample of flash carbonization charcoal with a much lower volatile matter content. The elemental analyses of these carbons showed a scattered progression from 87.9 to 95.13 wt % carbon with increasing HTT accompanied by concomitant decreases in the H and O contents of the samples. The high ash content of the 850 °C carbon must represent inhomogeneities present in the charcoal samples. Recall that the 1050 °C carbon was derived from a different macshell charcoal sample than the other carbons, and this might explain its high nitrogen content. Values of the H/C and O/C ratios of the macshell carbons (see Table 2) decreased monotonically, except for the 950 °C sample. Of the remaining carbons listed in Tables 1 and 2, the Leucaena wood carbon resembles the Kukui nut shell carbon (except for their respective ash contents). A comparison of the 950 °C carbons reveals a considerable range in the values of each of the properties listed in Tables 1 and 2.

FTIR Analyses. The FTIR spectra of the macshell carbons prepared at 650-850 °C are displayed in Figure 3. For comparison, the spectrum of the macshell charcoal substrate and that of a Sigma-Aldrich synthetic graphite are also indicated. Note that all spectra are displayed on a linear absorbance scale and each curve is drawn one unit higher than the one beneath it. This approach facilitates the comparison of the relative intensities of the spectra. Weak features at about 2350 cm⁻¹ belong to CO_2 absorption of air. H_2O adsorbed on the KBr reference material gives weak, broad, inverse bands at about 3400 and 1630 cm⁻¹ in the spectra of the carbons. There is a weak and sharp absorption band at about 1378 cm⁻¹ originating from a KBr impurity.

Table 1. Carbonized Charcoals Employed in This Work

feed	HTT,[b] °C	burnoff,[c] wt %	surface area,[d] m2/g	pore volume, mL/g	elemental analysis,[a] wt %					
					C	H	O	N	S	ash
macshell[e]	650	21	216	0.135	87.90	2.19	6.69	1.04	0.05	1.17
	750	22	169	0.115	90.71	1.63	5.97	0.95	0.05	1.12
	850	30	194	0.132	90.03	0.89	5.66	1.00	0.06	4.51
	950	32	244	0.164	89.98	0.90	6.04	1.11	0.05	1.61
	1050	22	NA	NA	95.13	0.37	2.82	1.43	0.05	1.07
Kukui nut shell[f]	950	NA[g]	22	NA	92.92	0.54	4.52	1.26	<0.05	1.49
coconut husk[h]	950	NA	437	NA	85.08	0.72	8.39	0.91	0.05	5.63
Leucaena wood[i]	950	NA	310	NA	92.15	0.46	3.99	1.15	0.05	2.45

[a] Measured by Huffman Laboratories, Inc. [b] Heat treatment temperature. [c] Mass loss during carbonization. [d] BET surface area.
[e] High- yield charcoal 961205 except at 1050 °C, which was flash carbonization charcoal 020510. [f] High-yield charcoal 941114. [g] NA = not available. [h] High-yield charcoal 941202. [i] High-yield charcoal 940721.

Table 2. H/C and O/C Ratios[a] for the Carbonized Charcoals Employed in This Work

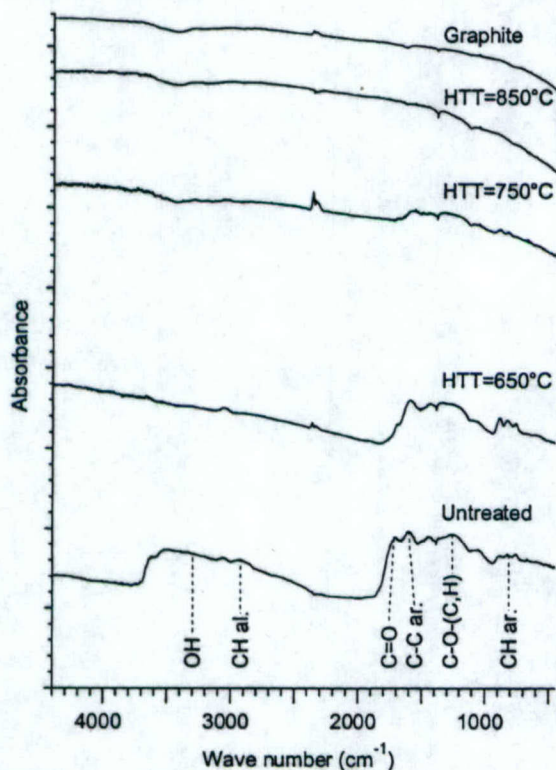| feed	HTT, °C	H/C	O/C
macshell	650	0.2969	0.0571
	750	0.2141	0.0494
	850	0.1178	0.0472
	950	0.1192	0.0504
	1050	0.0463	0.0223
Kukui nut shell	950	0.0693	0.0365
coconut husk	950	0.1008	0.0740
Leucaena wood	950	0.0595	0.0325

a Ratios on a mole basis.

Figure 3. Effect of HTT on the FTIR spectra of macshell char. The spectrum of the synthetic graphite is shown for comparison. (Each curve is drawn one unit higher than the curve beneath it.)

As expected, the macshell charcoal has an alkyl aromatic structure with many oxygen-containing (C-O-H, C=O, and C-O-C) functional groups that give rise to characteristic bands in the infrared spectrum.[27] During carbonization, these functional groups are destroyed. At 650 °C, the O-H groups (3700-2000 cm⁻¹), the aliphatic C-H groups (3000-2800 cm⁻¹), and in a great part the C=O groups (~1700 cm⁻¹) decompose, and condensed aromatic structures form with characteristic C-H out-of-plane bending modes (three main band components) between 900 and 700 cm⁻¹. These findings corroborate earlier thermogravimetry-mass spectrometry (TG-MS) studies of the carbonization of macshell charcoal.[27,28] The TG-MS data revealed major peaks associated with the evolution of H_2O, CH_4, CO, and CO_2 below 650 °C. At 750 °C, most of the aromatic C-H groups were lost. This loss corresponded to a TGMS peak in the evolution of H_2 at about 750 °C. A weak C-H absorption remains at about 880 cm⁻¹. It is assigned to lone H atoms at the edges of the condensed aromatic sheets.[29] A weak, broad band with some subbands can be observed between 1700 and 1000 cm⁻¹ as a result of the skeletal stretching and bending modes of aromatic structures containing residual O and/or N heteroatoms. At 850 °C, the intensity of this weak, broad feature further diminishes and so does the aromatic C-H (~880 cm⁻¹) band.

With increasing carbonization temperature between 650 and 850 °C, the overall intensity of the infrared spectrum decreases along with the loss of functional groups. The baseline in the spectra of the carbonized charcoals is shifted upward. This baseline shift (increasing diffuse absorption) is assigned to low-energy electron excitations of condensed aromatic structures. It is a well-known phenomenon in carbonized coal spectra.[29] Graphite has no characteristic infrared band(s) in the investigated spectral region, and the FTIR method is not sensitive to long-range ordering during graphitization.[30] Graphitization can be followed by Raman spectroscopy;[31] however, the best method is XRD[32] (see below).

All of the carbons obtained from the macshell, Leucaena, coconut husk, and Kukui nut shell charcoals with HTT of 950 °C show spectra very similar to each other as well as to the spectrum of graphite (see Figure 4). Leucaena has the highest N content, but the spectra

of carbons obtained from this precursor do not show significant differences from the spectra of other carbons in the region of the C=N and C-N stretching bands between 1700 and 1000 cm^{-1}. Small differences in the
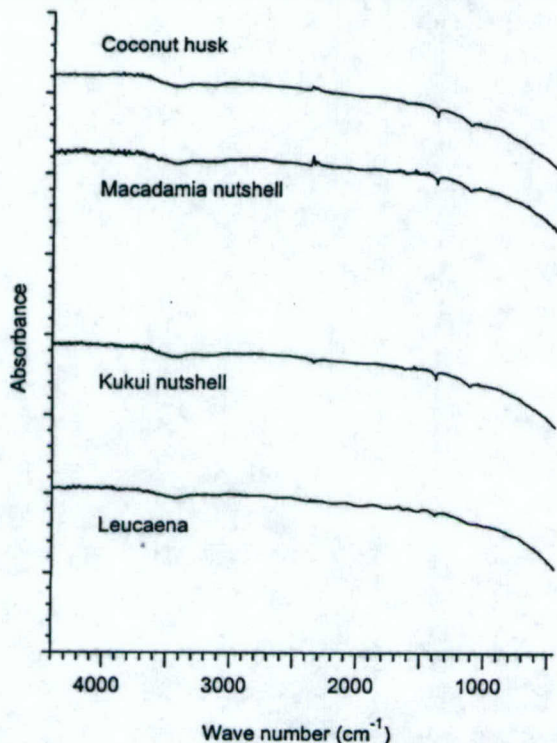

Figure 4. FTIR spectra of carbons treated at 950°C. (Each curve is drawn one unit higher than the curve beneath it.)

baseline positions and shapes probably represent particle size and scattering effects rather than electron mobility changes. These effects hardly can be eliminated from the DRIFT spectra of the carbonized charcoals and graphite.

XRD Analyses. For reference, Figure 5 displays XRD spectra of synthetic and natural graphite samples. Figure 6 displays spectra of macshell charcoals carbonized at increasing temperatures. Unexpectedly, the XRD spectra undergo almost no visible change with increasing HTT above 750 °C. Table 3 demonstrates this observation. The scattering domains of the macshell carbons contain only two or three layers in the 002 direction.[33-37] Small increases in both L_{002} and ε indicate some increase of ordering as a function of HTT in the macshell experiments. The estimated aromaticity γ_a [34,37] of the domains does not significantly increase with HTT
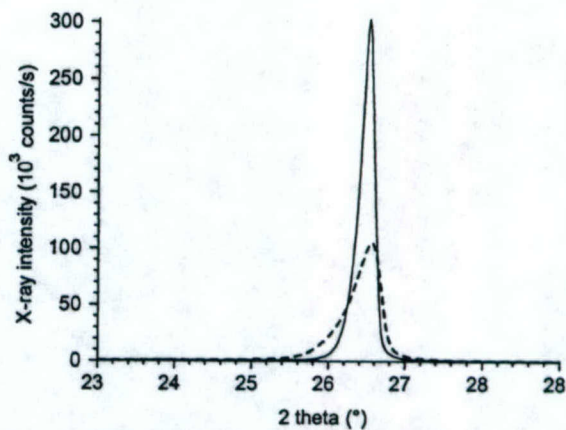

Figure 5. XRD spectra of a natural (-) and a synthetic (- - -) graphite, used as references.
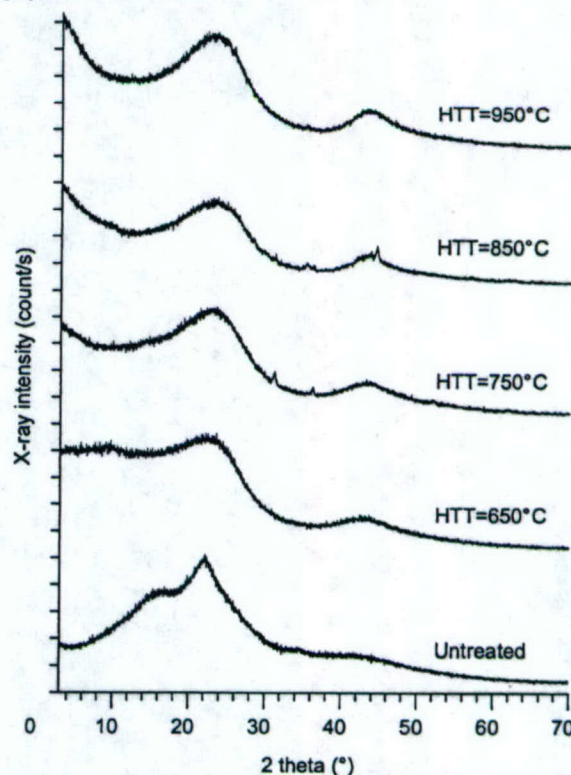

Figure 6. Effect of the HTT on the XRD spectra of the macshell carbon.

Table 3. Results of the XRD Analyses

feed	HTT, °C	fwhm,[a] deg (2θ)	$L002$,[b] Å	ε,[b] %	d(002),[c] Å	γ_a [d]
macshell		8.69	6	19.2	4.01	0.74
	650	8.44	7	17.9	3.98	0.79
	750	7.98	7	16.8	3.87	0.96
	850	7.78	8	16.3	3.79	0.97
	950	7.77	8	16.3	3.76	0.99
Kukui nut shell	950	8.01	7	16.9	3.85	0.99
coconut husk	950	9.67	6	22.8	3.89	0.99
Leucaena wood	950	8.66	6	18.7	3.83	0.99
synthetic		0.45	233	0.8	3.35	1.00

graphite

natural graphite	0.18	918	0.3	3.36	1.00

a fwhm: width at the half peak height of reflection (002). *b L002*
and ε: average crystallite size and deformation (lattice strain) determined from single-line profile Fourier (Voigt method) analysis. *c* d(002): distance between crystallite planes in the 002 direction. *d* ça: aromaticity factor (see text).

above 750 °C. Figure 7 displays the XRD spectra of the 950 °C carbonized charcoals. These spectra are similar, except for the presence of small peaks that arise from the presence of inorganic species (mineral impurities) in the carbon. The broad, featureless peaks displayed in Figure 7 bear little resemblance to the broad peak at $2\theta = 25°$ associated with the XRD spectra of a turbostratic carbon (Monarch 71) displayed in Figure 5 of Walker and Seeley,[38] the heat-treated coals and petroleum coke displayed in Figure 4 of Senneca et al.,[39]
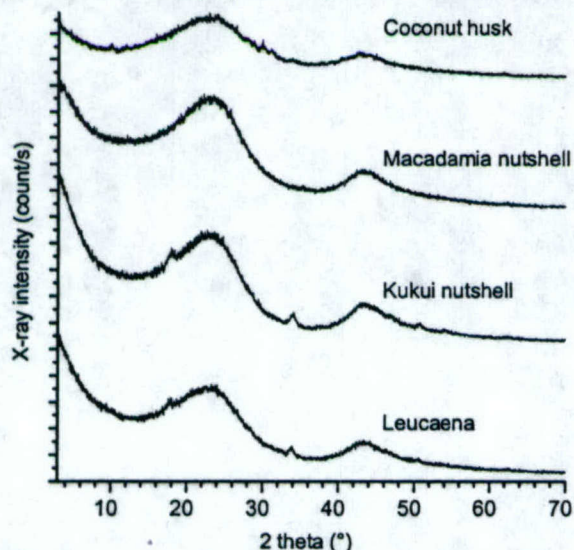

Figure 7. Comparison of the XRD spectra of charcoals carbonized at 950°C.

or the sharp peaks associated with heat-treated Australian black coals reported by Lu et al.[37] As indicated in Table 3, the scattering domain of these carbons contains only two or three layers in the 002 direction. The size of these domains is significantly smaller than those (six or seven layers) reported by Kercher and Nagle[40] for various hardwood and softwood mediumdensity fiberboard charcoals. Values of ε for these carbons exceed that of the 750 °C macshell carbon. The estimated aromaticity γ_a of these carbons is high (much higher than those reported by Lu et al.[37] for Australian black coals) but significantly lower than that of graphite.

Surface Area and Pore-Volume Distributions.
Table 1 displays the BET surface areas and (in some cases) the total pore volumes of the carbonized charcoal samples discussed above. Although the carbonization technique employed in this study was not designed to enhance the porous structure of the substrate, some of the biocarbon samples evidenced surprisingly high BET surface areas (e.g., 437 m²/g). Earlier workers reported values between 100 and 200 m²/g for macshell charcoal carbonized at 900-950 C.[16-19,41] In the case of the macshell carbon, the lack of a clear trend in the development of

surface area with increasing HTT may reflect gross heterogeneities in the surface properties of the macshell charcoal. Both macshells and Kukui nut shells are rich in oil that forms a coke during pyrolysis. This coke must have a low surface area. It is possible that the scatter in the macshell data and the very low surface area of the Kukui shell carbon are a result of coked nut oils. More generally, we remark that 50 years ago Franklin called attention to the existence of "a large volume of extremely small holes" within highly porous, nongraphitizing carbons (e.g., sugar charcoal).[42] The presence of extremely narrow pores in the biocarbons listed in Table 1 complicates the determination of their surface areas and pore volume distributions. In an earlier paper,[17] we presented scanning electron microscopy photographs of macshell charcoals, but these do not display the nanoporous structures that are responsible for the high surface areas of these carbons.

Electrical Resistivity. Because few studies have been reported of the electrical properties of packed beds of biocarbons, we initiated this work with measurements of a commercially available B&S coconut shell AC and a commercial graphite powder that serve as reference materials. The B&S AC is attractive because it can be sieved to a useful particle size (20-40 mesh) and it is quite homogeneous. The graphite powder is a logical reference material, but its very fine particle size makes it difficult to handle.

Figure 8a displays the resistivity and bed length as a function of applied compressive pressure for a 0.506-g packed bed of 20-40-mesh AC. After an initial compression of the bed, the influence of the compressive pressure on the measured resistivity and length of the bed and its apparent bulk density are reproducible with little hysteresis. Although Mrozowski[23] observed creep in his measurements of packed-bed resistivity, we detected no significant, systematic creep over a 60-min period. In Figure 8a, the resistivity of the bed decreases to a value of 0.41 Ω·cm at a bulk density of 0.61 g/mL under a compressive pressure of 7.63 MPa. Note that, after the initial compaction, the packed bed is virtually incompressible. Parts b and c of Figure 8 display identical behavior for packed beds of 1.0 and 1.5 g (respectively). Figure 8d confirms the expected ohmic behavior of the packed bed under a compressive pressure of 7.6 MPa. The slope of the solid, least-squares line (filled symbols) yields a resistivity of 0.44 Ω·cm. This value is in good agreement with the individual single-point values. Data points (open symbols) along the dashed line represent values of the measured resistance offset by the measured empty-cell resistance. This empty-cell resistance included the contact resistance between the two Ni electrodes as well as the resistance of the two Ni electrodes, etc. The measured empty-cell resistance was largely independent of the applied pressure. All of our reported values of resistivity were corrected by subtraction of the measured emptycell resistance from the measured total resistance at the pressure of interest. The *y* intercept of the solid line (8 mΩ) in Figure 8d represents the sum of the empty-cell resistance and the contact resistances between the two Ni electrodes and the carbon bed. The *y* intercept of the dashed line

represents the difference between the empty-cell Ni-Ni contact resistance and the two Ni-C contact resistances. This difference approximates the error incurred when we correct for the Ni-C contact resistance by use of the Ni-Ni (empty-cell) contact resistance. As displayed in Figure 8d, this error is small (<1 mΩ) relative to the resistance values of the packed bed (>40 mΩ). Related data for a smaller particle size (<105 μm) are displayed in Figure 8e. In this case the AC reaches a bulk density

of 0.81 g/mL (see Table 4) with a resistivity of 0.26 Ω·cm under a compressive pressure of 11.5 MPa. At 7.86 MPa, the measured resistivity (0.35 Ω·cm) of the <105-μm powder (with a bed density of 0.78 g/mL) is somewhat less than the value (0.41 Ω·cm) associated with the 20-40-mesh material (with a bed density of 0.61 g/mL) under a compressive pressure of 7.63 MPa. This comparison suggests that the electrical resistivity
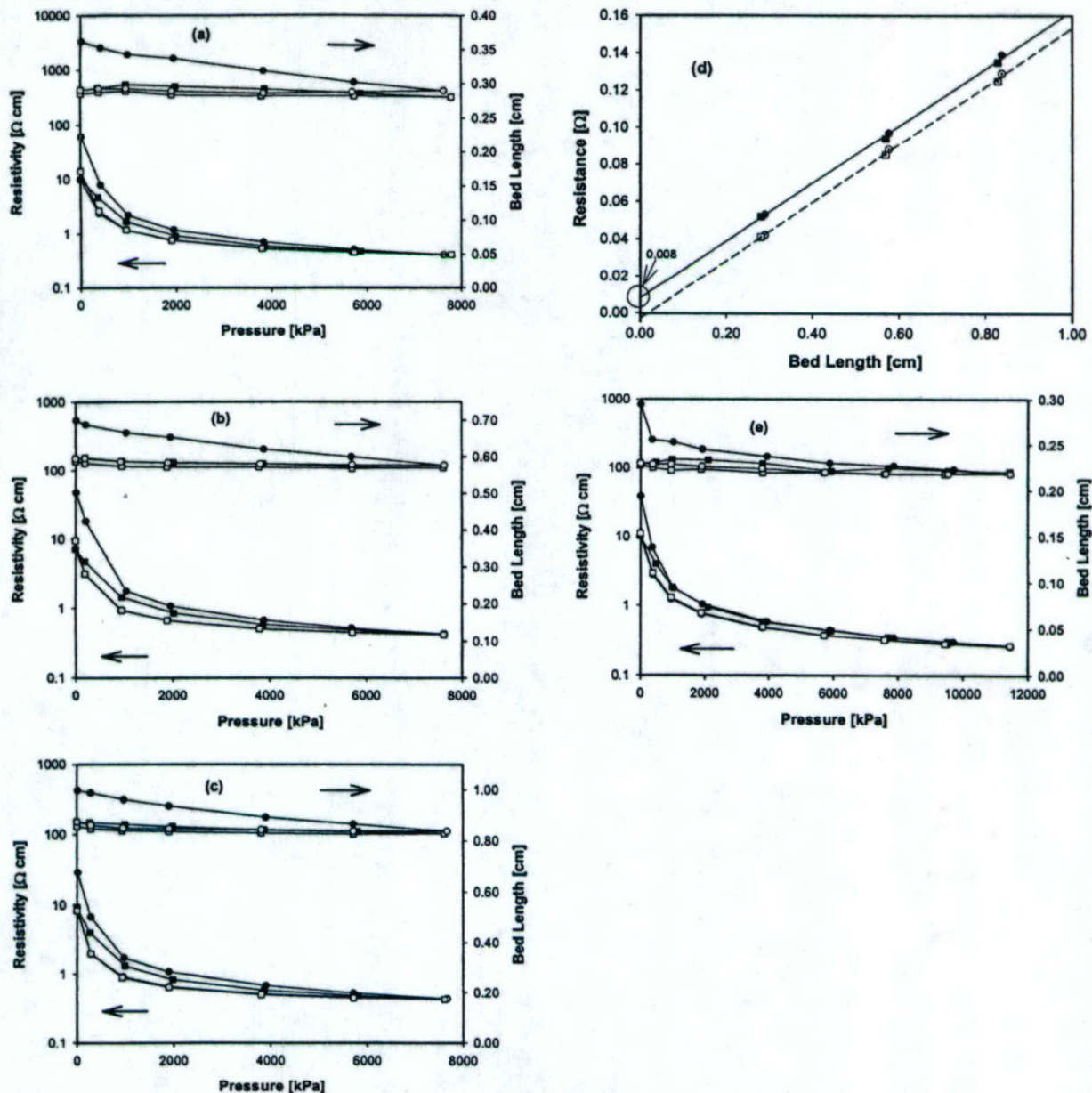

Figure 8. Resistivity (lower set of curves) and bed length (upper set of curves) vs compressive pressure for a packed bed of (a) 0.5 g, (b) 1.0 g, and (c) 1.5 g of 20-40-mesh AC; (d) ohmic behavior of the carbon packed bed at 7.6 MPa; and (e) resistivity and bed length vs compressive pressure for a 0.5-g packed bed of <105-μm AC powder. Symbols for parts a-c and e: ($\bullet$) pressurization 1; ($\bigcirc$) depressurization 1; ($\blacksquare$) pressurization 2; ($\square$) depressurization 2. Symbols for part d: ($\bullet$,$\blacksquare$, and solid line) measured resistance for pressurizations 1 and 2 and the least-squares regression line; ($\bigcirc$,$\square$ and dotted line) corrected resistance by subtraction of the empty-cell resistance for pressurizations 1 and 2 and the least-squares regression line.

of the packed bed is not strongly dependent upon either the particle size or the apparent bulk density of the bed (see below).

Figure 9 displays similar data for a 2.00-g packed bed of 1-2-μm graphite powder. The very fine particle size combined with the lubricity of the graphite powder

causes the bed to be unusually compressible. Under a compressive pressure of 7.77 MPa, it evidenced a resistivity of 0.029 Ω·cm at a bulk density of 1.41 g/mL. We remark that the compressive pressure caused the packed bed of graphite particles to become a wafer that retained its integrity when removed from the apparatus,

although the wafer was easily broken by hand. By way of comparison, the density of solid graphite is 2.26 g/mL, and the electrical resistivity of single crystals of graphite is anisotropic, with values as low as 40 $\mu\Omega\cdot$cm in the a-b plane at 300 K[43]

We have no knowledge of the conditions that were employed to produce the commercial AC used to acquire the data displayed in Figure 8. In particular, we have no knowledge of the carbon's HTT, i.e., its peak temperature. To put a floor on this value, we carbonized the AC in the muffle furnace at 950 °C and measured its resistivity as a function of compressive pressure. The values displayed in Figure 10 follow trends similar to those of Figure 8 but with a resistivity of 0.25 $\Omega\cdot$cm and a bulk density of 0.60 g/mL under a compressive pressure of 7.61 MPa. The carbonization treatment had little effect on the packed-bed density, but it lowered the resistivity by 43%. Evidently, the commercial activation

Table 4. Summary of the Resistivity and Bulk Density Values of Packed Beds of Carbon under a Compressive Pressure of ca. 7.6 MPa

feed	HTT, °C	particle size,[a] mesh	sample weight, g	resistivity,[b] Ωcm	density,[b] g/cm3	energy content,[c] MJ/kg	energy density,[c] GJ/m3
macshell	650	20-40	0.24	6.6×10^3	0.70	35.0	24.5
	750	20-40	0.37	2.9×10^1	0.65	35.0	22.8
	850	20-40	0.45	5.8×10^{-1}	0.65	33.8	22.0
	950	20-40	0.50	1.1×10^{-1}	0.58	34.9	20.2
	1050	20-40	0.51	5.9×10^{-2}	0.61	35.1	21.4
Kukui nut shell	950	20-40	0.50	1.8×10^{-1}	0.82	34.9	28.6
coconut husk	950	20-40	0.49	1.8×10^{-1}	0.46	33.4	15.4
Leucaena wood	950	20-40	0.50	1.6×10^{-1}	0.44	34.6	15.2
	950	<105 µm	0.50 0.51	1.1×10^{-1}	0.78	34.6	27.0
ACd		20-40		4.2×10^{-1}	0.63	NA	NA
		20-40	1.00	4.3×10^{-1}	0.62	NA	NA
		20-40	1.50	4.3×10^{-1}	0.64	NA	NA
carbonized		<105 µm	0.50 1.00	3.3×10^{-1}	0.81	NA	NA
AC[d]	950	20-40		2.3×10^{-1}	0.63	NA	NA
graphite powder		1-2 µm	2.00	2.9×10^{-2}	1.41	NA	NA

[a] U.S. standard sieve size or particle size before the heat treatment. [b] Resistivity and density values upon the second depressurization. [c] Estimated using the correlation of Cordero et al. (see text). [d] AC) activated carbon.
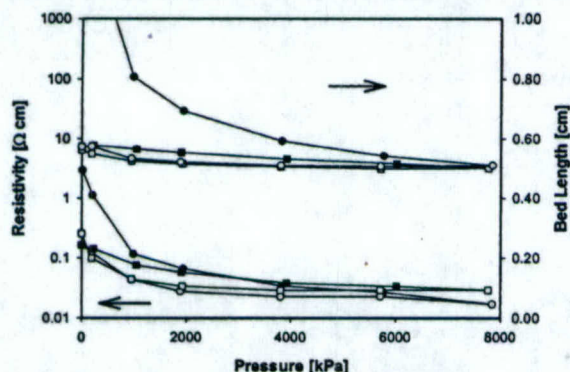

Figure 9. Resistivity (lower set of curves) and bed length (upper set of curves) vs compressive pressure for a 2.0-g packed bed of 1-2-µm graphite powder: (●) pressurization 1; (O) depressurization 1; (■) pressurization 2; (□) depressurization 2.
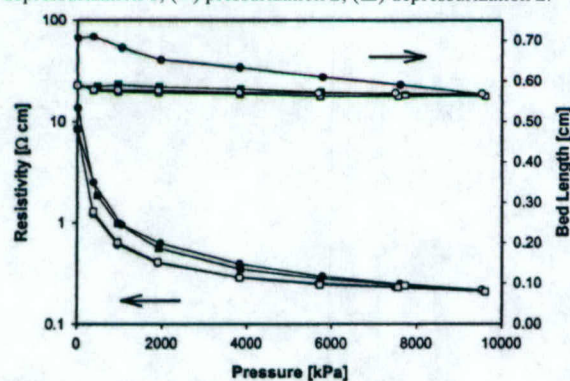

Figure 10. Resistivity (lower set of curves) and bed length (upper set of curves) vs compressive pressure for a 1.0-g packed bed of 20-40-mesh carbonized AC: (●) pressurization 1; (O) depressurization 1; (■) pressurization 2; (□) depressurization 2.

treatment did not involve a peak temperature above 950°C. Data for carbonized coconut husk charcoal powder displayed in Figure 11 can be compared to that of the AC displayed in Figure 10. Under a compressive
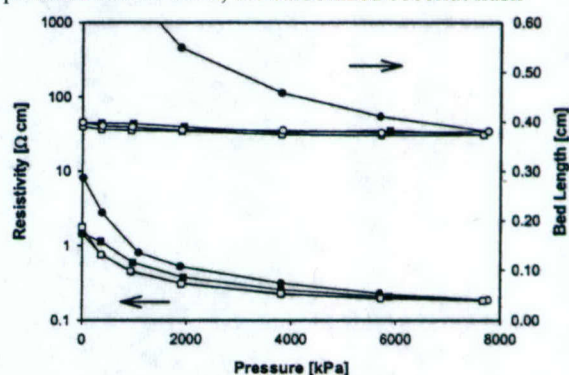
pressure of 7.77 MPa, the carbonized coconut husk

Figure 11. Resistivity (lower set of curves) and bed length (upper set of curves) vs compressive pressure for a 0.49-g packed bed of coconut husk carbonized charcoal powder: (●) pressurization 1; (O) depressurization 1; (■) pressurization 2; (□) depressurization 2.

charcoal offers a resistivity of 0.19 Ωcm at a bulk density of only 0.45 g/mL. Despite its low density, the coconut husk carbonized charcoal is a better conductor of electricity than the commercial coconut shell AC. Ostensibly, this result appears to contradict the claim of some earlier workers[44-46] that increasing the porosity of a carbon decreases both its thermal and its electrical conductivities. We remark that oxygen chemisorption can increase the electrical resistivity of a carbon;[47] hence, the relatively low electrical conductivity of the AC may reflect its aggressive chemisorption of oxygen from the air.

As shown in Figure 12, a packed bed of the 20-40-mesh macshell carbonized charcoal (950 °C) evidences an electrical resistivity of 0.12 Ωcm at a bulk density of 0.53 g/mL under a compressive pressure of 7.97 MPa. To learn more about the effects of HTT on the electrical resistivity of carbonized charcoals, we also carbonized macshell charcoal at HTT of 1050, 850, 750, and 650

°C. Figure 12 displays the effect of compressive pressure on the resistivity of each of these carbons,
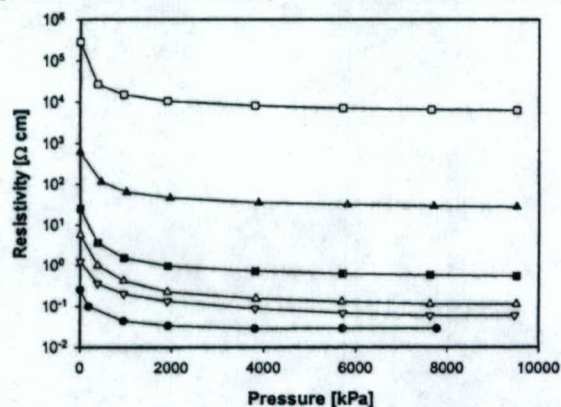

Figure 12. Resistivity vs compressive pressure for ca. 0.5-g packed beds of 20-40-mesh macshell charcoals carbonized at 650, 750, 850, 950, and 1050 °C and graphite powder (for comparison): (□) 650 °C, (▲) 750 °C, (■) 850 °C, (△) 950 °C, (▽) 1050 °C, (●) graphite. Each curve shows depressurization 2.

which decreases by more than 5 orders of magnitude with an increase of HTT from 650 to 1050 °C. As displayed in Figure 12, the 1050 °C macshell carbon's resistivity is about twice that of the graphite powder. Because these values approach the limit of detectability of our equipment, the exact ratio may differ somewhat from a factor of 2. Under a compressive pressure of 7.8 MPa, the apparent bulk density of the packed bed decreases from 0.71 to 0.58 g/mL as the HTT increases from 650 to 950 °C. This decrease is due to increased porosity of the carbon at higher HTT.

The 20-40-mesh Kukui shell carbon (see Figure 13) evidences a electrical resistivity (0.18 Ω·cm) similar to those of the coconut husk and macshell carbons but at a bulk density of 0.82 g/mL. The apparent bulk density (0.44 g/mL) of the 20-40-mesh Leucaena wood carbonized charcoal at 7.61 MPa (see Figure 14) is less than the macshell and Kukui shell carbons; nevertheless, its electrical resistivity (0.16 Ω·cm) is almost the same. To gain further insight into this matter, we carbonized Leucaena charcoal powder (<105 μm) and measured its resistivity. As displayed in Figure 14a, the powder evidences a slightly lower resistivity at the highest compressive pressures employed. On the other hand, the bulk density of the packed bed of powder (0.78 g/mL in Figure 14b) is nearly double that of the 20-40-mesh particles. Taken together, these findings indicate that the porosity of a carbonized charcoal does not significantly influence the electrical conductivity of the carbon.

For comparison sake, Espinola et al.[48] reported a resistivity of 1.24 Ω·cm for a packed bed of Babacu nut carbon at 19.6 MPa and 0.272 Ω·cm at 98 MPa. Likewise, they reported a resistivity of 0.92 Ω·cm for Eucalyptus lignin carbon at 19.6 MPa and 0.19 Ω·cm at 98 MPa. Unfortunately, Espinola et al. did not indicate the HTT of their carbons; consequently, this comparison is not very meaningful.

Discussion

The transformation of biomass into charcoal involves the loss of 60% or more of the substrate's mass with the

evolution of nearly 4 mol of gas/mol of "monomer".[14] During the transformation, the pyranose ring framework
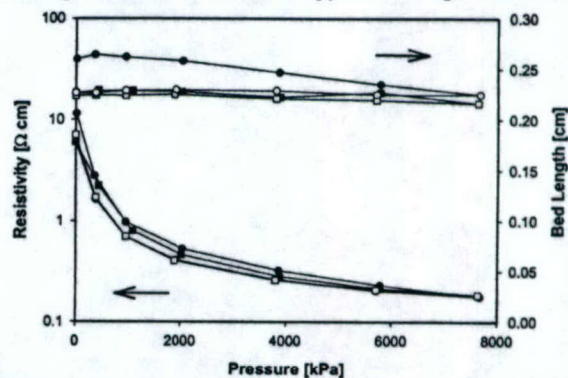

Figure 13. Resistivity (lower set of curves) and bed length (upper set of curves) vs compressive pressure for a 0.5-g packed bed of 20-40-mesh Kukui shell carbonized charcoal: (●) pressurization 1; (O) depressurization 1; (■) pressurization 2; (□) depressurization 2.
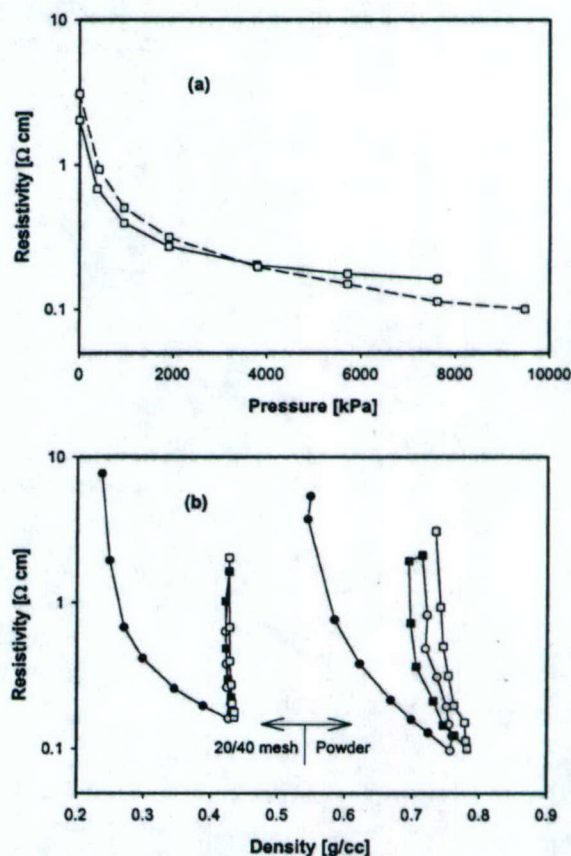

Figure 14. (a) Resistivity vs compressive pressure and (b) resistivity vs apparent density for packed beds of 20–40 mesh and <105-lm Leucaena wood carbonized charcoal. (a) Solid line: 20-40 mesh. Dashed line: powder. Each curve shows depressurization 2. (b) Left side: 20-40 mesh. Right side: powder. Symbols: (●) pressurization 1; (O) depressurization 1; (■) pressurization 2; (□) depressurization 2.

of the cellulosic fibers that compose biomass is grossly rearranged to form aromatic structures. Because this transformation does not involve a liquid phase, the product carbonaceous solid is inherently porous at the molecular level.[14] Franklin elucidated some aspects of this transformation in her classic XRD study of crystallite growth in graphitizing and nongraphitizing

carbons.[42] She found that oxygen-rich substances (e.g., sugar) form nongraphitizing carbons that have relatively low densities and are microporous, very hard, and composed of a randomly oriented, cross-linked structure of graphitelike crystallites. The nanoporous structure combined with the random orientation of the crystallites prevents graphitization, even at HTT as high as 3000 °C. Nevertheless, we remark that Franklin employed a sugar charcoal produced via a 2-h heat treatment at 1000 °C prior to carbonization at 2160 °C and higher, whereas we observe graphitelike electrical resistivities following carbonization at 950-1050 °C for only 10 min. Surprisingly mild conditions impart graphitelike electrical properties to nongraphitizing carbons.

In a series of papers, Mrozowski and coworkers [23,26,49-54] showed that the electrical resistivity of a packed bed of coke particles (subject to HTT of 1200 °C or more) decreased with increasing pressure (to the -0.5 power) and also decreased with increasing particle size (to the -0.25 power). No limit to the conductivity was reached at pressures as high as 100 MPa. The dependence of resistivity on pressure evidenced hysteresis and changed with increasing time at constant pressure (i.e., "creep"). On the other hand, we observed no creep and little hysteresis after an initial compaction of the bed. Furthermore, we found that neither the compressive pressure applied to the packed bed, the size and porosity of the particles composing the bed, nor the porosity of the bed had a big impact on its electrical resistivity under a compressive pressure of 5-10 MPa. We believe that some of these differences can be explained by a crushing of the bed at the high pressures employed by Mrozowski. Our equipment would not accommodate such high compressive pressures. Furthermore, such pressures are not needed to obtain a workable anode in a fuel cell. Moreover, the stability of the packed bed (as in our work) would be a desirable property of an electrode employed in a fuel cell.

There are similarities between the 9 orders of magnitude decrease in the electrical resistivity of compacted packed beds of fossil coke subject to increasing HTT as high as 1100 °C reported by Mrozowski[50] and the macshell biocarbon resistivities listed in Table 4. On the other hand, Pinnick[54] showed that a plot of log σ vs (HTT)[-1] for a typical coke fell along a perfectly straight line, whereas such a plot of our data does not fall on a straight line. Some of the differences between our findings and those of Mrozowski may be due to the fact that all of the carbons employed in his work became liquid when heated and remained liquid up to 450 °C. As mentioned earlier, there is no liquid-phase precursor to charcoal. It is well-known that charcoal retains the form and structure of its biomass precursor to such an extent that the appearance of a charcoal can be used to identify its origin.[55]

The plot of log σ vs the H/C ratio displayed by Waters[56] for fossil carbons resembles the data displayed in Tables 2 and 4. Waters also observed a plateau in electrical resistivity for atomic ratios H/C < 0.1. On the other hand, the value of O/C reported by Waters was a factor of 5-10 smaller than the values obtained in this work.

The 950 °C carbonized charcoals tested in this work spanned a large range of carbon contents, ash contents, H/C and O/C ratios, surface areas, porosities, particle sizes, and packed-bed densities. Nevertheless, at a given HTT, their FTIR spectra, XRD spectra, and electrical resistivities were quite similar to each other. Furthermore, at HTT g 950 °C, their FTIR spectra and their electrical resistivities were similar to those of graphite particles. On the other hand, the XRD spectra of macshell charcoal underwent virtually no change at increasing HTT from 750 to 950 °C. Evidently, the 3 orders of magnitude decrease in electrical resistivity (with increasing HTT from 750 to 950 °C) is not associated with any change in the crystal structure of the biocarbon. Furthermore, the biocarbon XRD spectra do not resemble those of graphite or turbostratic carbons. These facts cause us to visualize carbonized charcoal to be a macromolecular, cross-linked, threedimensional, aromatic structure replete with conjugation and π bonds that facilitate the conduction of electrons[56,57] as well as nanopores, and micromolecular cracks.[14] The evolution of about four molecules of gas per molecule of biomass "monomer" during carbonization leaves behind many dangling bonds (unpaired electrons) that may also contribute to the electrical conductivity of the carbon.[23,49-51,56] Nevertheless, Shafizadeh and co-workers[58] showed that the concentration of unpaired electrons ("free radicals") in cellulose char peaked at HTT between 500 and 600 °C and thereafter declined by a factor of 5 at a HTT of 800 °C. Consequently, there is no evident relationship between the concentration of unpaired electrons in biocarbons and their electrical resistivity. The fossil carbon literature also contains speculations about the potential effects of mineral impurities on the electrical resistivity of the carbon. These impurities may act as donors or acceptors and thereby improve the electrical conductivity of the carbon semiconductor.[23,49-51,56] It is evident that biocarbonsalso contain mineral impurities that could influence their electrical conductivity. Nevertheless, if we recognize that these biocarbons were produced from greatly different biomass substrates that must represent different ash compositions, it would be a case of real serendipity if they all contained an influential impurity that imparted to each carbon a similar electrical conductivity.

If we employ the correlation[59] proposed by Cordero et al. for the higher heating value (HHV) of charcoal [i.e., HHV/MJ = 0.3543 x (% fC) + 0.1708 x (% VM)], where % fC and % VM are the percentage fixed carbon and volatile matter contents of the charcoal, respectively,.and assume that the 950 °C charcoals contain only ash and fixed carbon, then the energy content of these carbons is about 35 MJ/kg (see Table 4). This value is somewhat lower than those of liquified natural gas (LNG; ca. 55 MJ/kg), propane (ca. 50 MJ/kg), and crude oil (ca. 44 MJ/kg) but much higher than those of most coals. Table 4 also displays the energy density of these carbons on a volumetric basis. These values range from 15.2 to 28.6 GJ/m³ and can be compared to the energy density of gasoline (i.e., octane with a lower heating value of 32 GJ/m³), ethanol (ca. 21 GJ/m³), LNG (23 GJ/m³), and propane (24 GJ/m³). When it is recognized that these carbon packed beds retain

their bulkdensity after an initial compaction, it is evident thatdense carbon packed beds are attractive energy carriers with energy densities comparable to those of conventional liquid fuels.

Conclusions

1. After an initial compaction, a packed bed of carbonized charcoal particles is virtually incompressible and evidences ohmic behavior under a compressive pressure of 7.6 MPa. The contact resistance between the bed and the two electrodes is negligible at this pressure. We observed no creep, little hysteresis, and little effect of pressure (between 5 and 10 MPa) on the resistivities of packed beds of carbonized charcoals after the initial compaction.
2. Surprisingly mild conditions (HTT ~ 950 °C) impart graphitelike electrical properties to all of the charcoals that we studied.
3. The electrical resistivity of a packed bed of carbonized charcoal is not strongly dependent upon the particle size of the bed material, the surface area or the microporosity of the bed material, or the apparent bulk density of the packed bed.
4. The energy content of carbonized charcoal (ca. 35 MJ/kg) is somewhat lower that of than crude oil but higher than those of most coals. The energy density of a compact bed of carbonized charcoal (15.2-28.6 GJ/ m³) is comparable to that of conventional liquid fuels (e.g., propane, LNG, and ethanol).
5. Some carbonized charcoals have surprisingly high BET surface areas (e.g., 437 m²/g), whereas others have negligible surface area. The presence of extremely narrow pores in carbonized charcoals complicates the determination of their surface areas and pore-volume distributions.
6. Increasing the HTTs between 750 and 950 °C has no significant effect on the XRD spectra of macshell charcoals. A wide range of charcoals carbonized at 950 °C manifest nearly identical XRD spectra. The scattering domains of graphite crystallites in the carbonized charcoals are less than three layers thick.
7. All biocarbons obtained from macshell, Leucaena, coconut husk, and Kukui nut shell charcoals with HTT of 950 °C show FTIR spectra very similar to each other, as well as to the spectrum of graphite.
8. A comparison of the 950 °C biocarbons reveals a considerable range in the values of their C, H, O, and ash contents and the H/C and O/C ratios. None of these values is closely associated with the electrical conductivity of the biocarbon.
9. The transformation of biomass into biocarbon involves the loss of 60% or more of the substrate's mass with the evolution of nearly 4 mol of gas/mol of "monomer" of biomass. During this transformation, the pyranose ring framework of the cellulose fibers that compose biomass is grossly rearranged to form aromatic structures. Because this transformation does not involve a liquid phase, many bonds are left dangling, giving rise to a carbonaceous solid that is highly reactive and inherently porous at the molecular level. The findings of this work cause us to visualize carbonized charcoal to be a macromolecular, cross-linked, three-dimensional, aromatic structure replete with conjugation and ∂ bonds that facilitate the conduction of electrons, as well as nanopores, and micromolecular cracks.
10. In light of the facts that (a) under compressive pressure a compact packed bed of carbonized charcoal can have an electrical resistivity comparable to that of a compact packed bed of graphite particles, (b) a compact carbonized charcoal packed bed can have a very large surface area and high reactivity as well as an energy density comparable to that of conventional liquid fuels, and (c) the wholesale price of biomass charcoal is competitive with gasoline and natural gas, we conclude that compact packed beds of carbonized charcoal have promising applications as electrodes and consumable anodes in biocarbon fuel cells and batteries. To explore these applications further, we are currently testing a biocarbon fuel cell that employs the packed bed apparatus described herein as its anode. Results of this work will be the subject of future papers.

Literature Cited

(1) Vielstich, W. *Fuel Cells*; Wiley-Interscience: London, 1965.
(2) Williams, K. R., Ed. *An Introduction to Fuel Cells*; Elsevier Publishing Co.: Amsterdam, The Netherlands, 1966.
(3) Bockris, J. O. M.; Srinivasan, S. *Fuel Cells: Their Electrochemistry*; McGraw-Hill Book Co.: New York, 1969.
(4) Anbar, M.; McMillen, D. F.; Weaver, R. D.; Jorgensen, P. J. Method and Apparatus for Electrochemical Generation of Power from Carbonaceous Fuels. U.S. Patent 3,970,474, 1976.
(5) Anbar, M. Methods and Apparatus for the Pollution-Free Generation of Electrochemical Energy. U.S. Patent 3,741,809, 1973.
(6) Pesavento, P., personal communication, 1998.
(7) Gur, T. M.; Huggins, R. A. Direct Electrochemical Conversion of Carbon to Electrical Energy in a High-Temperature Fuel Cell. *J. Electrochem. Soc.* **1992**, *139*, L95.
(8) Ford, A. R.; Greenhalgh, E. Industrial Applications of Carbon and Graphite. In *Modern Aspects of Graphite Technology*; Blackman, L. C. F., Ed.; Academic Press: London, 1970; p 258.
(9) Coutinho, A. R.; Luengo, C. A. Preparing and Characterizing Electrode Grade Carbons from Eucalyptus Pyrolysis Products. In *Advances in Thermochemical Biomass Conversion*; Bridgwater, A. V., Ed.; Blackie Academic & Professional: London, 1993; p 1230.
(10) Coutinho, A. R.; Luengo, C. A. Mass Balance of Biocarbon Electrodes Obtained by Experimental Bench Production. In *Developments in Thermochemical Biomass Conversion*; Bridgwater, A. V., Boocock, D. G. B., Eds.; Blackie Academic & Professional: London, 1997; p 305.
(11) Coutinho, A. R.; Rocha, J. D.; Luengo, C. A. Preparing and characterizing biocarbon electrodes. *Fuel Process. Technol.* **2000**, *67*, 93.

(12) Antal, M. J.; Croiset, E.; Dai, X. F.; DeAlmeida, C.; Mok, W. S. L.; Norberg, N.; Richard, J. R.; Majthoub, M. A. High-Yield Biomass Charcoal. *Energy Fuels* **1996**, *10*, 652.

(13) Antal, M. J.; Allen, S. G.; Dai, X.; Shimizu, B.; Tam, M. S.; Gronli, M. G. Attainment of the theoretical yield of carbon from biomass. *Ind. Eng. Chem. Res.* **2000**, *39*, 4024.

(14) Antal, M. J.; Gronli, M. G. The Art, Science, and Technology of Charcoal Production. *Ind. Eng. Chem. Res.* **2003**, *42*, 1919.

(15) Antal, M. J.; Mochidzuki, K.; Paredes, L. S. Flash Carbonization of Biomass. *Ind. Eng. Chem. Res.* **2003**, *42*, 3690.

(16) Dai, X.; Antal, M. J., Jr. Synthesis of a High-Yield Activated Carbon by Air Gasification of Macadamia Nut Shell Charcoal. *Ind. Eng. Chem. Res.* **1999**, *38*, 3386.

(17) Tam, M. S.; Antal, M. J., Jr. Preparation of Activated Carbons from Macadamia Nut Shell and Coconut Shell by Air Activation. *Ind. Eng. Chem. Res.* **1999**, *38*, 4268.

(18) Conesa, J. A.; Sakurai, M.; Antal, M. J. Synthesis of a High-Yield Activated Carbon by Oxygen Gasification of Macadamia Nut Shell Charcoal in Hot, Liquid Water. *Carbon* **2000**, *38*, 839.

(19) Tam, M. S.; Antal, M. J.; Jakab, E.; Varhegyi, G. Activated Carbon from Macadamia Nut Shell by Air Oxidation in Boiling Water. *Ind. Eng. Chem. Res.* **2001**, *40*, 578.

(20) Langford, J. I. A rapid method for analysing the breadth of diffraction and spectral lines using the Voigt function. *J. Appl. Crystallogr.* **1978**, *11*, 10.

(21) Delhez, R.; de Keijser, T. H.; Mittemeijer, E. J. Determination of crystallite size and lattice distortions through X-Ray difraction line profile analysis. *Fresenius' Z. Anal. Chem.* **1982**, *312*, 1.

(22) de Keijser, T. H.; Langford, J. I.; Mittemeijer, E. J.; Vogels, A. B. P. Use of the Voigt functions in a single-line method for the analysis of X-ray diffraction line broadening. *J. Appl. Crystallogr.* **1982**, *15*, 308.

(23) Mrozowski, S. Studies of Carbon Powders Under Compression I. *Proceedings of the Third Conference on Carbon*; Pergamon Press: New York, 1959; p 495.

(24) Rosa, M. L. *Nuovo Cimento* **1916**, *12*, 284.

(25) Gottstein, G. *Ann. Phys.* **1914**, *43*, 1079.

(26) Loebner, E. E. Thermoelectric Power, Electrical Resistance, and Crystalline Structure of Carbons. *Phys. Rev.* **1956**, *102*, 46.

(27) Varhegyi, G.; Szabo, P.; Till, F.; Zelei, B.; Antal, M. J.; Dai, X. TG, TG-MS, and FTIR Characterization of High-Yield Biomass Charcoals. *Energy Fuels* **1998**, *12*, 969.

(28) Varhegyi, G.; Szabo, P.; Antal, M. J. Kinetics of Charcoal Devolatilization. *Energy Fuels* **2002**, *16*, 724.

(29) Friel, J. J.; Mehta, S.; Follweiler, D. M. Electron Optical and IR Spectroscopic Investigation of Coal Carbonization. In *Coal and Coal Products: Analytical Characterization Techniques*; Fuller, E. L., Ed.; American Chemical Society: Washington, DC, 1982; p 294.

(30) Mapelli, C.; Castiglioni, C.; Meroni, E.; Zerbi, G. Graphite and Graphitic Compounds: Vibrational Spectra from Oligomers to Real Materials. *J. Mol. Struct.* **1999**, *480-481*, 615.

(31) Kwizera, P.; Dresselhaus, M. S.; Dresselhaus, G. Raman Spectra and Staging of Intercalated Graphite Fibers. *Carbon* **1983**, *21*, 121. **5150** Ind. Eng. Chem. Res., Vol. 42, No. 21, 2003

(32) Kim, D.-Y.; Nishiyama, Y.; Wada, M.; Kuga, S. Graphitization of Highly Crystalline Cellulose. *Carbon* **2001**, *39*, 1051.

(33) Biscoe, B. E.; Warren, B. E. An X-Ray Study of Carbon Black. *J. Appl. Phys.* **1942**, *13*, 364.

(34) Yen, T. F.; Erdman, J. G.; Pollack, S. S. Investigation of the Structure of Petroleum Asphaltenes by X-Ray Diffraction. *Anal. Chem.* **1961**, *33*, 1587.

(35) Cullity, B. D. *Elements of X-ray Diffraction*; Addison-Wesley: Reading, MA, 1978.

(36) Schwager, I.; Farmanlan, P. A.; Kwan, J. T.; Weinberg, V. A.; Yen, T. F. Characterization of the microstructure and macrostructure of coal-derived asphaltenes by nuclear magnetic resonance spectrometry and X-Ray diffraction. *Anal. Chem.* **1983**, *55*, 42.

(37) Lu, L.; Sahajwalla, V.; Harris, D. Characteristics of Chars Prepared from Various Pulverized Coals at Different Temperatures Using Drop-Tube Furnace. *Energy Fuels* **2000**, *14*, 869.

(38) Walker, P. L.; Seeley, S. B. Fine Grinding of Ceylon Natural Graphite. *Proceedings of the Third Conference on Carbon*; Pergamon Press: New York, 1959; p 481.

(39) Senneca, O.; Salatino, P.; Masi, S. Microstructural changes and loss of gasification reactivity of chars upon heat treatment. *Fuel Process. Technol.* **1998**, *77*, 1483.

(40) Kercher, A. K.; Nagle, D. C. Microstructural evolution during charcoal carbonization by X-ray diffraction analysis. *Carbon* **2003**, *41*, 15.

(41) Dai, X. *Pyrolytic and Oxidative Syntheses of High-Yield Carbons from Biomass*. Ph.D. Thesis, University of Hawaii at Manoa, Honolulu, HI, 1998.

(42) Franklin, R. Crystallite growth in graphitizing and nongraphitizing carbons. *Proc. R. Soc. London A* **1951**, *209*, 196.

(43) Mantell, C. L. *Carbon and Graphite Handbook*; Interscience: New York, 1968.

(44) McEnaney, B.; Mays, T. J. Porosity in Carbons and Graphites. In *Introduction to Carbon Science*; Marsh, H., Ed.; Butterworths: Boston, 1989; p 154.

(45) Alekhina, M. B.; Shumyatakii, Y. I.; Skubak, E. A.; Savchenko, S. G. Correlation Between Electrophysical Properties and Parameters of Porous Structure of SKT Activated Charcoal. *Russ. J. Appl. Chem.* **1993**, *66*, 1413.

(46) Hutcheon, J. M. Manufacturing Technology of Baked and Graphitized Carbon Bodies. In *Modern Aspects of Graphite Technology*; Blackman, L. C. F., Ed.; Academic Press: London, 1970; p 49.

(47) Golden, T. C.; Jenkins, R. G.; Otake, Y.; Scaroni, A. W. Oxygen Complexes on Carbon Surfaces. In *Proceedings of the Workshop on the Electrochemistry of Carbon*; Sarangapani, S., Akridge, J. R., Schumm, B., Eds.; The Electrochemical Society: Pennington, NJ, 1983; p 61.

(48) Espinola, A.; Miguel, P. M.; Salles, M. R.; Pinto, A. R. Electrical Properties of Carbons-Resistance of Powder Materials. *Carbon* **1986**, *24*, 337.

(49) Mrozowski, S. Electric Resistivity of Polycrystalline Graphite and Carbons. *Phys. Rev.* **1950**, *77*, 838.

(50) Mrozowski, S. Semiconductivity and Diamagnetism of Polycrystalline Graphite and Condensed Ring Systems. *Phys. Rev.* **1952**, *85*, 609.

(51) Mrozowski, S. Semiconductivity and Diamagnetism of Polycrystalline Graphite and Condensed Ring Systems. *Phys. Rev.* **1952**, *86*, 1056.

(52) Loebner, E. E. Thermoelectric Power of Carbons and Graphite. *Phys. Rev.* **1951**, *84*, 153.

(53) Loebner, E. E. Thermoelectric Power of Carbons and Graphite. *Phys. Rev.* **1952**, *86*, 1056.

(54) Pinnick, H. T. Electronic Properties of Carbons and Graphite. *Proceedings of the First and Second Conferences on Carbon*, Buffalo, NY, 1953, 1955; p 3.

(55) Klar, M. *The Technology of Wood Distillation*; Chapman & Hall: London, 1925.

(56) Waters, P. L. Semiconducting Properties of Carbonized Coal. In *Proceedings of the Fifth Conference on Carbon*; Mrozowski, S., Ed.; Pergamon Press: New York, 1963; p 131.

(57) Eley, D. D. *Nature* **1948**, *162*, 819.

(58) Shafizadeh, F.; Bradbury, A. G. W.; DeGroot, W. F., personal communication, 1984.

(59) Cordero, T.; Marquez, F.; Rodriguez-Mirasol, J.; Rodriguez, J. J. Predicting heating values of lignocellulosics and carbonaceous materials from proximate analysis. *Fuel* **2001**, *80*, 1567.